Signatures of degradation mechanisms from photovoltaic plants

Nikola Hrelja

INSTITUT POLYTECHNIQUE DE PARIS

NNT : 2020IPPAX090

Thèse de doctorat

Signatures of Degradation Mechanisms from Photovoltaic Plants

Thèse de doctorat de l'Institut Polytechnique de Paris
préparée à l'École polytechnique

École doctorale n°574 École doctorale de mathématiques Hadamard (EDMH)
Spécialité de doctorat : Mathématiques aux interfaces

Thèse présentée et soutenue à Fontainebleau, le 06 nov. 2020, par

NIKOLA HRELJA

Composition du Jury :

Anne Auger Directeur de recherche, Inria (RANDOPT)	Président
Fabrice Gamboa Professeur, Université de Toulouse (IMT)	Rapporteur
Roger French Professeur, CWRU Cleveland, Ohio, (SDLE)	Rapporteur
Florence Forbes Directeur de recherche, Inria Grenoble (MISTIS)	Rapporteur
Thierry Klein Professeur, Ecole Nationale d'Aviation Civile (ENAC)	Examinateur
Éric Moulines Professeur, Ecole Polytechnique (CMAP)	Directeur de thèse
Mike Van Iseghem Ingenieur de recherche, EDF R&D Tree	Co-directeur de thèse

"This project has received funding from the European Union's Horizon 2020 research and innovation programme under the Marie Sklodowska-Curie grant agreement No 721452"

Acknowledgements

This project has received funding from the European Union's Horizon 2020 research and innovation programme in the framework of the project "SolarTrain" under the Marie Sklodowska-Curie GA No 721452.

Contents

List of Figures

Acronyms

DDM Double Diode Model.

DOE Design of Experiments.

EDF Electricite de France.

EE Elementary Effect.

EL Electroluminescence.

EVA Ethylene-vinyl acetate.

FF Fill Factor.

IEA International Energy Agency.

IR Infrared.

LCOE Levelized Cost of Electricity.

LFM Loss Factor Model.

LHS Latin Hypercube Sampling.

NREL National Renewable Energy Laboratory.

ODE Ordinary Differential Equation.

PCE Polynomial Chaos Expansion.

PLR Performance Loss Rate.

POA Plane Of Array.

PR Performance Ratio.

PV Photovoltaic.

PVUSA Photovoltaics for Utility Scale Applications.

RMSE Root Mean Square Error.

SA Sensitivity Analysis.

SDM Single Diode Model.

STC Standard Test Conditions.

Résumé

La dégradation de la performance des centrales PV (photovoltaïque) au cours de leur durée de vie est généralement déterminée par la variation de la puissance au point de puissance maximale (Power at maximum power point P_{mpp}). Cependant, la même quantité de pertes en P_{mpp} peut avoir des causes multiples, qui ont, chacune, des évolutions différentes dans le temps.

Les méthodes existantes de taux de perte de performance (Performance Loss Rate) ne sont pas adaptées pour identifier ces causes et mécanismes fondamentaux à partir des données de terrain. Le modèle physique d'EDF est une version sophistiquée d'un modèle à 2 diodes. Ce modèle dépend de paramètres dont les valeurs évoluent au cours du temps et peuvent reflètent ainsi les processus de dégradation. Lorsque les mesures des courbes courant-tension (courbes IV) sont disponibles, les paramètres du modèle physique peuvent être directement estimés. Toutefois les mesures de la courbe IV sont rarement effectuées sur les sites de production de PV et l'estimation des paramètres du modèle à 2 diodes est difficile à partir du nombre limité de variables mesurées. Le défi que nous nous attachons à relever est l'estimation des paramètres du modèle en utilisant uniquement le P_{mpp}, et la météo, permettant ainsi une évaluation plus précise de l'état de santé du système, plutôt que d'estimer uniquement la mesure de la perte de performance.

Une analyse de sensibilité a été réalisée sur différents modèles physiques photovoltaïques, à savoir le modèle à diode unique et le code d'EDF. Les trois paramètres les plus influents identifiés par notre méthodologie sont ont la résistance-série (R_s), la résistance shunt (R_{sh}) et le courant de court-circuit (I_{sc}). Ces paramètres identifiés ont été utilisés dans la calibration du modèle de performance PV.

L'algorithme proposé vise à identifier la distribution *a posteriori* des paramètres en calibrant le code de calcul en fonction des données observées. L'inférence bayésienne a été menée à l'aide de la méthode ABC (Approximate Bayesian Computation) car la vraisemblance des observations est un code de calcul et n'a pas d'expression close. Comme l'exécution du code de calcul est chronophage. Une expansion en chaos polynomial (PCE) a été utilisée comme modèle de substitution pour remplacer le code original et accélérer l'inférence. L'algorithme a été validé sur des données synthétiques simulées (Digital Power Plant) auxquelles nous avons ajouté un bruit de mesure gaussien, une erreur systématique et un scénario d'évolution de dégradation des paramètres. Les résultats sur les données synthétiques montrent que l'évolution des paramètres peut être estimée en dépit du bruit de mesure et des fluctuations importantes.

La méthode proposée a ensuite été appliquée à des données réelles collectées en fonctionnement à la centrale solaire de Bolzano (Italie, pendant la période 2011-2019). Notre méthode ne donne des résultats robustes qu'en été et en automne, la météo étant plutôt stable pour ce site pendant cette période. Au cours de ces mois, les résultats montrent que la baisse de puissance des modules exposés peut être attribuée à la baisse du I_{sc} alors que la R_s et la R_{sh} ne montrent pas de changement significatif sur 8 ans. Une analyse supplémentaire sera nécessaire pour définir plus précisément les mécanismes de dégradation qui peuvent être identifiés avec l'évolution des paramètres extraits et

leur corrélation avec les conditions de fonctionnement extérieures.

En perspective, nous suggérons d'utiliser notre méthode pour examiner un grand nombre de jeux de données ayant des mécanismes de dégradation connus et inconnus, afin de connaître et améliorer la robustesse de la méthode et l'évolution des paramètres qui pourraient se révéler être des caractéristiques plus intéressantes, et de suggérer des explications physiques permettant d'identifier les points de rupture et les changements des mécanismes de défaillance au cours du temps.

Mots Cles: Dégradation de performance, Centrales photovoltaïques, Analyse de sensibilité, Méta-modèles, Estimation d'un modèle non linéaire, Calcul bayésien approximatif

Abstract

The degradation of the PV (Photovoltaic) performance over its lifetime is usually determined with the variation of Power at maximum power point (P_{mpp}). However, the same amount of P_{mpp} loss can have different causes, which have, each, different expectations of evolution with time.

Existing Performance loss rate (PLR) methods are not suitable to identify these root causes and mechanisms from the field data. Physical performance models based on 2 diode models contain parameters that can reflect degradation over time. When IV curves measurements are available from the field the parameters of the physical model can be straightforwardly estimated. While the IV curve measurements are rarely available from the PV production sites the parameter estimation is challenging since only limited data about the observed system is available. Estimating the model parameters using only P_{mpp} is the challenge here allowing a more precise evaluation of the health state of the system, rather than estimating only the performance loss metric.

The proposed algorithm aims to identify posterior distribution of parameters by calibrating the computational code to the observed data with a robust Approximate Bayesian Computation (ABC) method. The ABC method expresses the probability of the observed data under a prior statistical model with certain parameter values. Polynomial Chaos Expansion (PCE) was used as a meta-model to replace the original code which was found to be too computationally expensive.

The algorithm has been validated on simulated synthetic data (Digital Power Plant) with an added Gaussian noise, some systematic discrepancy and a known parameter degradation evolution. The results on the synthetic data show that the evolution of parameters can be estimated in noisy measurement conditions.

The proposed method has then been applied to the real outdoor data. Firstly, the method only gives robust results in the summer and autumn. In these months, the results show that the power decline of the fielded modules can be attributed to the decline in the short circuit current (I_{sc}) while the parameters series (R_s) and shunt resistance (R_{sh}) do not show any significant change over 8 years. Additional analysis is needed to define the possible signatures of degradation mechanisms that can be identified with the evolution of extracted parameters and their correlation with outdoor operating conditions.

As a perspective, we suggest to use our new method to look into a big amount of data sets with known and unknown mechanisms in order to learn about the robustness of the method and the evolution of the parameters that could reveal more interesting characteristics, and suggest physical arguments for studying breaking points and changes in failure mechanisms.

Keys words : Photovoltaic degradation, Sensitivity analysis, Design of Experiment, Calibration

Chapter 1

Introduction

The introductory chapter describes the objective and outline of the thesis with brief chapter descriptions. In this chapter, the literature review is presented with an emphasis on the gaps this manuscript is trying to overcome. This brief thesis overview is intended to give the reader an insight into the physics of photovoltaics and degradation and serve as an introduction to the content of this thesis.

Contents

1.1 Thesis motivation

Because of the recent technological developments and increasing concerns about the sustainability and environmental impact of conventional fuel usage, the energy companies are focusing their research on producing cleaner, sustainable power from renewable energy sources. In recent years there has been a rapid growth in large scale photovoltaic (PV) power plant installation around the world where the majority of those installations are consisting of hundreds of thousand modules spread over hectares of land. The solar market has grown very fast and in some cases it is becoming a non-subsidized market with increased demand for performance certainty.

In 2018 Electricite de France (EDF) has announced to install in France 30 GW of photovoltaic power in the project called "Le Plan Solaire" between the years 2020-2035 where the majority will be constituted of large PV plants [23] (Figure 1.1). In this context, it is more and more important for EDF to accurately predict the power delivery over time and to quantify and define all the relevant risk factors of long term performance losses. This thesis is motivated by EDF's need to better understand and model the PV plant performance loss and degradation over its lifetime and giving access to the underlying physical mechanisms.

Figure 1.1: PV power plant from EDF Renewables installed in Puyloubier.

The degradation of PV modules over time directly reduces the electricity generation and increases the Levelized Cost of PV electricity. The PV plant operating lifetime is mainly determined by the stability and resistance of PV modules to different stressors which are closely related to the meteorological exposure of installed modules.

Depending on the meteorological exposure and the chosen technology the degradation rates and the prevailing degradation mechanisms will be different where certain degradation modes are more severe with specific climatic conditions; see for example the review by D. Jordan [44] and the references therein.

Measuring and understanding the mechanisms of degradation is important because it can help to predict the expected lifetime of a PV plant. The International Energy Agency (IEA) PVPS Task 13 document "Review of Failures of Photovoltaic Modules" [50] divided the typical failures of PV modules into the following three categories: infant-failures, midlife-failures, and wear-out-failures. Figure 1.2, taken from [50], shows the impact of these three categories of failures for PV modules on the nominal power as a function of the lifetime.

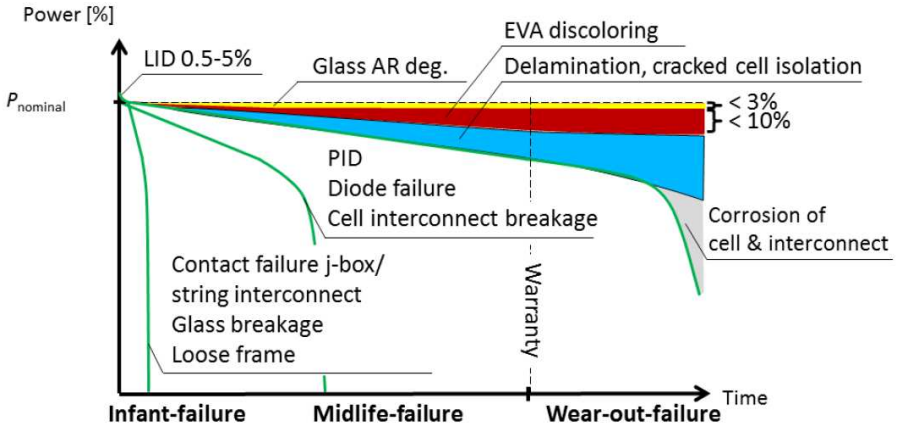

Figure 1.2: Three typical failure categories for wafer-based crystalline photovoltaic modules [50].

Infant-mortality failures occur in the beginning of the working life of a PV module where flawed PV modules are responsible for those failures. The most important failures in the field are j-box

failure, glass breakage, defective cell interconnect, loose frame and delamination.

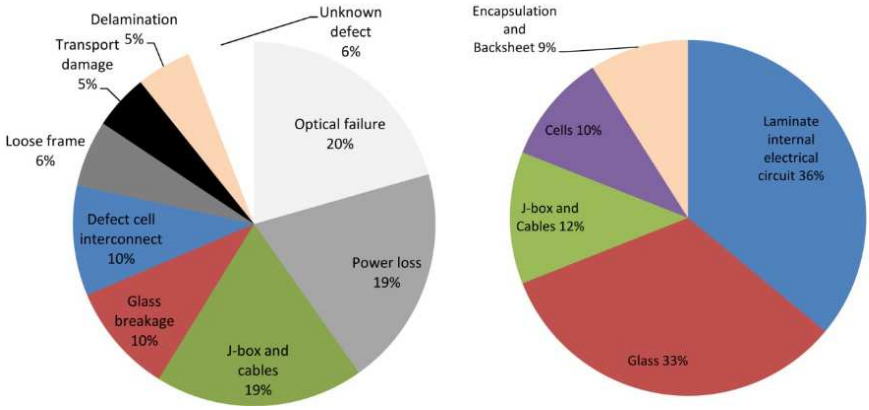

Figure 1.3: Figure (Left) Failure rates due to customer complains in the first two years after delivery. Figure (right) Field study of PV module failures found for various PV modules of 21 manufacturers installed in the field for 8 years [20].

Midlife failures are described in the study of DeGraff [20]. The Figure 1.3 shows the failure distribution of PV modules that have been in the field for 8 years. Around 2% of the PV modules are predicted not to meet the manufacturer's warranty after 11-12 years of operation. In the study the most prevalent failures are defected interconnections and PV module glass breakage. The failure rate of j-box and cables (12%), burn mark on cells (10%) and encapsulant failure (9%) are comparably high.

Wear out failures occur at the end of the working lifetime of PV modules. Where the working lifetime is defined as a power drop under a certain level, typically between 20% and 30% of the initial power. According to the study of Schulz [84] the predominant PV modules wear out failures are delamination, cell part isolation due to cell cracks and discolouring of the laminate. However, all these failures lead to a power loss between 0% and 20% and meet the manufacturer's power warranty. The PV modules used in the study of Schulz [84] are not representative for today. The lamination material being responsible for the delamination and discoloration are not in use in today's PV manufacturing as well the cell and module sizes deviate strongly from today's PV modules, this factors affect the cell part isolation of cells in a PV module.

In our approach, we want to fit a physical model to measured timeseries representing a significant part of the lifetime, so that signatures of degradation mechanisms become visible.

Various physical/mathematical models have been developed to predict the performance of the PV plant as the function of different weather variables (for example, the irradiance, the panel temperature, etc.) and physical model parameters. These physical model parameter typically depend on many physical parameters whose values are likely to change significantly during the lifetime of the PV panel. Moreover, the PV module manufacturers release the nominal value of the parameters when the module is installed, but these values are sometimes remarkably different from the ones which are measured.

In model calibration, the physical model parameters are estimated so that the measured values are matched with the simulated values and hopefully the model accurately represents the important features of the observed system. Figure 1.4 shows the modeling approach and calibration.

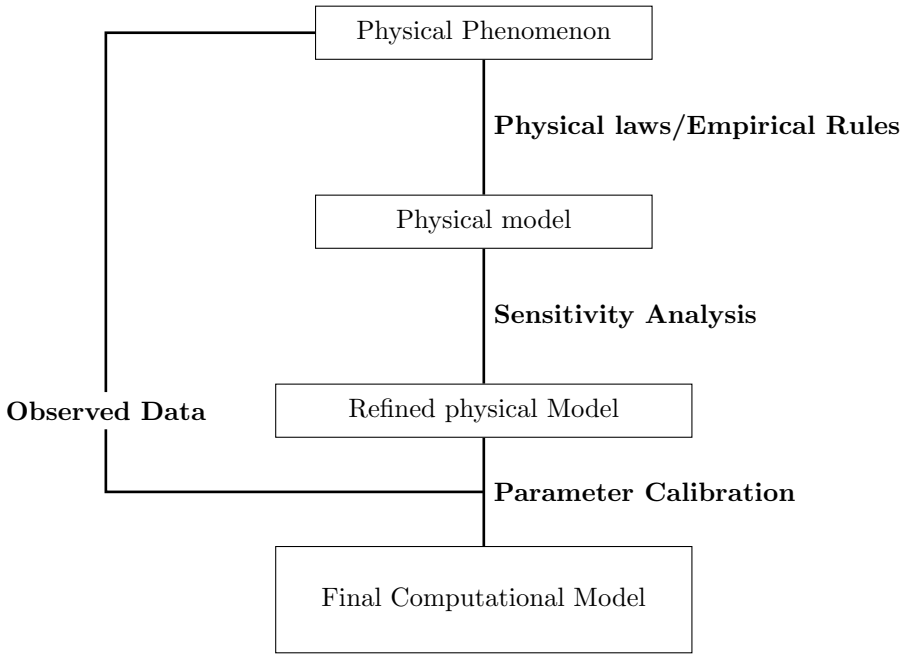

Figure 1.4: Modeling approach with calibration.

The different steps in our approach are :

- Identify the computational code parameters which are the most influential on the degradation of the PV plants.
- Calibrating them to observed values, in order to obtain their evolution.
- To overcome the intensive computation the meta-models are build as a surrogates for computational code.

Understanding the degradation related parameter evolution could help reveal the main mechanisms behind photovoltaic degradation.

1.2 Thesis organization and contributions

The thesis presents statistical tools and methods for numerical code calibration and parameter estimation for photovoltaic degradation analysis. The first chapter addresses the motivation and the problems of the thesis together with the literature review on various photovoltaic degradation calculation methodologies and the physical model for photovoltaic devices. It highlights the industrial need for a new method for degradation estimation based on a physical model that could be able to explain the mechanisms behind the degradation.

In the second chapter of the thesis, the Design of Experiments (DOE) is introduced. The motivation for using DOE is to obtain a deeper insight into the model structure. Because running computer models is usually time expensive the motivation is to find the design of experiment which provides maximum information on the model with a minimum number of code calls. A mathematical criterion needs to be defined which quantifies that the points of the input parameter space are well spread and are covering all the possible realizations of the computer code. For the appropriate design, the Latin Hypercube with the maximin design is used as a space-filling design. The method is applied to the EDF numerical code for photovoltaic performance estimation, called PVNOV [68]. The DOE insights are applied for building the meta-model.

The third chapter of the thesis is focusing on the sensitivity analysis performed on various photovoltaic physical models namely the single diode model and the EDF code for photovoltaic performance estimation based on the double diode model (PVNOV). Morris screening and Sobol analysis were applied to identify all the important parameters in both physical models which could be related to the degradation mechanism of the photovoltaic devices. The constraints of the sensitivity analysis were defined based on expert knowledge and available literature. Morris's method was firstly applied on both models to screen the non-influential variables which can be set to their nominal value for the rest of the study. Afterward, the Sobol method was applied to the parameters identified with the Morris method to obtain more granular information about the model parameters. Finally three parameters were identified as the influential ones (on degradation) namely the R_s, R_{sh} and the I_{sc}. These identified parameters will be used in the calibration of the PV performance model.

The fourth chapter focuses on various approaches of building meta-models together with their validation. The advantage of using meta-models or surrogate models is to alleviate the computational burden of expensive or time-consuming code at the cost of adding additional sources of uncertainty.

In order to stay within a limited number of code calls, the issue is to find the right design of experiment as discussed in chapter 2 which provides the maximum amount of information out of the original model.

Polynomial chaos expansion (PCE) was built as a surrogate for our time-consuming code. PCE surrogates the model with the series of orthonormal polynomials in the input variables, where the selected polynomials are in coherence with the probability distribution of the input variable.

The meta-model needs to be validated before we can use them as a replacement for the initial models. Cross-validation was applied and the meta-model error was calculated. The validation method is based on comparing the model prediction on simulation points that were not used in the meta-model's fitting process. An example of a PCE meta-model is presented. To compare the meta-model accuracy various sample sizes of LHS were used where, in general, more sample points give more information but at a higher expense of code calls.

The coefficient of determination was calculated and it shows good accordance between model

and meta-model. In the end, calibration on the meta-model was performed were the structural identifiability of the model vs meta-model was compared. The results show that the meta-model can be used as an equivalent replacement for the computational code without sacrifying accuracy.

In the fifth chapter, the model calibration is presented. Various optimization and calibration approaches are presented together with their strengths and drawbacks. The CMA-ES evolutionary algorithm is applied to the data from the EDF test site where the IV-curves of individual modules are available. Single diode model parameter evolution was estimated from 8 years of outdoor IV curve measurements under a range of operating conditions, all of this without translating to Standard Test Conditions (STC). The IV curves were selected in a narrow window of outdoor temperature and irradiance conditions.

The results show that the main aging factor is the decrease of short-circuit current and the increase of series resistance. Possible degradation modes affecting the analyzed module are yellowing and browning of Ethylene-vinyl acetate (EVA), delamination, and appearance of bubbles or anti-reflecting coating degradation. An increase in series resistance suggests that there is possible corrosion on metal bars or inter connectors in PV module. In the presented method the short circuit current I_{sc} and the series resistance R_s are time-dependent variables presenting the aging process of materials over time, thereby the I-V characteristics are not only a function of irradiation G and cell temperature T, but also a function of time t.

Because IV curves are rarely available from power plants the other part of the chapter is focused on calibration in the cases where the only available data is the measured power and the corresponding weather file. Before the calibration process, the parameter bounds need to be defined so that the interpretation of calibration results is physically meaningfully. The calibration on the outdoor data shows that the calibration is not converging because the parameter values are reaching their boundaries.

The structural identifiability of the code was tested with varying number of model parameters. The structural identifiability is a property of the model that ensures that the model parameter can be uniquely determined. The structural inevitability test was performed with two different sets of parameters. In the first case with parameters nDs, $R_s(\Omega)$, $R_{sh}(\Omega)$, Ms, $I_{sc}(A)$ and A_r the model is unidentifiable with the CMA-ES approach. The parameter values are not stabilizing even after 2000 function evaluations. The possible explanation is the over-parametrization of the model. When reducing the number of parameters to 3, the model becomes fully identifiable. One of the possible issues of the calibration procedure is the initial parameter constraints. The parameter bounds are defined with the physical meaning while in the calibration procedure they are reaching the bounds defined. Because the calibration is performed on noisy data, the increased discrepancy between the simulated and measured data is causing convergence issues.

The Approximate Bayesian Computation is presented which is more robust on measurement noise and does not require the specification of a likelihood function, and can be used to estimate posterior distributions of parameters for simulation-based models. The ABC avoids the direct evaluation of the likelihood function and approximates it with generated synthetic data from model simulations.

The calibration on the meta-model was performed to avoid the computational burden of time expensive code and to compare the calibration results obtained from both meta-model and full model.

In the sixth chapter, the paper is attached to the signatures of degradation mechanisms from fielded photovoltaic system monitoring data. Where all the steps presented in the manuscript

were applied all together. The EDF PV performance model is applied to calibrate outdoor power measurements and identify the physical parameter evolution with the ABC method, which is approximated with a PCE meta-model.

First, our algorithm has been validated on simulated synthetic data (Digital Power Plant) with added Gaussian noise, discrepancy and a prescribed parameter degradation evolution. The results on the synthetic data show that the evolution of the parameter can be estimated in noisy measurement conditions.

Then, our method is applied on the 8 years of outdoor power measurements (Eurac test facility) where the results show that the power decline of the fielded modules can be attributed to the decline in short circuit current I_{sc} while the parameters R_s and R_{sh} do not show any significant changes over the period of 8 years.

The seventh chapter is the discussion and perspectives of the thesis where the possible improvements and next steps are discussed.

1.3 Degradation of Photovoltaic Devices

Degradation of Photovoltaic (PV) modules is inevitable regardless of the module technology or meteorological exposure. The PV plant lifetime is mainly determined by the module design, manufacturing flaws and stability and resistance of PV modules to different external loads. These loads are closely related to differences in meteorological exposure depending on the location of the installation and are affecting various module technologies differently.

Depending on the chosen technology and its geographic location the degradation rates and prevailing degradation mechanisms will be different, where certain degradation modes are more severe under specific climatic conditions [44].

There are several degradation rate calculation methodologies which are based on various statistical approaches [44], [54]. The overall goal of the statistical methods is to calculate the trend of the PV performance time-series and to translate the slope of the trend to an annual Performance Loss Rate (PLR) in %/year [71]. The models available are trying to obtain performance data while taking into account the dependencies between the PV system output and measured meteorological data (irradiation, temperature, wind speed etc.). Two widely used models are the Performance Ratio (PR) and Photovoltaics for Utility Scale Applications (PVUSA) models [64], [17].

To compare the performance of different PV technologies in different climates the normalized metrics needs to be applied. Here the PV performance data is normalized to comparable unit free metrics or corrected in respect to outdoor conditions. The most frequently used performance metrics is the PR which is an indicator for the quality of PV installation.

PR is defined in the standard IEC 61724 [17] and calculated by dividing the final yield of a PV plant $Y_{f(a)}$ with the reference yield Y_{ref}. The PR is a ratio of measured values of power and irradiance with values obtained under STC. Where the STC conditions are defined as: Solar irradiation in plane of array: $G_{POA} = 1000W/m^2$, ambient temperature: $T_{AM} = 25\ °C$ and air mass $AM = 1.5$

PR

$$PR = \frac{Y_f}{Y_{ref}} = \frac{P_{AC}/P_{STC}}{G_{POA}/G_{STC}} \tag{1.1}$$

The PVUSA (Photovoltaic for utility scale application) [64] performance method is based on collecting solar, meteorological, and system power output data for a period of time, and regressing the system output against a combination of irradiance, wind speed, and ambient temperature. To calculate the P_{mpp} the following equation is used:

PVUSA

$$P_{mpp} = G_{POA}(a + b \times G_{POA} + c \times W + d \times T_{am}) \tag{1.2}$$

Where $G_{POA} = 1000W/m^2$, $T_{AM} = 20\ °C$ and wind speed $W = 1m/s$. Measurements at high irradiance values ($G \geq 800W/m^2$) in the plane of array Plane Of Array (POA) are selected and fitted to calculate monthly values for the coefficients a, b, c, d applying multivariate regression.

Example of the PVUSA methodology applied on a single CdTe module. The model is based on the linear correlation between the power of the panel and its meteorological values. The Figure 1.5 shows the Pearson correlation between the power, plane of array irradiance, module temperature, wind speed and ambient temperature. It can be seen that the correlation is the highest between irradiance and power (0.988) followed by correlation between power and module temperature (0.829).

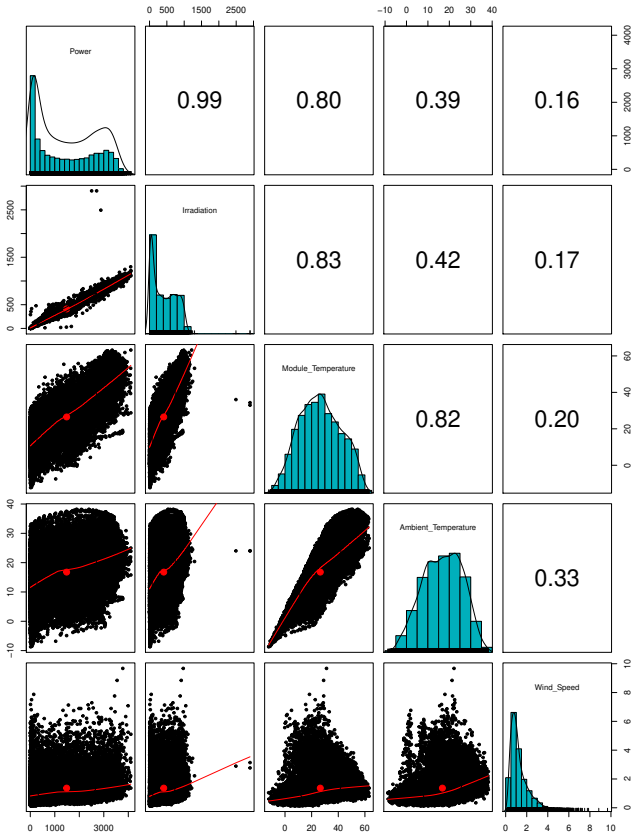

Figure 1.5: Pearson correlation factor between the power and the weather data as observed on EDF PV test zone data.

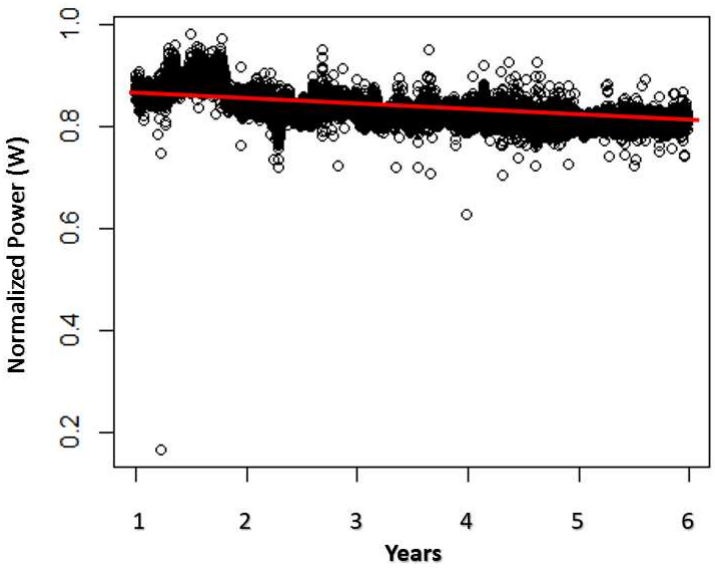

Figure 1.6: PVUSA methodology applied on CdTe modules.

Example of an PV module degradation estimation on CdTe module with a linear fit using standard least square (Figure 1.6). The red line corresponds to the overall degradation rate. Dividing the overall degradation rate with the number of analysed years we get 1.3568±0.00251% average degradation per year of exposure.

Comparison of the published degradation rates obtained with PR and PVUSA showed similar results for different technologies [59]. Some studies have shown different degradation rates by applying temperature correction and different averaged time [58].

The 6-k-values performance model describes system performance through the relative efficiency P_{REL} correlated to STC as a function of in-plane irradiance $G^{'}$ and module temperature T_{mod} [34].

6-k Model

$$P_{REL}(G^{'},T^{'}) = 1 + k_1 \ln(G^{'}) + k_2 \ln(G^{'})^2 + k_3 T^{'} + k_4 T^{'} \ln(G^{'}) + k_5 T^{'} \ln(G^{'}) + k_6 T^{'2} \quad (1.3)$$

The normalized irradiance and module temperature are given by:

$$G^{'} = G/G_{STC} \quad (1.4)$$

$$T^{'} = T_{mod} - T_{STC} \quad (1.5)$$

The equation (1.3) needs to be fitted to experimental data (from indoor or outdoor measurements) to obtain the empirical coefficients $k_1 - k_6$. The fit is can be done by a least-square procedure.

The coefficients $k_1, \ldots, k_6$ are calculated using data from different modules of the same PV technology. The fitted coefficients are used to calculate the relative efficiency like the ratio of the

module efficiency under given conditions of irradiance and temperature to the efficiency at STC conditions.

These methods have the advantage of calculating the real-time efficiency of the PV plant without disconnecting or interrupting the operation of PV plant. The drawback of the methods is that the information about underlying degradation mechanisms and pathways is missing.

On the other hand, methods that require the interruption of PV modules are often complicated and costly to perform but provide insights on the specific degradation modes. Typically applied methods are IV curves fitting, imaging techniques, material characterization techniques, and physical models.

Fitting the IV curves to the single or double diode model and then interpreting the extracted circuit parameters can be used to interpret the efficiency loss to the increased series or shunt resistance [32]. The Loss Factor Model (LFM) [86], [85] has been developed to fit measured IV curves to not only predict the energy yield but also estimate the root causes of observed degradation and seasonal variation with a physical meaning. The model is based on the set of normalized parameters that describe each IV curve and a set of fitting coefficients that describe how these parameters vary. The LFM allows PV modules of any technology to be characterized by six normalized, independent and physically significant coefficients plus correction factors for module temperature and spectral miss-match. The normalized coefficients are calculated from outdoor measured IV curves and from reference parameters as for example indoor flash measurements at standard test conditions STC. The loss factor model can be used to estimate the energy losses due to the shunt and series resistance variation.

Infrared (IR) and Electroluminescence (EL) imaging techniques can be used to identify faults and failures developing with PV modules. A great number of failures developed on PV modules can be detected using IR imaging, from hot-spots to mismatch losses or installation failures.

The sample Figure 1.7 shows an PV module with overheated cells. These cells are overheated due to failures in the cell and module manufacturing process. Some examples for failures during these production processes are inaccurate cell sorting, local short circuits within the solar cell or an insufficient electrical contact. Most of the overheated cells derive from internal cell problems [38].

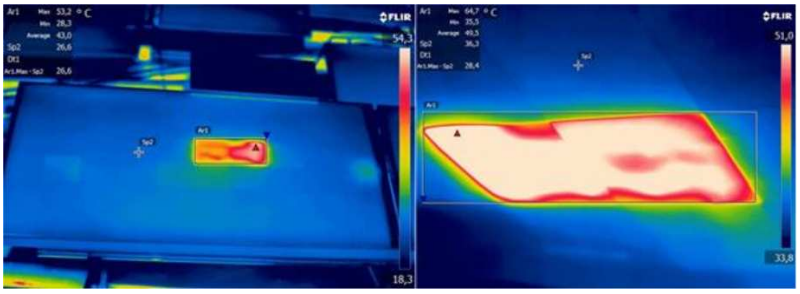

Figure 1.7: On the left side front view and on the right hand side rear side view of a PV module with overheated cell caused by internal cell problems [38].

EL imaging can be used to detect cell-fracture, deficient solder joints, short-circuited cell and bypassed sub-strings (Figure 1.8). Currently, drones and machine learning techniques are being used for automated image processing obtained from EL.

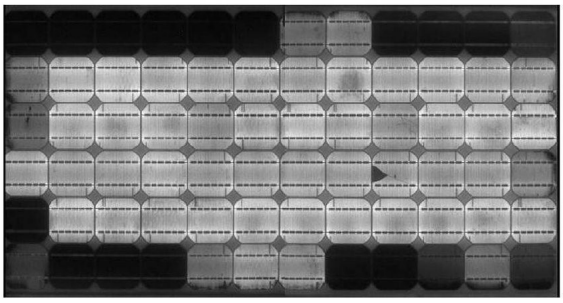

Figure 1.8: EL of PID affected module.

Material characterization methods can be used for finding the fundamental mechanisms behind PV degradation (sodium migration of potential-induced degradation PID [57]) but usually, they imply destructive testing. The physical models are trying to model the complex processes happening in the PV modules where several variables are interacting to produce a specific degradation mode. The drawbacks of the models are based on the limited understanding of all underlying processes and they are still only heuristic models, which do not include the influence of material parameters.

Machine learning techniques can be used to classify anomalous behavior in the IV curves data from the fielded PV modules/plants. Those models are trying to combine both data coming from the monitoring sites with the physical understanding of degradation.

Machine learning techniques can be utilized to classify and find anomalous behavior in the data, such as IV curves under short-circuited bypass diodes. Peshek et al. [69] used automated analytic of IV curves based on non parametric regression approach of local polynomial regression. In a population of IV curves acquired from time-series study the majority of curves are typical in shape and may fit the simplistic single diode model. The emphasis of the automated anomaly detection of I-V curves is to identify unusual curves exhibiting change points or inflection points. The focus of the approach is anomaly detection, and is not intended to analyze and fit the IV curves to the single diode model.

New techniques of modeling solar cell behavior have been developed that are largely data-driven and less restricted to the physics-based diode models. They benefit from progress in machine learning and statistical methods.

The Suns-Vmp method [93] monitors and diagnoses time-dependent degradation of solar modules by using real-time field data of power P_{mpp}, current I_{mpp} and voltage V_{mpp} at maximum power point to identify various degradation pathways. The Suns-Vmp algorithm pre-processes P_{mpp} data to reconstruct the IV characteristics synthetically based on irradiation variations in a certain period (couple of days) with Double Diode Model (DDM). The initial double diode circuit parameters are extracted in various operating conditions (irradiation and temperature) by using the data sheet values of the analyzed modules. With the initial guesses the possibility of the multiple solutions is eliminated. Synthetic IV curves are constructed by sampling P_{mpp} data over a given period (2-3 days). The natural variation of the G_{POA} and the cell/module temperature T_{mod} allows to track the changing I_{mpp} and V_{mpp}. The algorithm steps are summarized in Figure 1.9

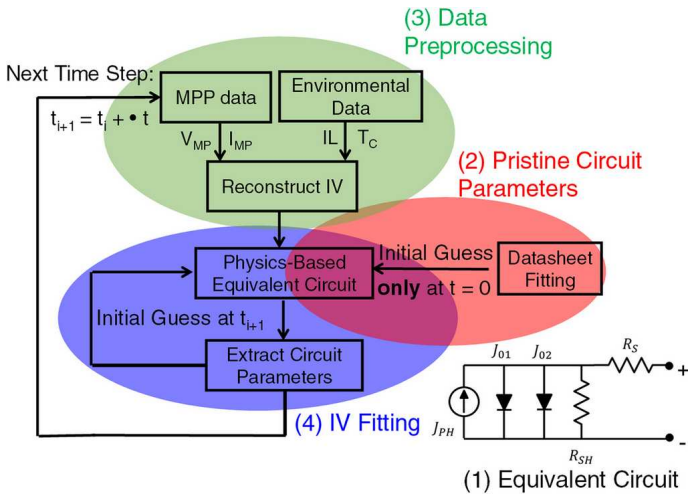

Figure 1.9: The flow chart of the Suns-Vmp method. Degradation mechanism will affect the circuit parameters [93].

With the G_{POA}, T_c, I_{mp}, V_{mp} the IV curves are reconstructed and calibrated to the measured P_{mpp}. After reconstructing P_{mpp} IV curves the double diode parameters are estimated with non-linear least-squares.

The results on the real data from National Renewable Energy Laboratory (NREL) site show the degradation of Fill factor while the V_{oc} and I_{sc} degradation are insignificant. The decrease of fill factor is assigned to rapid increase of series resistance.

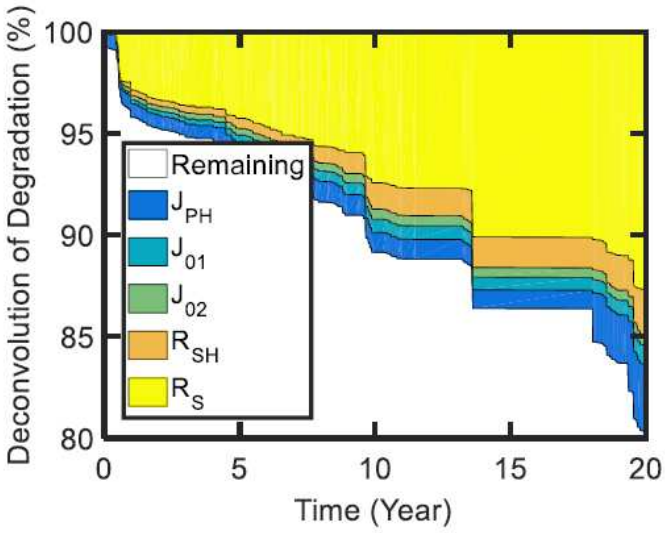

Figure 1.10: Temporal degradation deconvolution with respect to circuit parameters [93].

The Figure 1.10 shows the evolution of series resistance as the dominant contributor to efficiency reductions. The inspection shows that localized hot spots caused solder bond failure and eventually step wise increase of series resistance. Around 4% of power loss can be attributed to the reduction of J_{PH} caused by discoloration. The photo current reduction because of discoloration has occurred within the first year of installation.

The drawback of the method is that both current at maximum power point (I_{mpp}), and voltage at maximum power point (V_{mpp}) data is needed to reconstruct the full IV curves and extract the parameters in various operating conditions. Compared with the full IV outdoor measurements the mean absolute percentage error is less than 4 %.

1.4 Discussion

Combination of presented models and approaches into a hybrid one could allow monitoring and diagnosis of PV system reliability in real time by systematically analyzing the data coming from the monitored sites. Unfortunately using the statistical online methods it is not possible to determine which degradation mode occurs on the basis of calculated PLR's. The variation of P_{mpp} and FF over time is related to relative performance loss while the physical parameters of the PV diode models are more closely linked to the fundamental mechanisms of degradation. Because usually only limited data from PV plants is available (P_{mpp}) the challenge is how to diagnose possible failures and make reasonable PV life predictions using only P_{mpp} data. Using the physics based models parameter evolution could allow identifying failure modes and help build forecast models for their future evolution.

On the PV cell level the main mechanisms behind performance loss and possible failure are corrosion, LID, LeTiD (Light and elevated Temperature Induced Degradation), contact stability and cracked cells. At the module level degradation occurs due to the reliability issues on the cell level and because additional issues like glass breakage, delamination, bus bar failure, broken inter connector, front surface discoloration, moisture ingress, reduced inter layer adhesion, diode failures and hot-spots [71].

The studies on the crystalline silicon (c-Si) reports that the power degradation was mainly due to the short circuit current losses, followed by a smaller decrease in the fill factor [81]. The I_{sc} degradation is commonly caused by discoloration and delamination [73]. According to the studies of NREL the degradation and associated I_{sc} decline is associated with the ultraviolet (UV) light absorption at or near of the top of the silicon surface, which causes discoloration [66].

1.5 The physics of photovoltaics

A solar cell is basically a $p-n$ junction diode which utilizes the photovoltaic effect to convert light energy into electrical energy. The PV cell is constructed of a very thin layer of $n-type$ semiconductor which is grown on a thicker $p-type$ semiconductor. On the top of the $n-type$ semiconductor layer fine electrodes are installed which do not obstruct light to reach the thin $n-type$ layer. Below the $p-type$ layer there is a $p-n$ junction and at the bottom of the $p-type$ layer a current collecting electrode is installed. The whole assembly is encapsulated by thin glass to protect the solar cell (Figure 1.11).

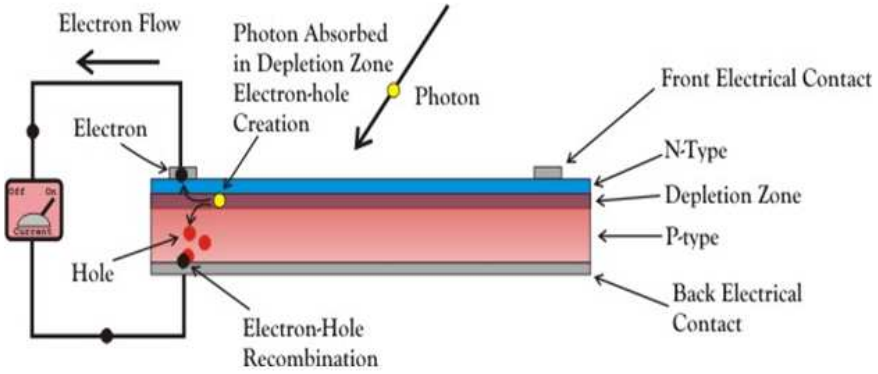

Figure 1.11: Solar cell schematics [14].

When light reaches the $p-n$ junction, the light photons can easily enter in the junction, through

the very thin $p-type$ layer. The light energy in the form of photons, supplies sufficient energy to the junction to create a number of electron hole pairs. The incident light breaks the thermal equilibrium condition for the junction. The free electrons in the depletion region can quickly come to the $n-type$ side of junction. Similarly the holes in depletion zone can quickly come to the $p-type$ side of the junction. Once the newly created free electrons come to the $n-type$ side they cannot further cross the junction because of the barrier potential of the junction. Because of the barrier potential of the junction the newly created holes once come to the $p-type$ side cannot cross. As the concentration of electrons becomes higher on the $n-type$ side of the junction and concentration of holes becomes higher in another side the $p-type$ side of the junction will behave as a battery cell. A voltage is set up which is known as a photo voltage (photo-current). If we connect a small load across the junction there will be a current flowing through it, the photocurrent.

Conventional PV cells operates as a diode. A diode allows current to flow in one forward direction but not in the reverse direction. To study the behaviour of PV cells IV curves (Current-Voltage) curves are used to define the PV cell/module operation within electrical circuit in various conditions. IV curves are used as a tool to determine the basic parameters of a PV cell and mathematically model its behaviour within the electrical circuit.

In the literature there are many different models available to express the physical behavior of solar cell/module under real outdoor conditions. Most commonly these models use a single diode model which is characterized by five unknown parameters or double diode model with 7 unknown parameters. The Figure 1.12 shows the IV curve of solar cell under defined temperature and irradiance conditions. The red curve (IV curve) shows the relationship between the voltage applied across an PV cell and the current flowing through it. The corresponding maximum power point (M_{pp}) is shown on the I-V curve. Loading the PV module such that the current is at maximum power point (I_{mpp}) and voltage is in maximum power point (V_{mpp}) will operate the PV module at the maximum power point (M_{pp}) and result in the maximum power generation. The power vs voltage curve (black curve) shows the point at which the power is a maximum (P_{max}) or power at maximum power point (P_{mpp}).

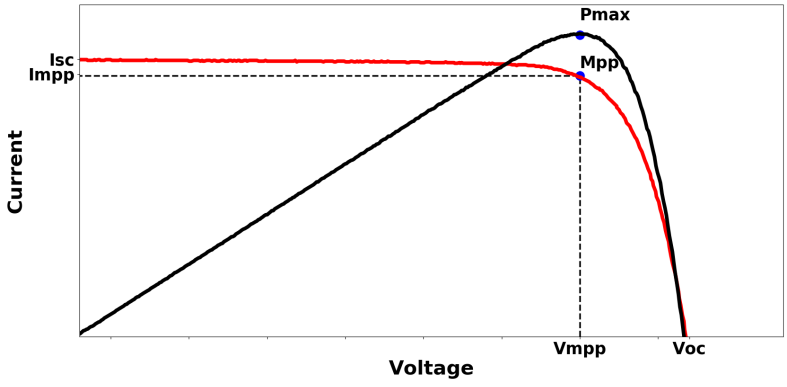

Figure 1.12: IV-Curve of a solar cell.

The degradation of the PV performance over lifetime is usually determined within the decrease of P_{mpp} (nominal power) and Fill Factor (FF) where both of the parameters are steadily decreasing. Fill factor is a measure of quality of the solar cell.

Fill Factor

$$FF = \frac{P_{max}}{P_T} = \frac{I_{mpp} \times V_{mpp}}{I_{sc} \times V_{oc}} \tag{1.6}$$

It is calculated by comparing the maximum power to the theoretical power P_T that would be the output at both the open circuit voltage V_{oc} and short circuit current together I_{sc}. The temporal evolution of the physical models parameters and the corresponding IV curves (if available) are much more linked to the fundamental mechanisms related to the degradation phenomena and could provide more insights on the PV degradation.

The Task 13 in the PVPS program of the IEA catalogued a collection of different IV curves related to the specific degradation modes and failures. The selection of the IV curves in blue color (Figure 1.13) indicated different features associated with different degradation mechanisms.

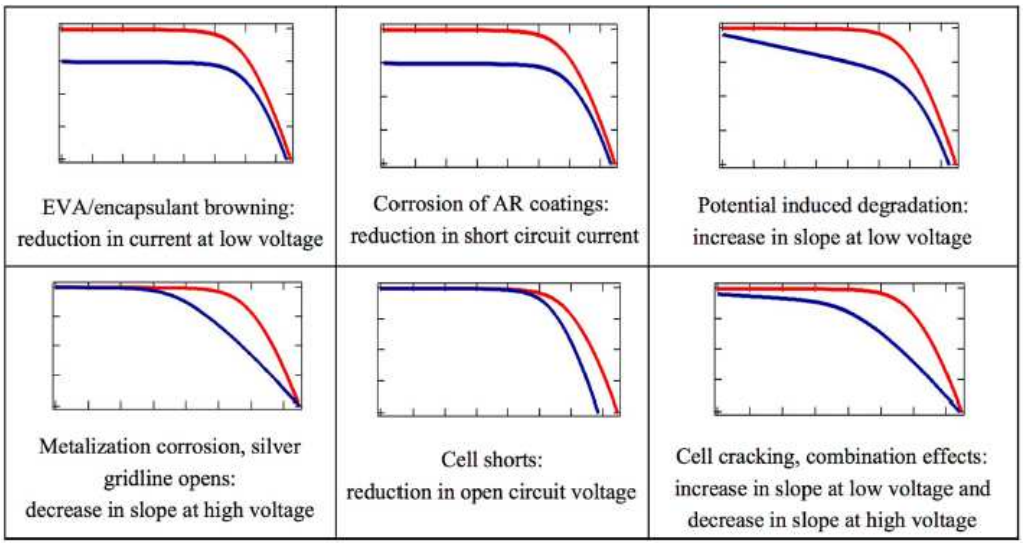

Figure 1.13: IV-Curve degradation. The red curve depicts the initial IV curve while the blue curve shows the degraded IV curve [50].

From the Figure 1.13 we can distinguish 4 failure signatures:

- Loss of I_{sc}
- Loss of R_{sh}
- Increase R_s
- Loss of V_{oc}

1.6 Physical models

Several numerical codes, based on the physical model have been developed to mimic the PV cell behaviour. In this section two models will be presented, firstly the simple one (single diode model) and the model developed by EDF based on the double diode model. What differentiates between them is their level of accuracy and complexity. Advanced PV models have additional constrains and parameters to model the behaviour of PV cells in various conditions and with various technologies.

1.6.1 Single Diode Model

For simplicity many researchers study the behavior of the Single Diode Model (SDM). From a modeling perspective, the accuracy achieved by the single diode model is often viewed as being adequate and it has good success reproducing the IV curve of the single cell. It is confirmed that this model provides an accurate prediction of an outdoor measurements especially for mono-c-Si and multi-c-Si technologies. Equivalent circuit models define the entire IV curve of a cell, module or array as a continuous function for a given set of operating conditions (Figure 1.14).

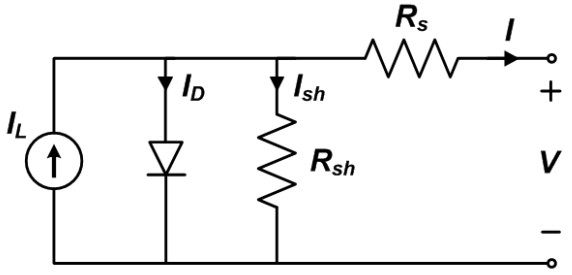

Figure 1.14: Single Diode Model Circuit.

The governing equation for circuit is formulated using Kirchhoff's current law for current I:

$$I = I_L - I_D - I_{sh} \tag{1.7}$$

The I_L represents the photocurrent in the cell, I_D represents the voltage-dependent current lost to recombination and I_{sh} represents the current lost due to shunt resistances. In this single diode model, I_D is modeled using the Shockley equation for an ideal diode:

$$I_D = I_0 \Big[\exp\Big(\frac{V + IR_s}{nV_T}\Big) - 1 \Big] \tag{1.8}$$

where n is the diode ideality factor, I_0 is the saturation current and the V_T is the thermal voltage given by:

$$V_T = \frac{Ns \times kT_c}{q} \tag{1.9}$$

where k is the Boltzmann's constant ($1.381 \times 10^{-23} J/K$), q the elementary charge ($1.602 \times 10^{-19} C$), N_s is the number of cells in series and T_c is the PV cell temperature. Writing the shunt current as $I_{sh} = (V + I \times R_s)/R_{sh}$ and combining this and the above equations results in the complete governing equation for the single diode model:

Single Diode Model

$$I = I_L - I_0 \exp\left(\frac{V + IR_S}{nV_T} - 1\right) - \frac{V + IR_S}{R_{sh}}. \tag{1.10}$$

The equivalent circuit of a practical PV cell. In literature it is also called as a five parameter model (I_L, I_0, R_s, R_{sh}, n). It takes into account different properties of solar cell. A single diode model is formulated by extending the ideal diode law to account for parasitic series and shunt resistances, and by adding auxiliary equations that describe how model parameters vary with irradiance and

cell temperature. The reference values are set on standard test conditions (STC) $G = 1000W/m^2$ and $T = 25°C$.

The five parameters are primary to all single diode equivalent circuit models:

- I_L light current (A),
- I_0 diode reverse saturation current (A),
- R_s series resistance (Ω),
- R_{sh} shunt resistance (Ω),
- n diode ideality factor (-),

The single diode model is characterized by 5 unknown parameters I_L (light or photo generated current) represents the charge carrier generation in the semiconductor layer of the PV cell caused by the incident irradiation ; I_0 diode reverse bias saturation current; R_s (series resistance) represents the internal losses due to current flow and the connection between cells; R_{sh} (parallel or shunt resistance) expresses the loses due to the high-current path through the semiconductor throughout the mechanical defects and the leakage current to the ground. The diode ideality factor n measures how closely the diode follows the ideal diode equation.

Having an explicit expression of I as a function of V is intractable regarding Equation (1.10). To solve the equation current can be expressed as a function of voltage $I = I(V)$ or voltage as a function of current $V = V(I)$ by using the transcendental Lambert's W-function [70]. Lambert W function is the solution $W(x)$ of the equation $x = W(x)\exp[W(x)]$. Using the function we may write $I = I(V)$. The principal branch of Lambert W function (W_0) is used in these calculations since the argument to W and the results are a positive real value. Defining the following parameter z is necessary to transform the single diode equation into a form that can be expressed as a Lambert W-function.

$$z = \frac{R_s I_0}{nV_T(1+\frac{R_s}{R_{sh}})}\exp\left(\frac{R_s(I_L+I_0+V)}{nV_T(1+\frac{R_s}{R_{sh}})}\right) \tag{1.11}$$

Then the module current can be solved using the Lambert W-function, $W(z)$ as [39]:

$$I = \frac{I_L + I_0 - \frac{V}{R_{sh}}}{1+\frac{R_s}{R_{sh}}} - \frac{nV_T}{R_s}W(z) \tag{1.12}$$

Lambert W function can be efficiently evaluated with high precision and the Equation (1.12) can be directly implemented for most of the range of an IV curve. However for equation (1.12) approaching V_{oc} (current I becomes small) numerical overflow can become a problem.

1.6.2 Double Diode Model

In the single diode model the ideality factor n of the diode is set on the constant value. In reality the ideality factor is a function of voltage across the device. At high voltage when the recombination in the device is dominated by the surfaces and the bulk regions the ideality factor is close to one. However at low voltage's, recombination in the junction dominates and the ideality factor approaches two. Double diode model (Figure 1.15) allows to model junction recombination by adding a second diode in parallel with the first and setting the ideality factor typically to two [24].

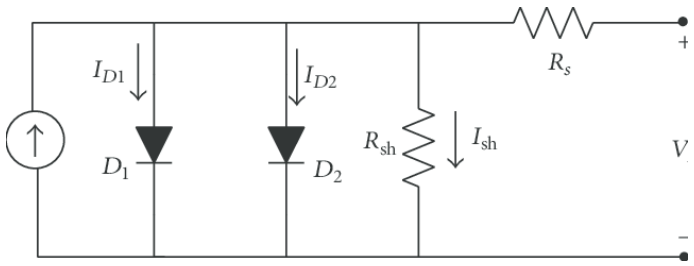

Figure 1.15: Double Diode Model Circuit.

Double Diode Model

$$I = I_L - I_{0_1} \exp\left(\frac{V + IR_s}{n_1 V_T} - 1\right) - I_{0_2} \exp\left(\frac{V + IR_s}{n_2 V_T} - 1\right) - \frac{V - R_s I}{R_{sh}} \tag{1.13}$$

- I_L light current (A),
- $I_{0_{1,2}}$ diode reverse saturation current (A) of diodes D_1 and D_2,
- R_s series resistance (Ohm),
- R_{sh} shunt resistance (Ohm),
- $n_{1,2}$ diode ideality factors of diodes D_1 and D_2,

Newton Raphson's iterative method is used to determine the parameter of the double diode model. The Newton Raphson Method is an iterative method for root finding. The method consist in an estimate of a given function $f(x)$ with an initial value x_0 which is the initial guess for the root. The function is rewritten using a Taylor series expansion in $(x - x_0)$ in the neighbourhood of x_0.

$$f(x) = f(x_0) + f^{'}(x_0)(x - x_0) + 1/2\, f^{''}(x_0)(x - x_0)^2 + r(x) \tag{1.14}$$

where $f^{'}(x)$ denotes the first derivative of $f(x)$ with respect to x, $f^{"}(x)$ is the second derivative, and the $r(x)$ is the reminder. Suppose the initial guess is very close to the real root of the equation. Then $(x - x_0)$ is small, and only first few terms in the series are important to get an estimate of the true root, given x_0. By truncating the series at the second term, we obtain the Newton-Raphson iteration formula [74].

$$x_{n+1} = x_n - \frac{f(x_n)}{f^{'}(x_n)} \tag{1.15}$$

In words, given the current estimate, x_n, the point $x_{(n+1)}$ is obtained by intersecting the tangent line of $f(x)$ in x_n with the x axis.

Compared to the single diode model, the double diode model can distinguish between recombination current in the quasi-neural vs space-charge regions, denoted by n_1 and n_2. The double diode model allows to identify more precisely various degradation mechanisms.

1.7 Numerical codes for simulating PV performance

To mimic the behaviour of photovoltaic power plants computational codes have been developed which intends to be as close as possible to the physical system. The physical model is only a

simplified representation of the real PV performance and may not take into account the existing influential variables and also depends on the uncertain physical constants in the model.

EDF's existing PV performance model written with the Modelica language allows to model the electrical behaviour of any PV device under given meteorological conditions [68]. There are 385 input parameters and variables for 3 different input groups for PV modeling. The variables represent the meteorological data while the parameters include those values which have an electrical meaning. Main parameter/variables groups for PV Modeling are:

- **Variables representing the meteorological file** (direct, diffuse irradiation, humidity, ambient temperature, wind speed etc.) applied as boundary conditions.
- **Technology related parameters** (heat conductivity, number of layers of PV panel, layers, thickness of PV panel , dirtiness of the panels),
- **Double Diode Model parameters** (17 parameters),

The double diode model parameters as defined in Dymola.

- **Np** Number of parallel cell chains,
- **Ns** Number of cells connected in series,
- **Scell** Surface of the cell,
- **Ms** Temperature exponent in saturation current,
- **nDs** Ideality factor of saturation current ,
- **Cs** Recombination ,
- **Mr** Temperature exponent in saturation current,
- **nDr** Ideality factor of saturation diode,
- **Cr** Recombination,
- **Eg** Energy Band-gap (technology dependent),
- **Rsh** Shunt resistance (no temperature and irradiance modeling in Dymola),
- **Rs** Series Resistance (no temperature or irradiance dependent modeling in Dymola),
- **Isc** Short circuit current,
- **Voc** Voltage at open circuit,
- **Alpha** Temperature coefficient of the current,
- **Ar** Transmission factor

Checking the accuracy of the code by confronting it with field experiments is called validation. The computational code depends on two kinds of inputs: variables and parameters.

The inputs variables are set during the field experiments and includes environmental variables that can be measured (i.e. boundary conditions) and model variables that are actually computed during the simulation and can change if parameter values change, where the parameters are generally interpreted as physical constants defining the physical model and they can contain so called tuning parameters which have no physical interpretation.

There are two major sources of uncertainties that could be linked to the physical model. In this context uncertainty relates to possible variations of an input variable and therefore variability within the model and its output.

The first source of uncertainty can come from inherent randomness found in climatic data, this type of variability cannot be controlled or optimized, the second source of variability in the yield estimation is caused by knowledge deficiency. The knowledge deficiency is due to either the uncertainty in the optimum value of input variables or from uncertainty of how the model behaves under alternate variable space regions. EDF experts judge that parameter uncertainty and input variable uncertainty are each responsible for about 4% of the output variability.

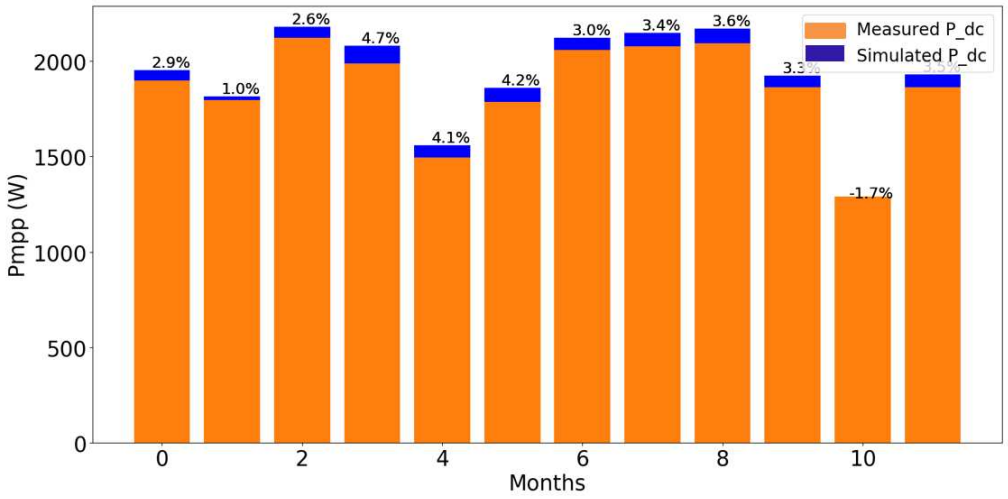

Figure 1.16: Average monthly difference between simulated and measured data in a period of 1 year.

The Figure 1.16 shows the average monthly difference between the measured and simulated data with the nominal parameter values. The simulated data is overestimating the real PV production for approximately 3% in the first year.

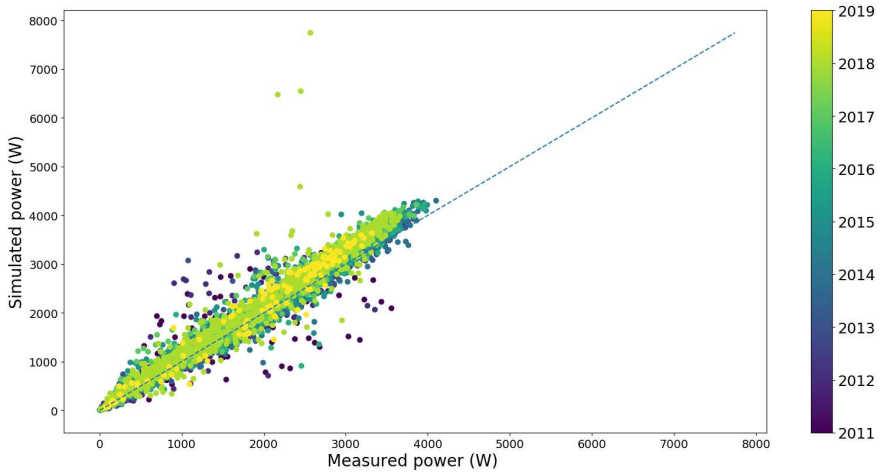

Figure 1.17: Hourly average comparison of simulated vs measured PV production in a period of 8 years.

Example of comparing the simulated vs measured hourly average PV production in a period

of 8 years Figure 1.17. The comparison shows that the model for simulating PV production fits the observed PV production well. The increasing discrepancy over time can be attributed to the degradation of the PV modules.

Chapter 2

Design of Experiments (DOE)

The chapter gives an overview of the various DOE strategies on computational codes. With the DOE the outputs are analysed while changing the input parameters. Latin Hypercube Sampling is presented with various distance designs. The motivation for using various DOE approaches is to get a best possible representation of the computer code with the smallest possible code calls. At the end an example of design of experiments on the EDF numerical code for simulating photovoltaic performance is presented.

Contents

2.1 Design of Experiments

In a computer experiment, observations are made on a response function by running a complex computer model at various choices of input variables. For any selection of input parameters (within the physical boundaries) and output $X = (x_1, \ldots, x_K)$ vector $Y = f(X)$ is produced by the computer code. For any condition of X we can perform an experiment and observe the output of the computer code. Because running computer models is usually time expensive the motivation is to estimate the relationship between the parameter inputs and the outputs of a model with a moderate numbers of runs.

The objective is to find the design of experiment which provides maximum information on the model with minimum numbers of code calls. In this context it is important to define a mathematical criteria which specifies that the points in the input parameter space are well spread.

Design of experiments techniques are widely applied in various simulation fields to minimize the computational expense of running such simulations. In the cases where the computer code is time consuming it is important to choose a sampling scheme that allows to have a good representation of the computer code with the smallest possible code calls. The classical experimental design methods tend to spread the sample points around the boundaries of the design space and leave only few at the center of the design space.

According to Sacks et. al. [79] and because computer experiments involve mostly systematic errors rather than random ones, a good DOE should fill the design space equally and not only concentrate on boundaries.

According to Sacks the classical approaches of experimental design like blocking, replication and randomization are irrelevant when it comes to deterministic computer experiments and the sample points should be chosen to fill the design space for computer experiments [80]. Simpson confirmed that the classical experimental design can be inefficient for deterministic computer codes and that the experimental design should be space filling [88].

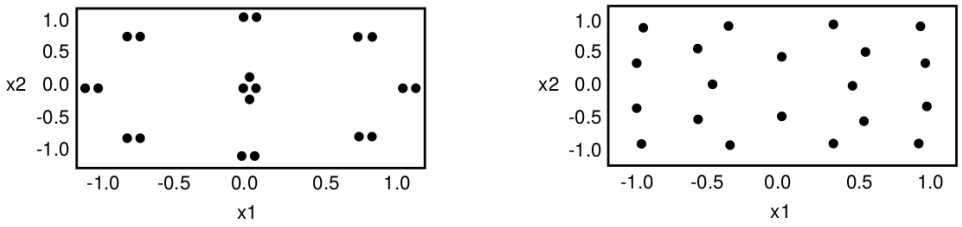

Figure 2.1: "Classical" design vs. "space filling" design [88].

The information desired from the code can be obtained from a study of the probability distribution of the output. Several input variables values of X , $x_1 \dots x_N$ must be selected as successive input sets in order to obtain the desired information concerning Y. In the case when the code is time consuming the N should be selected carefully.

The first idea of sampling is to generate N independent and identically distributed (iid) random variables from the uniform distribution with an identical probability distribution, this approach is called random sampling. Another possibility is to use stratified samples where all samples are sampled from each stratum. The sample space S of X is partitioned into I disjoint strata S_i. Let p=$P(X \in S_i)$ represent the size of S_i and obtaining a random sample $X_{ij}, j = 1 \dots, n_i$ from S_i we have a random sampling over the entire sampling space. McKay introduced an Latin Hypercube Design (LHD) also named Latin Hypercube Sampling (LHS) [60].

2.2 Latin Hypercube Sampling (LHS)

Latin hyper cube was the first type of design proposed specifically for computer experiments [60] and can be viewed as a K-dimensional extension of Latin square sampling. It is a matrix of n rows and k columns where n is the number of levels being examined and k is the number of input variables. Each of the k columns contains the levels $1, 2, \dots, n$, randomly permuted and the k columns are matched at random to form the Latin hyper cube. Latin hyper cubes can have flexible sample sizes from stratified samples, where input variables are sampled at n levels [80].

Let $\underline{x} = (x_1, \dots, x_d)$ be a random vector of input parameters. The Latin Hypercube Sample (LHS) distribute the N sample points where each parameter range is divided into N equal intervals and sample points are selected such that any hyper plane in the dimension contains one and only one sample point. Intervals are sampled without replacement to ensure even distribution of points with respect to each variable (Figure 2.2).

A drawback of Latin hyper cube sampling is that an existing design cannot be extended to higher sample sizes without re-positioning all sample points.

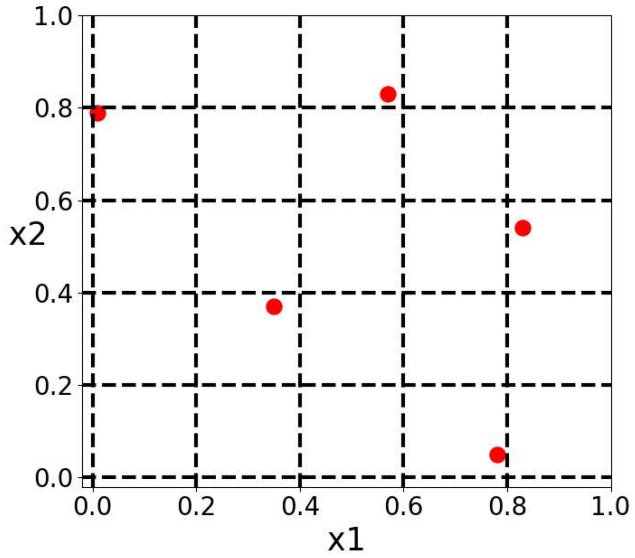

Figure 2.2: Example of 2 dimensional LHS.

When the code is time consuming the Latin Hypercube Sampling (LHS) design can help reducing the computational time while at the same time having a good representation of the parameters input space and of the computational model.

2.2.1 Space filling criteria

The LHS is not necessarily the best design for an exploratory design of experiments. The LHS is build under the assumptions that the input parameters vectors X are independent while following an uniform distribution on $[0,1]^k$. It is possible to perform LHS with a different distribution for X on $[0,1]^k$ but also with dependence between the components of X [90]. Some configurations of LHS do not fill up properly the parameter space. The LHS may consequently perform poorly in prediction of model output/meta-model building.

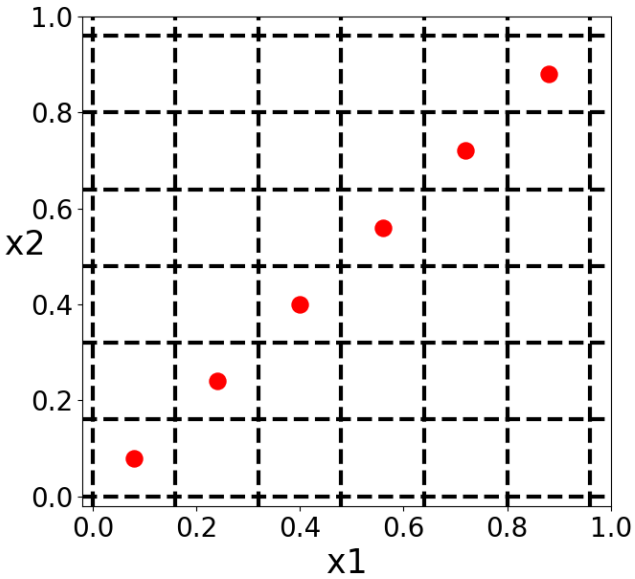

Figure 2.3: "6 points sampled with LHS".

Therefore some authors proposed to improve the LHS not only by improving one-dimensional space filling but also in higher dimensions. One option is to apply some optimality criterion such as entropy, discrepancy, minimax and maximin distances, etc. to avoid situations such as a design where the points are aligned Figure 2.3 [65].

Morris and Mitchell [63] propose maximin distance design found within Latin Hypercube classes because the maximin distance offer a compromise between the entropy/maximin criterion and good projective properties in each dimension. The Figure 2.4 bellow illustrates two maximin design with the Morris and Mitchell approach [63].

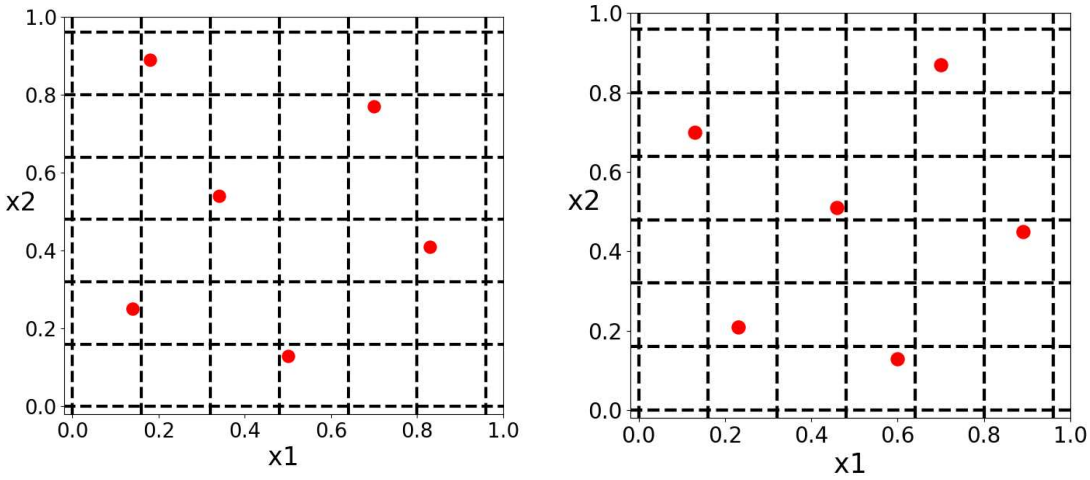

Figure 2.4: Two examples of maximin LHS for 2 parameters.

2.2.2 Minimax distance design

Let $\rho(\cdot,\cdot)$ be a metric such that:

$$\begin{aligned} &\rho(x_1,x_2) = \rho(x_2,x_1) \\ &\rho(x_1,x_2) \geq 0 \\ &\rho(x_1,x_2) = 0 \Leftrightarrow x_1 = x_2 \\ &\rho(x_1,x_2) \leq \rho(x_1,x_3) + \rho(x_3,x_2) \end{aligned} \tag{2.1}$$

Let $\rho(x,\mathcal{D}) = \min_{x_i \in \mathcal{D}} \rho(x,x_i)$ be the minimum distance to the design and let $\chi = [0,1]^p$ and

$$h = \max_{x \in \chi} \rho(x,\mathcal{D})$$

be the maximum distance in χ, the h is called the fill distance and it is the largest gap, the radius of the largest ball that can be placed in χ which does not contain any point in $\mathcal{D}$. To find a $\mathcal{D}$ to minimize h we need to:

$$\min_{\mathcal{D}} \max_{x \in \chi} \rho(x,\mathcal{D}) \tag{2.2}$$

this is called a minimax design and it can be presented as in Figure 2.5. With minimax we want to choose a minimal radius $r > 0$ and the set of centers $x_1 \dots x_n$ so that the design space $\mathcal{D}$ is covered by the union of all the spheres $B(x_i,r), i = 1,\dots,n$. Every point in $\mathcal{D}$ should be close by at least one of the selected points.

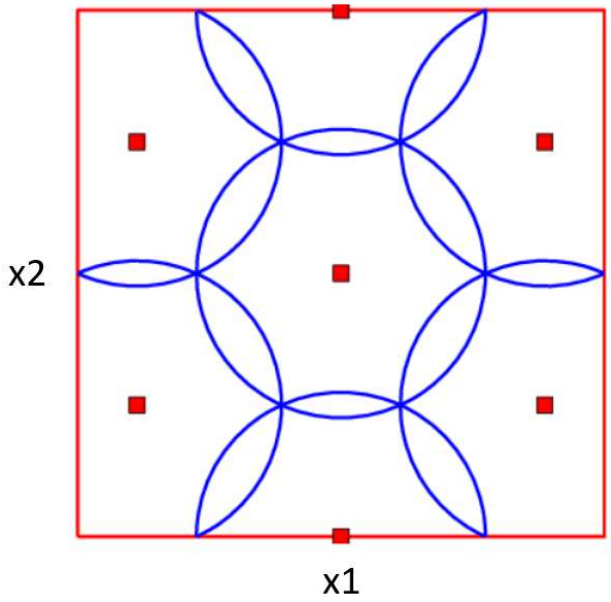

Figure 2.5: Example of minimax optimal design in a square for n=7. The design space $\mathcal{D}$ is covered by the union of all the spheres (blue curves) [72].

2.2.3 Maximin distance design

On the contrary, the maximin distance tries to create a maximum space between the points (Figure 2.6): The minimum distance between any two points in $\mathcal{D}$ is

$$2q = \min_{x_1, x_2 \in \mathcal{D}} \rho(x_1, x_2), \tag{2.3}$$

where q is the separation distance or packing radius- the radius which ensures that the points in $\mathcal{D}$ are as far apart from each other as possible. To find a $\mathcal{D}$ to maximise $2q$:

$$\max_{\mathcal{D}} \min_{x_1, x_2 \in \mathcal{D}} \rho(x_1, x_2). \tag{2.4}$$

The definition of maximin distance designs is very straightforward: because the number of design points is often relatively small with large design space we do not want to evaluate points which are close to each other. The problem is similar to the packing problem where we need to choose a maximal radius $r > 0$ and a set of centers $x_1 \dots x_n$ such that all the spheres $B(x_i, r), i = 1, \dots n$ are pairwise disjoint. The approach is the most well studied among all experimental designs [35].

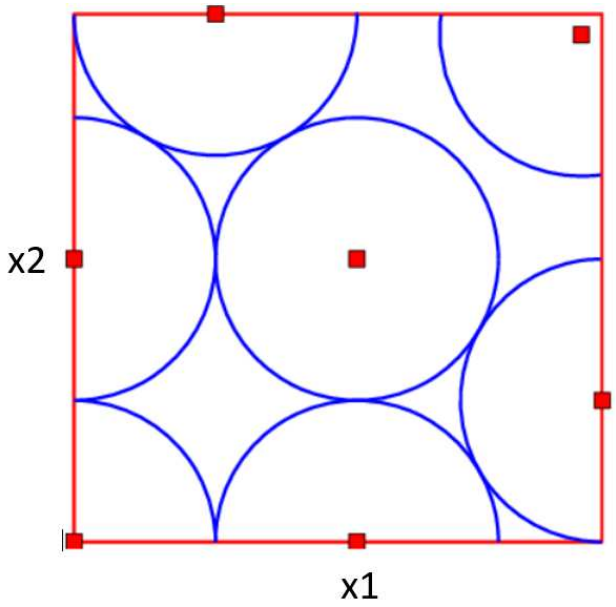

Figure 2.6: Example of maximin optimal design in a square for n=7. The spheres in maximin design are pairwise disjoint (blue curves) [72].

A maximin design tries to create a maximum space between the points and avoid replication. There are several other distance criteria available such as the L^2 discrepancy, the minimum spanning tree (MST) [26] etc. According to [45] the maximin design criterion ensures good space-filling in the full dimensional space.

2.3 DOE example on the Dymola code

The OpenTurns LHS library [6] was used for sampling from the Latin hyper cube. With samples obtained with LHS on 6 parameters (table 2.1). The LHS sampling was chosen because of the good coverage of the whole parameter space with minimal number of simulations. 100 parameter samples obtained from the LHS design were used to simulate the Dymola PV production of 10 PV modules for a period of 1 day in 15 minutes interval. The weather variables for simulation were obtained from the EDF PVZEN experimental site measurements together with the measured PV production for the same day.

Parameters	**Nominal value**	**Bounds**
A_r	0.2	[0.17,0.25]
I_{sc} (A)	5.724	[5.0-6.6]
R_s (Ω)	9e-5	[1e-5,14e-5]
R_{sh} (Ω)	0.1953	[0.014-1.5]
Ms	3	[2.7-3.6]
nDs	1	[0.9-1.2]

Table 2.1: Parameters and their bounds used for LHS sampling

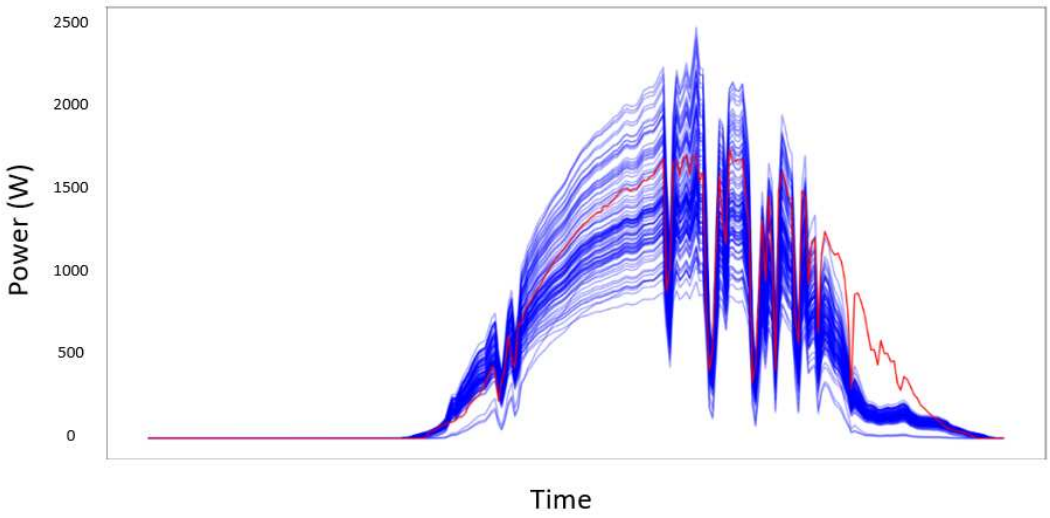

Figure 2.7: The measured daily production in PVZEN depicted in red with 100 realisations of Dymola code with 100 LHS samples in blue.

On the Figure 2.7 it can be seen that the computational code realizations (in blue) are not covering entirely the measured daily PV production (red) at PVZEN. The difference between the simulated and measured PV production is mostly evident at the end of day. The volatility of the PV production corresponds to the clouds passing across the PV modules.

The discrepancy between the model output and the measured data depends on the various factors. Possible explanations are:

- The model input weather file is inaccurate: the PV system is shaded while the pyranometer is still in the sunlight
- There is an issue with the modelled sun position

The spread of the computer code realisations increases with the irradiance values and it is the highest at noon while at the beginning and at the end of the day the obtained samples show less spread.

2.4 Conclusion

In this sections we looked to design of experiments (DOE) that allows to explore a computer model. DOE is used to analyse the response variation of the computer code which allows us to have the maximum information with the minimum code calls.

The presented methods allow to find space filling input parameter sets which will be used in the following chapters related to the meta-model building. Selecting an experimental design is a key step in building an efficient and accurate meta-model. Several criteria exist for the best sampling scheme selection. In the next chapter the DOE for sensitivity analysis is introduced which is based on factorial design and it is focused on the impact of input parameter displacement on the code output.

Chapter 3

Sensitivity Analysis

The chapter give an overview of the Sensitivity Analysis (SA) applied on two different physical models. Two different method are presented: Morris One Step At A Time and the Sobol analysis. The results are compared with the ones available in literature. The aim of this chapter is to give an overview of sensitivity analysis methods and apply them on two models: the simple single diode model and the more complex Dymola model that utilises the double diode model. The results of the sensitivity analysis give valuable insights on the model behaviour and allow to reduce the size of of the parameter vector. The selected parameters will be used for calibration in the following chapter.

Contents

3.1 Sensitivity Analysis

Sensitivity analysis (SA) occasionally termed uncertainty propagation analysis is the study of the relationship between inputs and outputs of a computational model [62].

Uncertainty propagation computes the output law given the input law, whereas SA measures the influence of each input uncertainty on the output uncertainty. The SA has become an crucial element of the development and evaluation of physical models, providing a strong framework for use in the development, operation, calibration, optimization and application of computational models. Given the selection of suitable techniques and frameworks, SA can provide information regarding the model structure, the dependence on input variables, the behaviour of the model at extreme values/events, and can be used as a decision making tool.

Sensitivity Analysis provides a framework and techniques that can identify important variables in the computation model. According to Saltelli [83] before applying a SA the objectives of the analysis needs to be specified clearly. These objectives may include:

- Identify and prioritize the most influential inputs
- Identify non-influential inputs in order to fix them to nominal values
- Map the output behaviour in function of the inputs by focusing on a specific domain of inputs if necessary
- Calibrate some model inputs using some available information (real output observations, constraints, etc.)

In the context of this thesis the sensitivity analysis is focused on the special domain of electrical parameters which could be related to the PV degradation, determination of the non-influential parameters that can be fixed without consequences on the output uncertainty. On the other hand reducing the number of parameters helps to increase the identifiability of the model parameters in the calibration process.

In a SA, model inputs are perturbed within predefined ranges, representing numerous realizations of the physical system. The model response is observed, with the sensitivity to variation of each input variable indicated by the magnitude of change of the response variable. The range of the input variable perturbation is generally the plausible values, often dictated by, but not limited to, the range of uncertainty of the input variable.

3.2 Morris OAT method

Morris method evaluates the influence of each input parameter by considering the impact of its variation on the model output while considering all the other input parameters constant. Each parameter is perturbed at one-step-at-a-time method (OAT) within the defined model parameter space, meaning that in each run only one input parameter is given a new value. The process is repeated until all the model parameters are changed and model outcomes evaluated. For each input parameter, two sensitivity measures are computed μ which assesses the overall influence of the parameter on the output and σ, which estimates the parameter's higher order effects, i.e. non-linear and/or due to interactions with other factors.

With the Morris method we can classify the model inputs in three groups: inputs having negligible effects, inputs having large linear effects without interactions and inputs having large non-linear and or interactions effects.

Trajectory design

Because the range of parameter values are not all of the same order, the sampling design of the Morris method is standardized over the interval $[0, 1]$. Thus for K parameters, the sampling plan will be contained in a hyper cube $[0, 1]^K$. For each parameter, the sampling plan is divided into p levels that divides the model parameter space into a uniform grid of points at which the model can be evaluated. The region of model evaluations is thus a K dimensional p level grid. A sequence of $K + 1$ points, in which each parameter changes only once by a predefined value Δ in $\{0, \frac{1}{p-1}, \frac{2}{p-2}, ..., 1\}$ is called a trajectory (Figure 3.1).

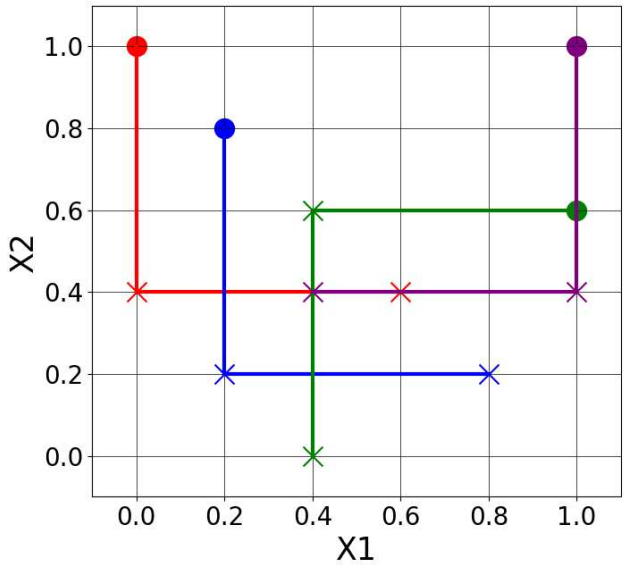

Figure 3.1: Example of a trajectory design in 2-dimensional input space with 4 trajectories. The input parameter space is uniformly divided into 6 equally divided levels. The filled circles are the random points from which the random grid jumps are carried out one-at-a-time.

In its paper Morris [62] advocates to select a step $\Delta = \frac{p}{2(p-1)}$, that ensures good coverage of the input space with few trajectories. However, such step selection might cause some loss of information on the parameter. For the rest of the thesis, the choice of step Δ will be chosen as $\Delta = \frac{1}{p-1}$. The starting point of a trajectory on the grid is randomly chosen and each sample differs only in one coordinate from the preceding one [62]. Then, a sign is also randomly selected (practically a Bernoulli random variable) to indicate the direction of displacement. One trajectory is used to compute the magnitude of variation in the model output due to the predefined variation of one parameter while keeping the other parameters constant. This output is called elementary effect (EE). The grid constructs a finite distribution of size $p^{K-1}[p - \Delta(p-1)]$ elementary effects per input parameter.

Usually the number of the trajectories r accomplished is between 4-5, depending on the number of input factors the computational cost of model evaluation and the choice of the number of levels. The technical scheme to generate trajectories is explained in detail in appendix A.

The elementary effect of parameter k for a model $f(x)$ with K parameters $x = (x_1, ..., x_K)$, contained in a hypercube $[0, 1]^K$ is defined as follow,

Elementary effect

$$EE_k = \frac{f(x_1, x_2, ..., x_k + \Delta, ..., x_K) - f(x_1, x_2, ..., x_K)}{\Delta} \tag{3.1}$$

Two indices computed with the EE's allow to compare the effect of the variation of each parameter on the output. The first is the expectancy of the EE and the second the standard deviation of the EE. The expectancy of the EE is obtained by sampling an n_r number of elementary effects associated with the k^{th} parameter sampled from the distribution of EE_k. The statistical summary of the EE_k from the sampled trajectories can be calculated. The arithmetic mean is defined as:

$$\mu_k = \frac{1}{n_r} \sum_{r=1}^{n_r} EE_k^r \tag{3.2}$$

As a change in a parameter value might result into a change of sign on the output, this may cause cancellation effect, Campolongo [11] proposed to use the mean of the absolute elementary effect to solve the issue. It is defined as:

Mean of the absolute elementary effect

$$\mu_k^* = \frac{1}{n_r} \sum_{r=1}^{n_r} |EE_k^r| \tag{3.3}$$

The next statistic is the standard deviation of the elementary effect associated with the k^{th} parameter from the obtained trajectories.

Standard deviation of elementary effect

$$\sigma_k = \sqrt{\frac{1}{n_r} \sum_{r=1}^{n_r} (EE_k^r - \mu_k)^2} \tag{3.4}$$

The standard deviation of the elementary effect gives an indication of the presence of interactions or non-linearity between the k^{th} parameter and the other parameters. If σ_k is small elementary effects have low variations on the support of the input. Thus the effect of a perturbation is the same all along the support, suggesting a linear relationship between the studied input and the output. On the other hand, the larger σ_k is, the less likely the linearity hypothesis is.

The three statistics when evaluated over a number of trajectories n_r can provide global sensitivity measured of the importance of the k^{th} parameter. According to Morris there are three possible categories of parameter importance:

- Parameters with non-influential effects. The parameters that have relatively small values of both μ_k^* and σ_k. The small values indicate that the parameter has a negligible overall effect on the model output.
- Parameters with linear and/or additive effects. Parameters with relatively large value of μ_k^* and relatively small value of σ_k. The small value of σ_k and the large value of μ_k^* indicate that the variation of elementary effects is small while the magnitude of the effects itself is consistently large for the perturbations in the parameter space.
- Parameters with non-linear or interaction effect have a relatively small value of μ_k^* and a relatively large value of σ_k. Opposite to the previous case a small value of μ_k^* indicates that the aggregate effect of perturbations is seemingly small while a large value σ_k indicates that the variation of the effect is large. The effect can be large or negligibly small depending on the other values of parameters at which the model is evaluated. Such large variations are a symptom of non-linear effects and/or parameter interaction.

To conclude, the Morris method allows to estimate the sensitivity measures (both μ^*, σ) starting both from a p-level grid. It allows to get the model response from parameter displacements and finally plot the sensitivity to get a qualitative estimate.

The advantage of the Morris method is that it provides a qualitative method for fast exploration of the behavior of a black-box computer code, at a low computational cost. However one of the main drawbacks of the method is that it is not possible to distinguish between nonlinear effects and interaction effects in the model which can be a critical in terms of model calibration. Moreover, because of the normalized grid, it does not really take into account the distributions of input parameters.

3.3 Morris OAT method applied on Single Diode Model

Prior to the analysis the boundaries of the parameter values needs to be defined. The defined parameter bounds needs to be selected carefully because they directly affect the sensitivity analysis results. The parameter bounds were set based on literature review and the expert knowledge.

Parameters	**Nominal value**	**Bounds**
I_{sc} (A)	5.724	[4.0-9]
R_s (Ω)	0.5	[0.3,1]
R_{sh} (Ω)	1200	[650-1600]
I_o	8.21235172e-8	[8.e-8,8.21235172e-07]
nDs	1.25	[1.-1.45]

Table 3.1: Parameter bounds used for sensitivity analysis on SDM.

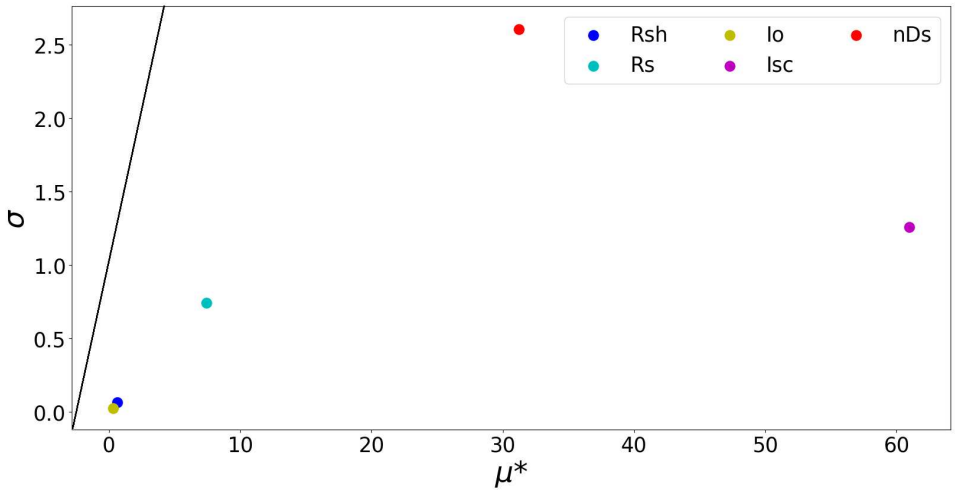

Figure 3.2: Morris OAT on Single Diode Model at STC conditions.

Based on the graph of elementary effect we can reveal three areas considering the axis x as μ^* and the y-axis σ:

- Low values of μ^* and σ the parameter is considered having a negligible impact on the output: I_o , R_{sh}
- High values of μ^* compared to σ the parameter has a strong linear effect on the output: I_{sc}

- High values of μ^* the parameter has either a strong non-linear effect on the output and/ or includes one or several interactions with other ones : nDs

Based on the Morris OAT results (Figure 3.2) the most influential parameters in the single diode model are the short circuit current I_{sc}, diode ideality factor nDs and series resistance R_s the parameters shunt resistance R_{sh} and saturation current I_o does not influence the model output.

The effect of different values of series and shunt resistance on the IV curves and the P_{mpp} is presented in Figure 3.3 and Figure 3.4.

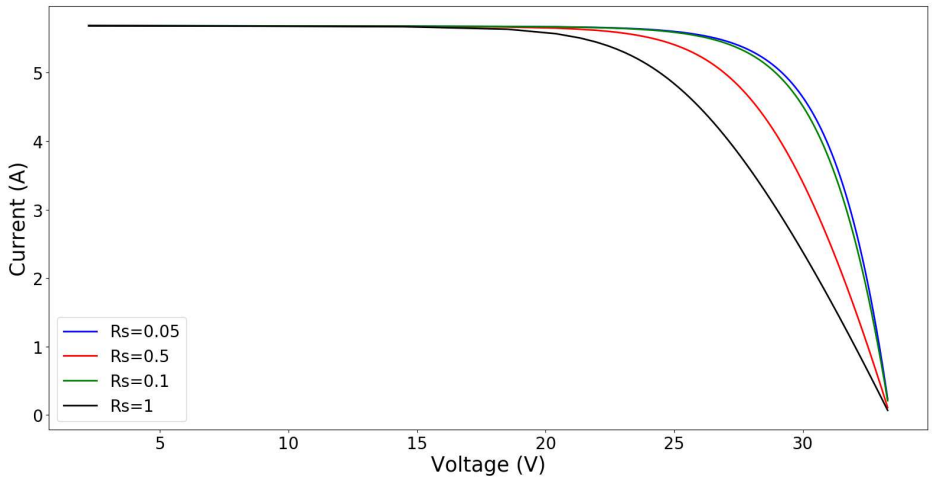

Figure 3.3: IV curve with different values of series resistance.

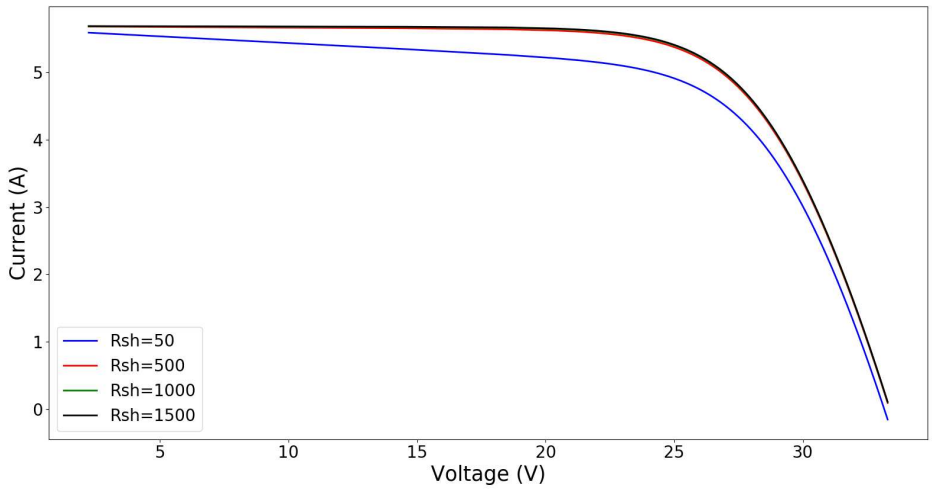

Figure 3.4: IV curves with different values of shunt resistance.

The IV simulations at STC conditions show that the high shunt resistance values do not have large effects on the power. The values above 500 Ω on cell level show only minor effects on the produced power in Figure 3.4. Based on this results we can expect that the model response to changes in shunt resistance values will have a threshold effect.

The changes in the values of the series resistance have bigger impact on the IV curve shape: Figure 3.3 shows small changes in the series resistance value cause big changes in the IV curve

shape.

3.4 Morris OAT method applied on the Dymola model

Parameters	Nominal value	Bounds
$Alpha\ (\%/K)$	0.037	[0.034-0.044]
A_r	0.2	[0.17,0.25]
$I_{sc}\ (A)$	5.724	[5.0-6.6]
$R_s\ (\Omega)$	9e-5	[1e-5,14e-5]
$R_{sh}\ (\Omega)$	0.1953	[0.014-1.5]
$Cr\ (A/m^2K^3)$	0.630	[0.450-0.842]
$Cs\ (A/m^2K^3)$	3291.9	[3003.759-4005.2]
Mr	2.5	[2.25-3.6]
Ms	3	[2.7-3.6]
nDr	2	[1.9-2.2]
nDs	1	[0.9-1.2]

Table 3.2: Parameter bounds used for sensitivity analysis.

A PV production was simulated with Dymola at a single time step at STC conditions to screen the model and identify the non-influential parameters that can be set on their nominal values during the whole study. The Morris method allows to identify variables which can be neglected in the further study but one of the drawbacks of the method is that can not differentiate between parameters that have interactions with other ones from those which have a non-linear effect on the output [25]. The SALib package was used for Morris method implementation [43].

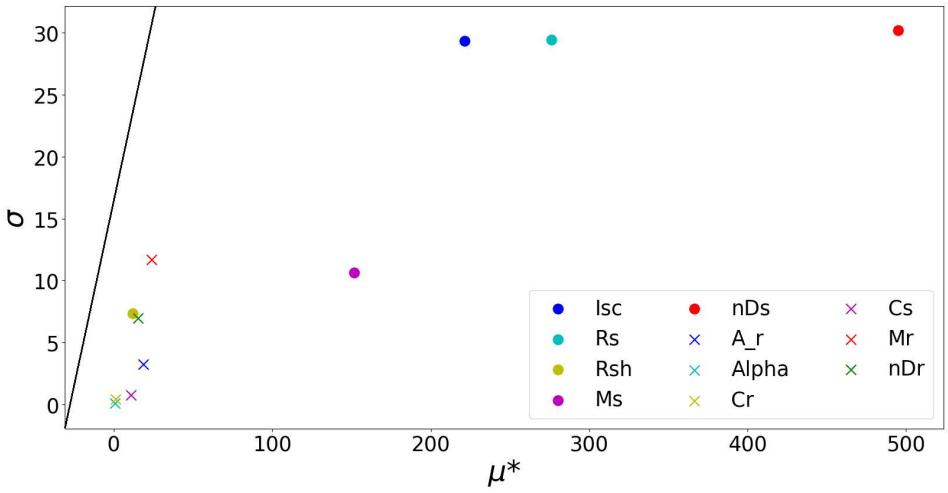

Figure 3.5: Morris OAT single time step at STC conditions.

Based on the results (Figure 3.5) the most influential Dymola model parameters are:

- I_{sc} short circuit current
- R_s Series Resistance
- R_{sh} Shunt Resistance

- Ms Temperature exponent in saturation current
- nDs Diode Ideality factor (Ideality factor of saturation current)
- A_r Transmission factor

The graph of the Elementary Effect (EE) can reveal three areas considering the axis x as μ^* and the y-axis as σ:

- for low values of μ_k^* and σ_k the k^{th} parameter is considered as having a negligible impact on the output (A_r and R_{sh}).
- for high values of μ_k^* compared to σ_k the k^{th} parameter has a strong linear effect on the output (R_s, I_{sc})
- for high values of μ_k^* the k^{th} parameter has either a strong non-linear effect on the output and/or includes one or several interactions with other ones nDs.

The results from a scalar output of the numerical code show that the parameters A_r and R_{sh} have a negligible impact on the power output. The results are expected because the parameter A_r is related to the transmission factor which is changing over the year according to the sun position and represents angular losses while the parameter shunt resistance R_{sh} effect depends on the irradiation levels where at low irradiation levels the effect is more severe.

The most influential parameters according to the Morris method are the series resistance R_s and short circuit current I_{sc}. Both parameters are closely related to the degradation of the PV cells. The effect of both parameters are directly related to the power output. The power output decrease linearly with the decrease of short circuit current while the series resistance affects the power near the open-circuit voltage where the the short circuit current is unaffected by the series resistance until it is very large. The parameters with a strong non-linear effect is the diode ideality factor nDs which measures how closely the diode follows the ideal diode equation but for modelling purposes is usually set on nominal value in silicon solar modules.

Morris method can only be applied on the function that create a scalar output however the method can be applied in various time steps over the period of a single day. In this case the sensitivity analysis takes into account the behaviour of the code on the whole time frame and not only at the instantaneous time. The impact of several parameter could seem negligible in a instantaneous time but they could not be negligible on another moment of the day. The sensitivity analysis is focused on all the influential parameters in the numerical code.

Single day PV simulation was selected for sensitivity analysis where the maximum POA reaches 800 W/m^2 at noon Figure 3.6. For the power two PV modules were selected where the maximum power generated is 314 W. The day is from 10.02.2011 the sunrise time 7:26 is while the sunset time is 17:35. A single time step corresponds to the 15 minutes interval starting on 7:30 and ending at 17:30.

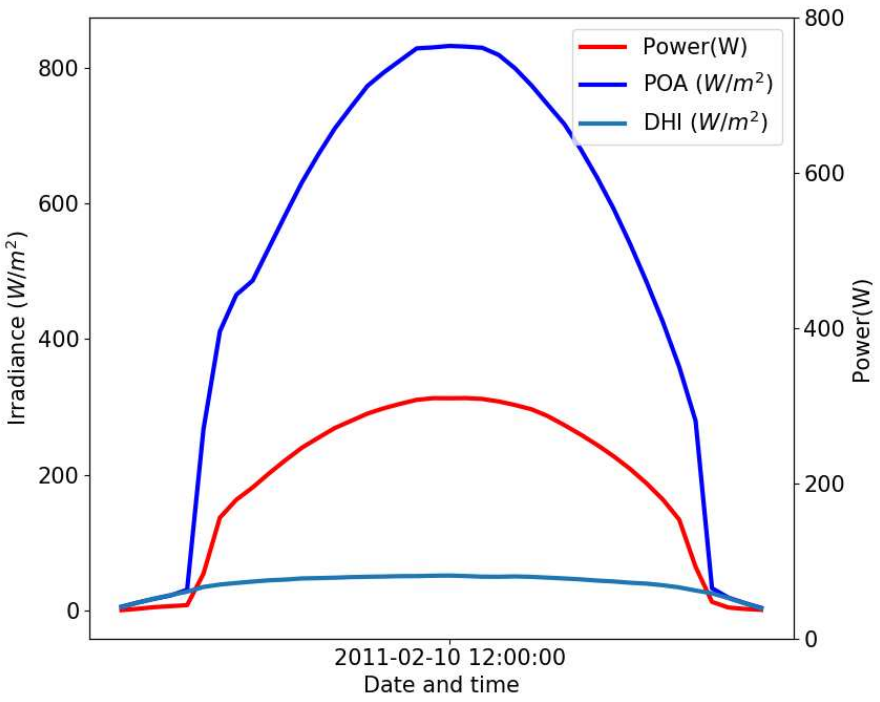

Figure 3.6: The selected day for sensitivity analysis.

The Morris method was applied on the period of a single day (Figure 3.6) to take into account the variation of outdoor operating conditions on the parameter values. Every point on the Figure 3.7 represents the 15 minutes time step starting from 7:45 and ending at 17:45.

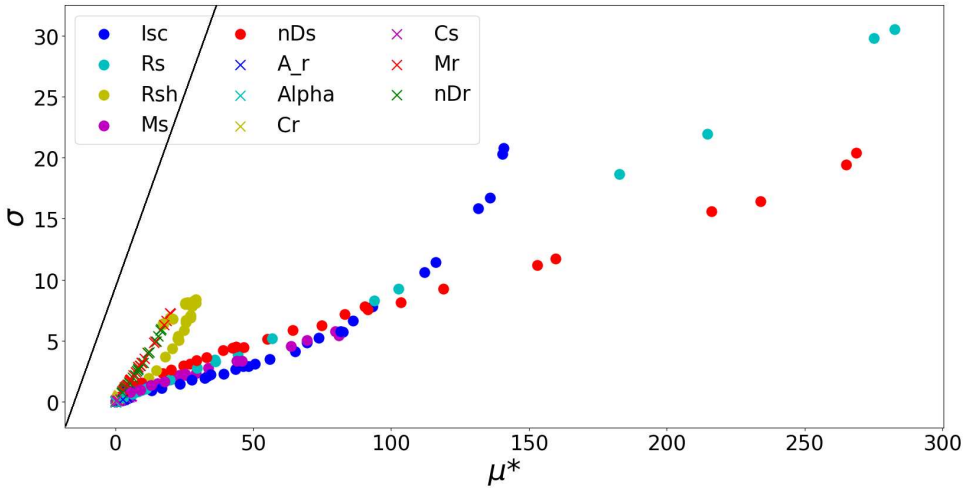

Figure 3.7: The Morris method performed on the period of a single day.

The results from the Figure 3.7 show similar patterns as the results obtained from the Morris method applied on the single scalar output. The most influential parameters are the short circuit current, series resistance, diode ideality factor and the shunt resistance. It can be seen on the figure that the parameters series resistance and diode ideality factor have a linear influence on

the power while the influence of the short circuit current and shunt resistance follows exponential relationship.

Mathieu Carmassi [13] illustrates the Morris study performed on the Dymola numerical code over two months time frame where the principal component analysis (PCA) was applied on the trajectories [13]. In the new subspace "new" indices μ^* and σ can be computed. On the new indices with PCA the temporal correlation can be visualised to find a new representation axis for the Morris indices. The results of the PCA are given in Figure 3.8.

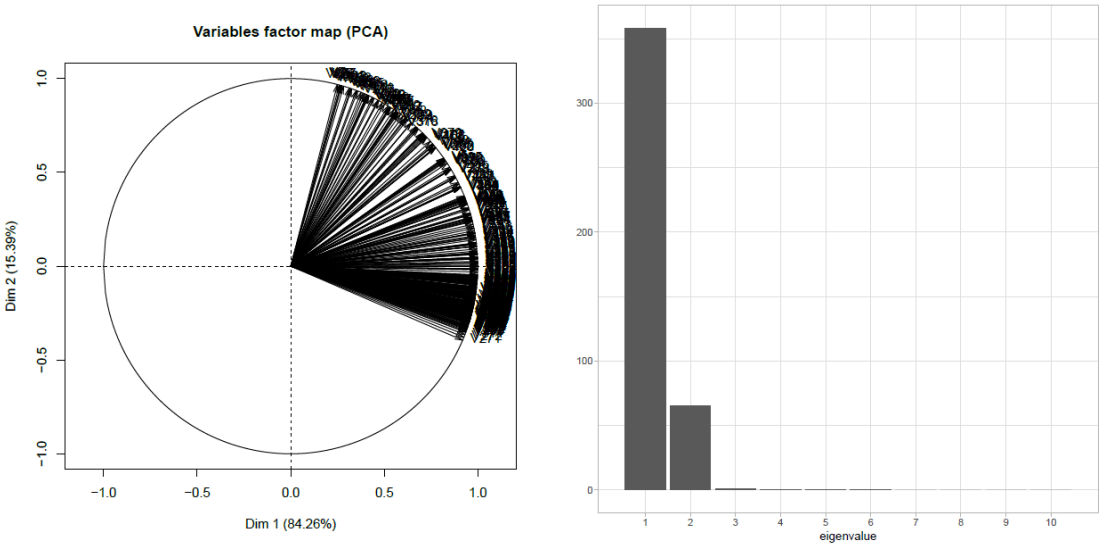

Figure 3.8: The PCA performed on the results given by the Morris method. On the left the correlation circle obtained by PCA and on the right the eigenvalues for the ten first axis [12].

Figure: 3.8 shows that the time series of the outputs, given by the Morris method can be projected on a 5 axis basis with keeping more than 99% of the information. This projection is in the new space is used to compute the new indices of the Morris method. illustrates all the indices in 5 axes of the dimensional subspace given by the PCA.

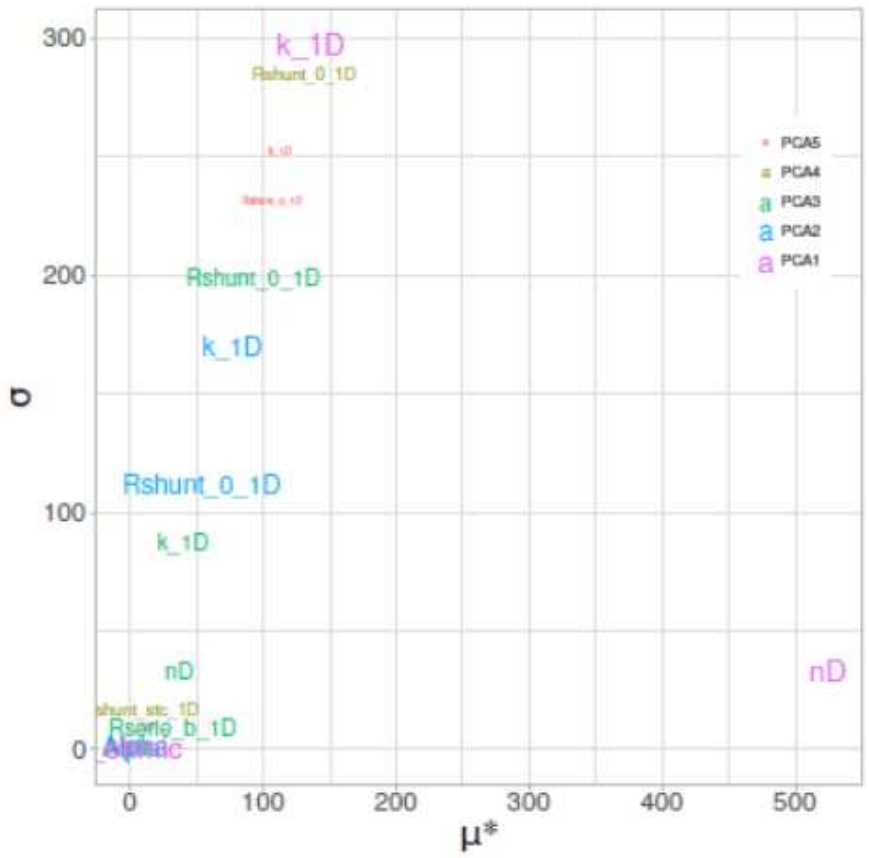

Figure 3.9: Morris OAT PCA [12].

According to Carmassi [13] the seven most important parameter in the Dymola model are the following:

- I_{sc} is the short circuit current
- nd is the diode ideality factor.
- R_{shunt} is the shunt resistance in STC conditions.
- R_{series} series resistance in STC conditions
- $Rshunt1D$ and $RshuntK1D$ coefficients that allow the shunt resistance to vary with the irradiation.
- $Paco$ is the maximum ac-power 'rating' for inverter at reference or nominal operating conditions, assumed to be an upper limit value.

Where the parameter shunt resistance is not important instantaneously but could be important at the conditions of low irradiation.

3.5 Sobol indices

The Morris method is a suitable method to detect parameters that have no impact on the model output and can be omitted from the analysis. The Sobol sensitivity indices can provide more granulated information about the parameters influence on the model output. The Sobol method attributes variance in the model output to parameters and the interactions between them. The

main idea of this method is to decompose the output variance into the contributions associated with each input factor i.

$$Y = f(X_1, ..., X_p) \tag{3.5}$$

The output Y is a scalar and the input factors $X_1, \ldots, X_p$ are supposed to be independent random variables described by known probability distributions. In order to quantify the importance of an input factor X_i on the variance of Y, we can fix it at its "true" value ,x_i^*. Where we want to know how much will this assumption change the variance of Y. The conditional variance:

$$V_{X-i}(Y|X_i = x_i^*) \tag{3.6}$$

where the variance is taken over the $(p-1)$ dimensional parameter space X_{-i}, consisting in all factors but X_i. Because the true value of X_i is unknown, we average over all possible values of X_i:

$$E_{Xi}(V_{X_{-i}}(Y|X_i)) \tag{3.7}$$

The smaller this quantity, the more important the contribution of X_i to the variance of Y. Using the law of total variance we can write:

$$V(Y) = V_{X_i}(E_{X-i}(Y|X_i)) + E_{X_i}(V_{X-i}(Y|X_i)) \tag{3.8}$$

and normalizing

$$1 = \frac{V_{Xi}(E_{X-i}(Y|X_i))}{V(Y)} + \frac{(E_{Xi}(V_{X-i}(Y|X_i))}{V(Y)} \tag{3.9}$$

The first-order sensitivity index for factor X_i, is given by the first term in equation above

$$S_i = \frac{V_{Xi}(E_{X-i}(Y|X_i))}{V(Y)} \tag{3.10}$$

From normalized equation we get that the first-order sensitivity index verifies $S_i \leq 1$.

If the function 3.10 is integrable over $[0,1]^p$ than it can be decomposed into terms of increasing dimensionality as follows [89]:

$$f(X_1, ...X_p) = f_0 + \sum_{i=1}^{p} f_i(X_i) + \sum_{1 \leq i < j \leq p} f_{ij}(X_i, X_j) + ... + f_{1...,p}(X_1, ..., X_p) \tag{3.11}$$

If the input factors are mutually independent then there exist a unique decomposition such that all the summands in Equation 3.11 are mutually orthogonal. Using this results, it can be shown that the variance of the output $V(Y)$, can be also decomposed into:

$$V(Y) = \sum_{i=1}^{p} V_i + \sum_{1 \leq i < j \leq p} V_{ij} + ... + V_{1,...,p} \tag{3.12}$$

where $V_i, V_{ij}, ..., V_{1,2...,p}$ denote the variance of $f_i, f_{ij}, ..., f_{1,...,p}$ respectively:

$$V_i = V(E(Y|X_i))$$
$$V_{ij} = V(E(Y|X_i, X_j)) - V_i - V_j$$
$$V_{ijk} = V(E(Y|X_i, X_j, X_k)) - V_{ij} - V_{ik} - V_{jk} - V_i - V_j - V_k$$
$$\vdots$$

$$V_{1,\dots,p} = V(Y) - \sum_{i=1}^{p} V_i - \sum_{1\le i<j\le p} V_{ij} - \dots - \sum_{1\le i_1<\dots<i_{p-1}\le p} V_{i1},\dots,i_{p-1}$$

For simplicity the indices for the variance and the mean are omitted. The first-order indexes defined in Equation 3.10 can be deduced from the first p terms of the decomposition

First order sensitivity indexes are expressed as:

First Order Sensitivity

$$S_i = \frac{V_i}{V(Y)} = \frac{V(E(Y|X_i))}{V(Y)} \tag{3.13}$$

The other terms of decomposition in Equation 3.12 can be interpreted like a higher sensitivity indexes. The second sensitivity index S_{ij} explains the amount of variance between X_i X_j (i.e. sensitivity to X_i and X_j not expressed in V_i nor V_j).

$$S_{ij} = \frac{V_{ij}}{V(Y)} \tag{3.14}$$

The third-order sensitivity index S_{ijk}, expresses the amount of variance of Y explained by X_i, X_j and X_k and not taken into account in the first and second order sensitivity indexes.

$$S_{ijk} = \frac{V_{ijk}}{V(Y)} \tag{3.15}$$

For every p input factor we can define $2^p - 1$ sensitivity indexes.

Homma and Salteli [33] introduced an additional index the total sensitivity index, ST_i, that accounts for all the contributions to the output variation due to factor X_i (the first order index plus all the interactions):

$$ST_i = \sum_{k\subseteq i} S_k \tag{3.16}$$

It can be shown that this total-order index can be expresses as:

$$ST_i = 1 - \frac{V_{X-i}(E_{Xi}(Y|X_{-i})}{V(Y)} \tag{3.17}$$

Again using the law of total variance and normalizing:

$$1 = \frac{E_{X-i}(V_{Xi}(Y|X_{-i})}{V(Y)} + \frac{E_{X-i}(V_{Xi}(Y|X_{-i}))}{V(Y)} \tag{3.18}$$

The second term in the equation above is giving the total-order indices:

Total-order indices

$$ST_i = \frac{E_{X-i}(V_{Xi}(Y|X_{-i}))}{V(Y)} \tag{3.19}$$

The first order index measures the total output variance caused by the parameter i without the interactions with other parameters. The total order index removes parameter i from the analysis and attributes the resulting reduction in variance to that parameter [33]. Where the difference between the parameter's first and total order indices represents the effect of the interactions with other parameters.

Test of Sobol method on Ishigami function

We estimate the Sobol indices for the Ishigami function, defined for $x_1, x_2, x_3 \in [-\pi, +\pi]$ by:

$$f(x_1, x_2, x_3) = \sin(x_1) + a\sin(x_2)^2 + bx_3^4 \sin(x_1)$$

We set a=7 and b=0.1 and assume that the random variables x_1, x_2, x_3 are independent and identically distributed according to the uniform distribution on the interval $[-\pi, +\pi]$:

$$x_1, x_2, x_3 \sim \mathcal{U}(-\pi, +\pi)$$

The scatter plots in Figure 3.10, represent the output function of each parameter and allow to visualize the behavior of the function according to a specific parameter.

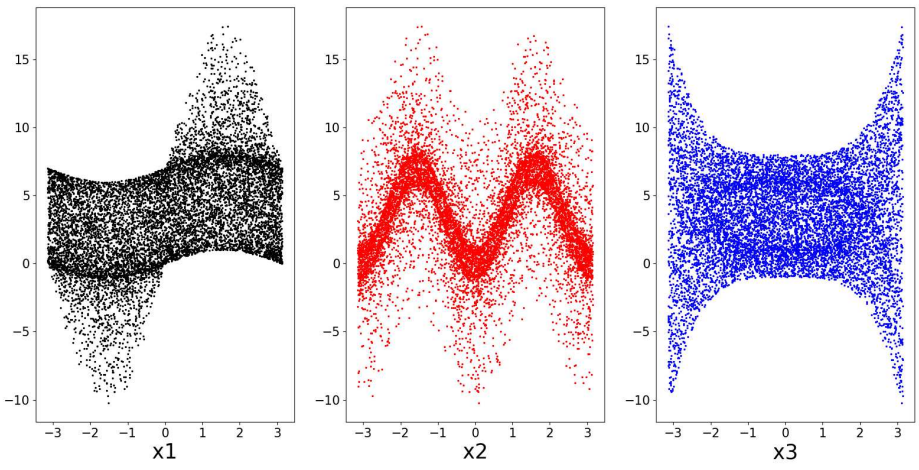

Figure 3.10: Scatter plots of the Ishigami function where the output is given function of the each parameter.

Before performing a Sobol sensitivity analysis, we need to generate samples on which the sensitivity indices will be estimated. Monte Carlo sampling based methods have been developed for Sobol indices estimation but this methods are costly in terms of number of model calls. To improve the efficiency of Sobol indices estimation the Saltelli sampler was used [82]. The sampler is based on quasi-Monte Carlo method, which generates a quasi random sequences of samples. The

procedure is explained in detail in appendix B. Using quasi-Monte Carlo instead of Monte Carlo samples can sometimes reduce the computational cost by a factor ten [83].

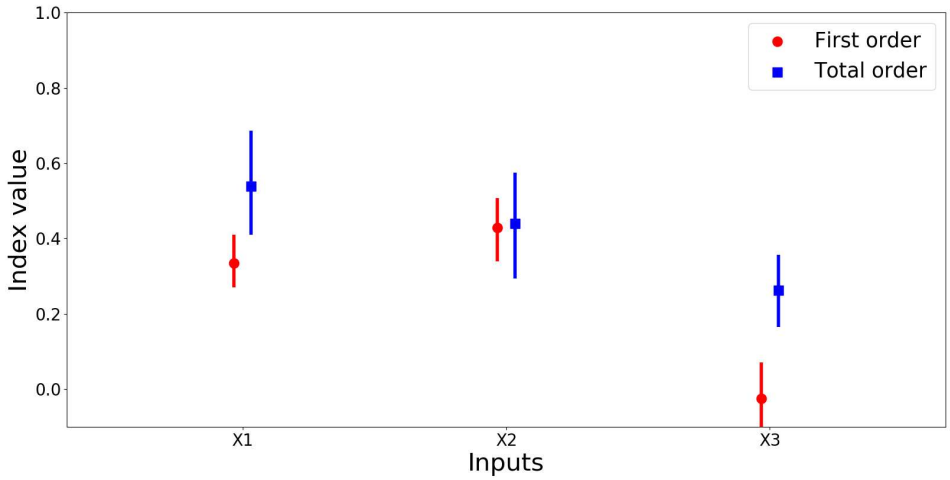

Figure 3.11: Sobol's index computed for the Ishigami function and the boxplots representing the variability of 1000 bootstrap iterations.

The results of the first order and the total effect Sobol's indices obtained on the Ishigami function are represented in Figure 3.11. We can see that the most significant variable is x_1 with a total order Sobol index close to 0.6. If the total-order indices are substantially larger than the first-order indices, then there is likely higher-order interactions occurring. The first order index of x_1 is close to 0.3 which implies that it's interactions alone produce almost 30% $(0.6 - 0.3)$ of the total variance. The variable x_2 has the highest first order Sobol index but has little interactions with other variables. The total order index and the first order index are almost the same. The variable x_3 has a first order index close to zero. However, it has an impact to the total variance because of it's interactions with x_1.

3.6 Sobol indices applied on Single Diode Model

Before applying the Sobol analysis the sample size needs to be defined. The sample size depends on the complexity of the model and the number of the parameters evaluated. The general rule is that the sample size needs to be scaled with the number of the model parameters. It should be noted that increasing the number of function evaluations increases the computational cost as well. The sample size selection can be tested using Bootstrap confidence intervals, where in general the uncertainty of one input should be around 10%. In cases where the uncertainty is bigger the sampling size needs to be increased.

Sobol analysis was applied on the SDM model parameters where the parameters boundaries were the same as defined in the Morris method. For Sobol indices estimation the Saltelli sampler [82] was used with 10000 generated samples.

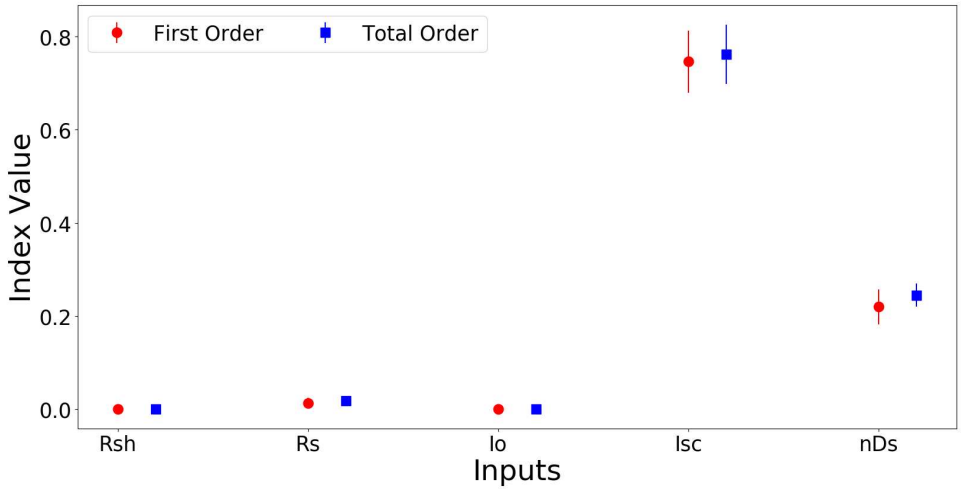

Figure 3.12: Sobol Analysis on SDM.

Parameters	Total Order Indices	Total Order 95% CI	First Order Indices
R_{sh} (Ω)	0.000082	0.000009	0.000031
R_s (Ω)	0.017393	0.002765	0.012282
I_o (A)	0.000024	0.000003	0.000063
I_{sc} (A)	0.762342	0.637520	0.746446
nDs	0.037865	0.244917	0.219417

Table 3.3: Sobol Analysis results on SDM.

According to the Figure 3.12 we see that the variable I_{sc}, with a total Sobol index close to 0.8, is the most significant variable, taking into account its direct effect on the model output. Its first order effect is close to the total order effect so there is no interaction with other variables in the model. The second most influential variable based on the total Sobol index is the nDs with the value of total Sobol index above 0.2, the first order index is close to the total order index so it has no or little interaction with other variables. We see that the variability of the estimates for I_{sc} and nDs is quite high even with a relatively large sample size. The calculated confidence intervals are based on the standard error of the mean for the total order indices estimates. The confidence intervals are estimated with 1000 bootstrap samples. The total order and first order Sobol indices for the parameters R_{sh}, R_s and I_0 is close to zero this means that those parameters are non-influential.

Both total-order sensitivity indices and first order sensitivity indices have similar values, which indicate no significant second order interactions between the parameter values. The differences between the first order indices and the total effect are small which means that no non-linear effects affects the input parameters.

The results obtained with the Sobol analysis corresponds to those obtained by Zarahatos [103] the most important parameter is the I_{sc} followed by the diode ideality factor nDs. The ranges for nDs and I_{sc} were set at about their maximum bounds for a crystalline silicon PV cell, while the range of parameter values for R_s and R_{sh} are to the certain degree limited.

The results of the single diode sensitivity analysis can be interpreted with regard to the physics of single diode model. Because the $P_{mpp} = I_{max} \times V_{max}$ on the IV curve where I_{max} usually scales linearly with the I_{sc}. The voltage at open circuit denoted as V_{oc} typically scales logarithmically with

the I_{sc} where V_{max} behaves like V_{oc}. Increase in I_{sc} affect I_{max} linearly and V_{max} logarithmically. Because the I_{sc} affects both I_{max} and V_{max} it is logical to be the most important parameter influencing the P_{max}.

3.7 Sobol indices applied on the Dymola model

To evaluate if the model parameters show any interaction which could have an effect on the whole calibration process the Sobol sensitivity analysis was applied. The interaction would mean that two (or more) parameters have a different influence on the model output together than separated. The PV production was simulated for a period of two days with the nominal values.

For the Sobol analysis the SALlib package was used [43]. Sobol sensitivity analysis is a global variance based method that attributes variance in the model output to individual parameters and the interaction between parameters. In theory, Sobol indices range is [0,1]; the more the indice is close to 1 the more the variable is important towards the output of the function.

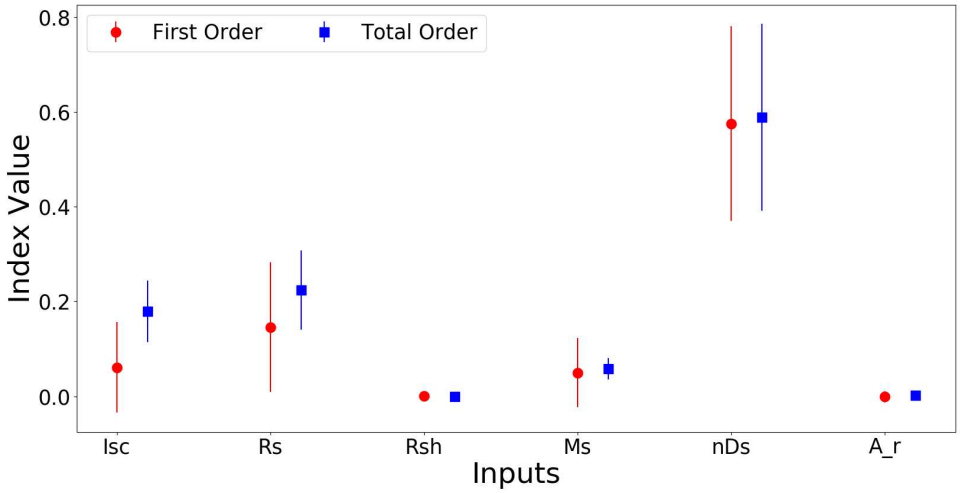

Figure 3.13: Sobol Analysis on Dymola model.

Parameters	Total Order Indices	Total Order 95% CI	First Order Indices
I_{sc} (A)	0.1795	0.0645	0.0612
R_s (Ω)	0.2244	0.0836	0.1458
R_{sh} (Ω)	0.000177	0.000259	0.00064
Ms	0.058	0.0223	0.0499
nDs	0.588	0.196	0.575
A_r	0.001	0.00001	0.00001

Table 3.4: Sobol Analysis results on Dymola model.

The confidence intervals are based on the standard error of the mean for the total order indices estimates. The Standard error is estimated with 1000 bootstrap re samples. The differences between the first order indices and the total effects are practically equal which means that no non-linear effects affect the input parameters (Figure 3.13).

Based on the total order indices the most influential parameters on the model output are: diode ideality factor nDs, series resistance R_s, short circuit current I_{sc}, temperature exponent in

saturation current Ms, transmission factor Ar, shunt resistance R_{sh}. If the total order indices are substantially larger than the first order indices, then there is likely higher order interactions occurring.

3.7.1 Second order indices

The second order indices is extending the analysis by looking at pairs of variables and their possible interactions. Pairwise comparison of 6 parameters were performed to see any possible interactions between them.

The second-order Sobol' index (S_{ij}) expresses the contribution of the interactions of the pairs of variables X_i and X_j on the output variance. More precisely this is second-order interaction screening, since we consider pairs of variables. The pairwise interactions can explain some important model properties and how the parameters are related.

If the total-order indices are substantially larger than the first-order indices, then there is likely higher-order interactions occurring. We can look at the second-order indices to see these higher-order interactions:

Parameters	**Second order indices**
$I_{sc} - R_s$	-0.000189
$I_{sc} - R_{sh}$	0.051859
$I_{sc} - Ms$	0.000106
$I_{sc} - nDs$	-0.001348
$I_{sc} - A_r$	-0.001815

Table 3.5: Second order indices on I_{sc}.

Parameters	**Second order indices**
$R_s - R_{sh}$	-0.000118
$R_s - Ms$	-1e-06
$R_s - nDs$	-9e-06
$R_s - A_r$	-2.3e-05

Table 3.6: Second order indices on R_s.

Parameters	**Second order indices**
$R_{sh} - Ms$	-0.008458
$R_{sh} - nDs$	0.008983
$R_{sh} - A_r$	-0.00834

Table 3.7: Second order indices on R_{sh}.

Parameters	**Second order indices**
$Ms - nDs$	0.000658
$Ms - A_r$	0.000328

Table 3.8: Second order indices on Ms.

Parameters	**Second order indices**
$nDs - A_r$	-0.001475

Table 3.9: Second order indices on nDs.

Based on the results the parameters do not show strong interactions between each other. We can see there are possible interactions between the parameter I_{sc} and R_{sh} and between R_s and R_{sh}. Some computing error will appear in the sensitivity indices. For example, we observe a negative value for the $I_{sc} - R_s$ index. Typically, these computing errors shrink as the number of samples increases.

To take into account the variation of the outdoor operating conditions on the parameter values the Sobol method was applied on the single day (Figure: 3.6) on 10.02.2011 starting at 7:30 and ending at 17:30 with the highest POA irradiance around 900 W/m^2.

The results from the daily analysis are comparable with those obtained in the initial Sobol analysis at STC conditions. (Figures 3.14 and 3.15). The additional information is on the temporal effect on parameter influence during the course of a day where some parameter show no influence at the beginning of the day (series resistance) while the parameter shunt resistance shows opposite behaviour.

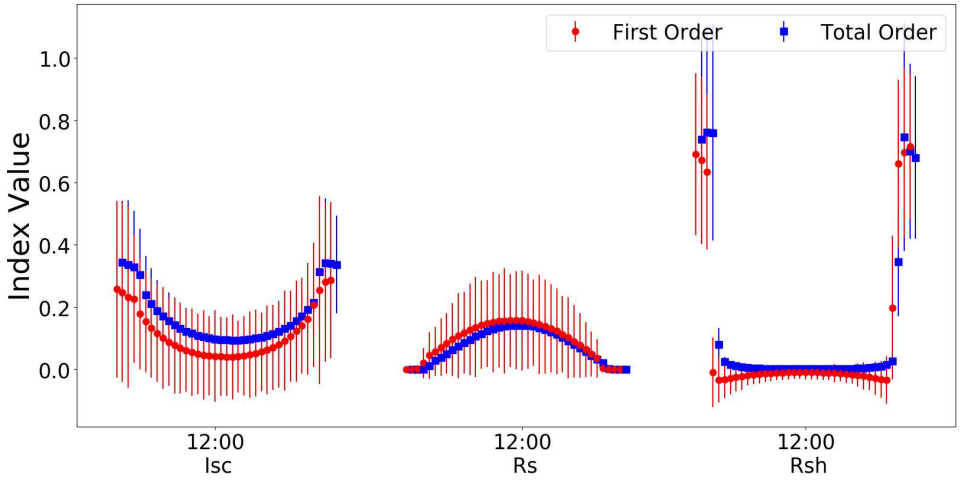

Figure 3.14: Sobol Analysis performed on the period of single day 1.

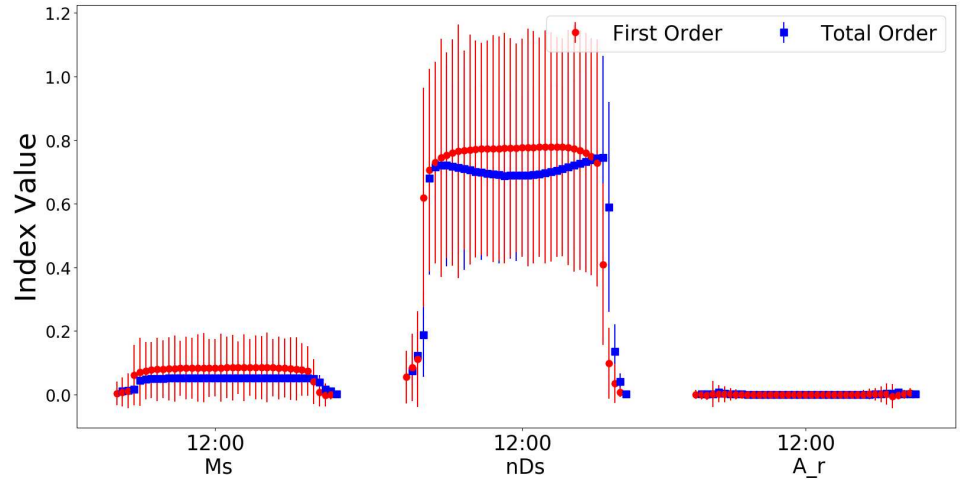

Figure 3.15: Sobol Analysis performed on the period of single day 2.

The most influential parameters in the model are nDs, R_s and I_{sc}. The parameter shunt

resistance R_{sh} is influential only at low irradiation levels at the beginning and end of the day. The parameters R_s and nDs are the influential at the highest irradiation levels while the parameter Ms and A_r doesn't show any variation over the course of a day.

3.8 Conclusion

Sensitivity analysis with Morris and Sobol method was performed on both Single Diode and Dymola model to map the output behaviour of the models with focus on a specific domain of parameter inputs which could be related to degradation of photovoltaic modules.

The motivation of using the sensitivity analysis is to reduce the size of the parameter vector and identify which parameters can be set on their nominal values during the calibration process. At the same time by reducing the number of the model parameters, due to the model over-parametrisation we are increasing the identifiability of the parameter values. Parameter identifiability cannot be achieved for calibrating a certain parameter if the selected parameter does not have any significant contribution to the model responses. At the same time calibrating the full model can be computationally intensive.

The Morris method allows to get a fast exploitation of the code behaviour identifying only a small number of influential parameters. To take into account the variation of the outdoor operating conditions the Morris method was applied on the period of a single day because the impact of several parameter could seem negligible in a instantaneous time but they could not be negligible on another moment of the day. The results in both cases show similar results.

The Sobol analysis shows the temporal influence on parameter values from the variations of outdoor operating conditions. This information could be used for estimating the values of shunt resistance only at certain period of the day (sunrise, sunset) but at the same time the effect of series resistance at this times is negligible.

The Morris method allows to simplify the model before using Sobol analysis which provides more granulated information of the model behaviours. Both methods show comparable results on both models. Sobol analysis allows to calculate the possible interactions between model parameters. Pairwise comparison of parameters was performed and it does not show any interactions.

In the following chapters the calibration with both models will be presented to identify the parameter values with the single diode model and with the more advanced Dymola model.

Chapter 4

Meta-Models

In this chapter the main motivation for using surrogate models is presented together with the various meta-model building approaches and their validation. The polynomial, Kriging and neural network meta-models are presented. For the meta-model validation the generalisation error and the coefficient of determination were calculated. Polynomial Chaos Expansion (PCE) is build and validated on an example data.

Contents

4.1 Meta-models

Often the physical models are highly complex and computationally expensive. Meta-models or surrogate models are usually employed to approximate or emulate computationally costly experiments or simulation models of complex physical phenomena [10]. In this cases it can be useful to replace the complex computational code by a mathematical model called meta-model or surrogate model at the cost of adding an additional source of uncertainty.

Meta-modeling is based on classical Design of Experiment (DOE) theory where polynomial functions are used as response surfaces or meta-models. As a numerical DOE is applied to a computational codes, each experiment involves an evaluation of the model, and thus computational cost depends on the computational resources and the number of runs (i.e. experiments). A large number of runs will increase drastically the needed resources. An optimal strategy is to choose the most efficient DOE and to use a method for reducing the computational cost of each run. An efficient DOE should minimise the number of runs and optimize the space-covering of the runs to gain insights into the relationship between the input variables and the output results of

computer simulations. The error made by the surrogate strongly depends on the numerical design of experiments used to fit the meta-model.

The physical phenomena can be represented by a computational model f considered as a deterministic function where the X in the sequel is used for a random vector $X = \{x_1, \ldots, x_M\}$ denote the M-dimensional input parameter vector of the computational model and $Y = \{y_1, \ldots, y_N\}$ the N dimensional response vector of the model. The physical model f is usually not accessible in closed form and may represent a complex computational process.

A meta-model $\widehat{f}$ is a function such that $\widehat{Y} = \widehat{f}(X)$ is as close as possible to the Y and have comparable mathematical properties. Non-intrusive methods for meta-model building are relying on multiple calls of the original model which is used as a "black-box" without any modification.

The Design of Experiment is used to analyse the set of realisations of the computational model f with carefully selected X inputs and the response vector of the model Y.

There are multiple advantages of using the meta-models [27].

- Model simplification
- Improvement and enhancement of optimisation efficiency by performing optimisation in a more computationally efficient way than the detailed model
- Efficiency of optimization is improved
- Parallel computation is supported

Besides the commonly used polynomial functions a variety of approximation models and techniques exist for constructing surrogate models/meta-models of computationally heavy computer codes Sacks et al. [80] proposed the use of a stochastic model, called Kriging, to treat the deterministic computer response as a realization of a random function with respect to the actual system response.

4.1.1 Polynomial meta-model

One of the simplest meta-model representations is the polynomial meta-model also known as polynomial response surface model [19]. The most common approach in building meta-models is with the second order polynomial which can be represented in the matrix form [67].

$$\widehat{\mathbf{f}}(x) = \widehat{\beta_0} + x^{\cdot}\widehat{b} + x^{\cdot}\widehat{B}x \tag{4.1}$$

Where the $\widehat{\mathbf{f}}(x)$ is the response variable predicted by the meta-model, $x = [x_1, x_2, \ldots, x_m]^{\cdot}$ is a column vector of input variables, $\widehat{b} = [\widehat{\beta_1}, \widehat{\beta_2}, \ldots, \widehat{\beta_m}]^{\cdot}$ is a column vector of the linear model parameters. $\widehat{B}$ is an $m \times m$ symmetric matrix of the second order model parameters while m is the number of data points.

$$\widehat{B} = \begin{bmatrix} \widehat{\beta}_{11} & \widehat{\beta}_{12}/2 & \ldots & \widehat{\beta}_{1m}/2 \\ \widehat{\beta}_{12}/2 & \widehat{\beta}_{22} & \ldots & \widehat{\beta}_{2m}/2 \\ \vdots & & \vdots & \vdots \\ \widehat{\beta}_{1m}/2 & & \ldots & \widehat{\beta}_{mm} \end{bmatrix} \tag{4.2}$$

Eventually the model parameters can be obtained using least squares regression [88].

4.2 Polynomial Chaos Expansion (PCE)

A popular class of meta-models (surrogate models) are the polynomial chaos expansions (PCE). The PCE is closely related to the previously presented Sobol sensitivity analysis. The use of polynomial chaos expansions in the context of sensitivity analysis has been originally presented in Sudret [91] using a non intrusive least-square method. It is shown that the computation of Sobol indices can be computed analytically from the PCE expansion coefficients [91]. The computation cost is thus transferred to the obtention of the PCE coefficients, the subsequent post-processing being almost cost-less. Only elementary mathematical operations are needed to compute the Sobol indices from the polynomial expansion coefficients [91]. The basic idea behind PCE is that PCE surrogates the computational model with the series or orthonormal polynomials in the input variables where the selected polynomials are in coherence with the probability distribution of input variables [100].

The physical model can be described by a numerical model f where the model f has M uncertain input parameters which can be represented by independent random variables $\{X_1, ..., X_M\}$ gathered into a random vector X of prescribed joint probability density function $f_D(x)$, thus the model response denoted as $Y = f(X)$ is also random. For simplicity Y is assumed to be scalar. Denoted by the ψ_α are the multivariate polynomials which are orthonormal with respect to the joint PDF (Probability distribution function) f_D of the input random vector X $E[\psi_\alpha(X)\psi_\beta(X)] = 1$ if $\alpha = \beta$ and 0 otherwise. Provided that the random variable Y has a finite variance, it can be expressed as bellow (Equation 4.3), where the equality has to be interpreted in the L^2:

$$Y = f(X) = \sum_{\alpha \in \mathbb{N}^M} a_\alpha \psi_\alpha(X) \tag{4.3}$$

This expansion is called as the generalized polynomial chaos (PC) representation of Y where the a_α are unknown deterministic coefficients. The input random vector X is supposed to have independent components $X_i, i = 1, ..., M$. The joint probability density function may be cast as:

$$f_D(x) = \prod_{i=1}^{M} f_{D_i}(x_i), \tag{4.4}$$

where $f_{D_i}(x_i)$ is the marginal PDF of X_i. Let $\{\pi_j^{(i)}, j \in \mathbb{N}\}$ be a family of orthonormal polynomials with respect to f_{D_i}. Most common distributions can be associated to a specific type of polynomials e.g. normalized Hermite (resp. Legendre) polynomials for standard normal variables (uniform variables over $[-1, 1]$) [78]. The multivariate basis $\{\psi_\alpha, \alpha \in \mathbb{N}^M\}$ of the representation on Equation (4.3) is build by tensorizing the M resulting families of uni-variate polynomials as follows:

$$\psi_\alpha(X) = \prod_{i=1}^{M} \pi_{\alpha_j^{(i)}}(X_i) \tag{4.5}$$

For the sake of computation expense the accurate PCE of true model is a infinite series and needs truncation Equation (4.3) in order to retain only finite number of terms. Commonly those polynomials are retained whose total degree $|\alpha| = \sum_i \alpha_i$ does not exceed a given p:

$$Y = f(X) \approx \sum_{|\alpha| \leq p} a_\alpha \psi_\alpha(X) \tag{4.6}$$

The random response Y is thus equivalent to computing the finite set of unknown coefficient $\{a_\alpha, |\alpha| \leq p\}$. This may be done using non-intrusive techniques respectively known as projection

and regression methods.

Projection strategy

The PC coefficients can be computed using a projection strategy which exploits the orthonormality of the PC basis. By pre-multiplying eq.(4.6) by ψ_α and by taking the expectation we can get the exact expression of each coefficient a_α:

$$a_\alpha = E[\psi_\alpha(X)f(X)] = \int_{D_X} \psi_\alpha(x)f(x)f_D(x)dx, \tag{4.7}$$

where D_X denotes the support of density f_D. The multidimensional integral Equation (4.7) may be computed either by simulation techniques (Monte Carlo, Latin Hypercube) or quadrature (full tensor product quadrature) [9].

Regression strategy

An alternative to the projection strategy the regression strategy consist in adjusting the truncated PCE expansion in eq: (4.6) to the model under consideration. The equation (4.6) can be recasted using a vector notation as:

$$Y = f(x) \approx f_p(X) = a^T\psi(X) \tag{4.8}$$

where a gathers the coefficients $\{a_\alpha, |\alpha| \leq p\}$ and ψ the basis polynomials $\{\psi_\alpha, |\alpha| \leq p\}$. Let $\mathcal{X} = \{x^{(1)}, ..., x^{(N)}\}^T$ be a set of N realisations of the input random vector, and $\mathcal{Y} = \{y^{(1)}, ..., y^{(N)}\}^T$ be the corresponding model evaluations $\{y^{(i)} = f(x^{(i)}), i = 1, ..., N\}$ the set $\mathcal{X}$ is called experimental design. The coefficient in Equation (4.6) are estimated by minimizing the squared residual as shown below:

$$\widehat{a} = \underset{a\in\mathbb{R}^P}{\arg\min} \left[\sum_{i=1}^{N} \left(f(x^i) - a^T\psi(x^{(i)})\right)^2 \right] \tag{4.9}$$

Where P denotes the number of multi-indices in the set $\{a_\alpha, |\alpha| \leq p\}$ which is given by:

$$P = \binom{p+M}{p} \tag{4.10}$$

the solution is:

$$\widehat{a} = (\Psi^T, \Psi)^{-1}\Psi^T\mathcal{Y} \tag{4.11}$$

The data matrix Ψ is defined by:

$$\Psi = \begin{pmatrix} \psi_{\alpha_1}(x^{(1)}) & \cdots & \psi_{\alpha_p}(x^{(1)}) \\ \vdots & \ddots & \vdots \\ \psi_{\alpha_1}(x^{(N)}) & \cdots & \psi_{\alpha_p}(x^{(N)}) \end{pmatrix} \tag{4.12}$$

In order to make this problem well-posed, the experimental design $\mathcal{X}$ must be selected in such way that the information matrix $\Psi^T\Psi$ is well conditioned. This implies that the size of N the design (the number of model evaluations) has to be large enough, and necessarily greater than P.

Sparse PCE

The PCE approach is powerful in a wide range of applications but it has limitations in the case of high-dimensional input. This is because the number of the unknown expansion coefficients grows exponentially with the number of the input parameters, which is commonly referred to as the "curse of dimensionality" [49]. To overcome this difficulty, sparse least squares schemes may be used. These methods are aimed at identifying a small set of significant coefficients in the model response approximation. Eventually, a sparse polynomial response surface, i.e. a polynomial which only contains a low number of non-zero coefficients, is obtained by means of a reduced number of possibly costly model evaluations. Here we focus on sparse regression schemes based on $\mathcal{L}_1$-penalization as implemented in the Open Turns [6], [5], [78] Equation (4.13) known as the LASSO method (Least absolute shrinkage and selection operator). The proposed approaches do not provide only one approximation, but a collection of sparse approximations with non-decreasing sparsity indices (number of non zero coefficients)

$$Minimize \sum_{i}^{N} (f(x^i) - a^T \psi(x^i))^2 + C\|a\|_1^2, \tag{4.13}$$

where $\|a\|_1 = \sum_{j=0}^{P-1} |a|$ and C is a non negative constant. The LASSO provides a sparse meta-model, i.e. it discards insignificant variables from the set of predictors, the sparsity index decreases as C increases. For a given $C \geq 0$, the solution of the optimization problem Equation (4.13) may be obtained via quadratic programming.

4.2.1 Isoprobabilistic transformation

For standard distributions, the associated families of orthogonal polynomials are well-known [100]. For example if X is Gaussian then the best corresponding family is the Hermite polynomial family. In OpenTurns [5], [6], four types of polynomial families are implemented:

- Hermite family for Gaussian variables $\mathcal{N}(0, 1)$
- Legendre family for Uniform variables $\mathcal{U}(-1, 1)$
- Laguerre family for Gamma variables $\mathcal{G}(k, 1, 0)$
- Jacobi family for Beta variables $\mathcal{B}(r, t, -1, 1)$

The input random vector X under consideration may have other types of marginal PDF that belongs to the mention group but with other parameters or marginal PDF not belonging to the group (e.g. lognormal distribution) or the X may have correlated components. In this context the original input random vector X is recast as a random vector whose whose margins are independent and have PDF's among the ones mentioned. In OpenTurns the input random vector can have two different forms. An input random vector X with independent margins $\{f_{x_1}(x_1), ..., f_{x_M}(x_M)\}$ or a Gaussian vector X with correlated components. Once the original input random vector has been transformed, the PCE is applied and produces PCE expansion which is a function of a set of reduced variables.

In practical uncertainty quantification problems the random variables which model the input parameters are usually not standardized. The selection of the orthonormal polynomials is performed with the use of isoprobabilistic transformation (e.g. the Rosenblatt transformation). The isoprobabilistic transformation τ of random vector X into a set of reduced variables U can be performed as follows [92]:

$$X = \tau(U). \tag{4.14}$$

Depending on the marginal distribution of each input variable X_i, the associated reduced variable U_i may be standard normal $\mathcal{N}(0,1)$, standard uniform $\mathcal{U}(-1,1)$, etc. Then the random model response Y is cast as a function of the reduced variables by composing the computational model f and the transform τ:

$$Y = f(X) = f \circ \tau(U) = \sum_{\alpha \in \mathbb{N}^{\mathbb{M}}} y_\alpha \Psi_\alpha(U). \tag{4.15}$$

For example when dealing with independent uniform distributions with support $D_{x_i} = [a_i, b_i], i = 1, ..., d$, the isoprobabilistic transform reads [92]:

$$X_i = \frac{a_i + b_i}{2} + \frac{b_i - a_i}{2} U_i \quad U_i \sim \mathcal{U}([0,1]).$$

In the case of Gaussian independent variables $\{X_i \sim \mathcal{N}(\mu_i, \sigma_i), i = 1, ..., d\}$, the one-to-one transformation is:

$$X_i = \mu_i + \sigma_i U_i \quad U_i \sim \mathcal{N}(0,1)$$

4.2.2 Kriging

Originally used for mining exploration models by the South African mining engineer called Krige. The mathematics were further developed by the Matheron [48]. Later on, Kriging models were applied to the Input/Output data of deterministic simulation models. These models have k-dimensional input where k is a given positive integer (whereas geostatistics considers only two-dimensional input) [80].

More recently the kriging was applied to random simulation models by Van Beers and Kleijnen [48]. Kriging models a deterministic response as the realisation of a stochastic process by means of a kriging basis function. It uses spatial correlation between the sampled points to interpolate the values in the spatial field.

The generic kriging prediction equation can be written as following:

Let Y is an Gaussian process on $\mathbb{R}^d$ where Y is observed at $x_1, x_2, ..., x_n \in \mathbb{R}^d$ and the covariance function C of Y is known and the mean function of Y is 0. Let the $Y_n = (Y(x_1), ..., Y(x_n))^t$ is the Gaussian observation vector, R is the $n \times n$ covariance matrix of $Y_n : (R)_{i,j} = C(x_i, x_j)$. Let the $x_{new} \in \mathbb{R}^d$ be a new input point for the Gaussian process Y where we want to predict $Y_{x_{new}}$.Let the r be the n covariance vector between y and $Y(x_{new}) : r_i = C(x_i, x_{new})$

Then with the Gaussian conditioning theorem we can get the conditional mean of $Y(x_{new})$ given the observed values in Y_n:

$$\hat{\mathbf{f}}(x_{new}) := \mathbb{E}(Y(x_{new}|Y_n)) = r^t R^{-1} Y_n \tag{4.16}$$

Where we also have the conditional variance:

$$\hat{\sigma}^2 := var(Y(x_{new})|Y_n) = C(x_{new}, x_{new})) - r^t R^{-1} r \tag{4.17}$$

Example of Kriging prediction on picture 4.1

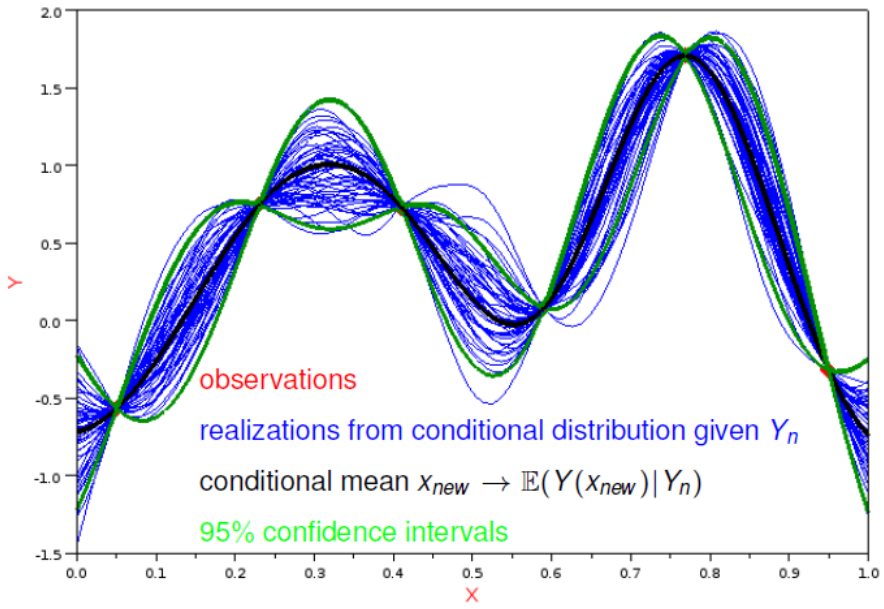

Figure 4.1: Example of one-dimensional data interpolation by kriging, with 95% confidence intervals. Red circles indicate the location of the data. The kriging interpolation, shown in black, runs along the means of the normally distributed confidence intervals shown in green [4].

4.2.3 Karhunen–Loève decomposition

Before applying the Polynomial chaos expansion on the field function we first compute the Karhunen-Loève decomposition of the output proces on the function $f(x)$ with known trajectories. Then we create a polynomial chaos decompositions between the coefficients of the input and output processes. Finally, we create a meta-model of the whole field model by combining the KL decomposition and the polynomial chaos.

Among the collection of random field discretization methods, the Karhunen-Loève (K-L) decomposition (in some references as K-L expansion) is one of the most widely used techniques for dimension reduction, since it can capture the variability of the uncertain quantity using a few number of random variables [28].

The Karhunen-Loève decomposition (K-L decomposition) is a representation of a stochastic process as an infinite linear combination of orthogonal functions, analogous to a Fourier series representation of a function on a bounded interval. The transformation is also known as eigenvector transform, and is closely related to principal component analysis (PCA) technique widely used in data analysis in many fields. The K-L is enabling a stochastic field to be represented with a minimum number of degree of freedom [55].

If the K-L decomposition is applied to a given stochastic field, we get a set of empirical eigenfunctions. When we want to reproduce that stochastic field with a certain criterion of accuracy, it can be represented with a minimum number of degree of freedom when employing these empirical eigenfunctions [7].

According to Grigoriu [28], the K-L decomposition is particularly applicable for the representation of homogeneous and non-homogeneous, as well as strongly correlated random fields. However, the major drawback of the method lies in the solution of the associated integral eigenvalue problem, given by an homogeneous Fredholm integral equation of the second kind. Most of the methods used for the estimation eigenvalue problem, e.g. Galerkin and Nyström methods, result in a reasonable computational cost, since they often deal with the assembly of dense covariance matrices.

The K-L decomposition allows to build finite approximations of stochastic processes which are optimal with respect to the norm L^2 [5], [6].

We suppose that $C : \mathcal{D} \times D \to \mathcal{S}_d^+\mathbb{R}$ is a covariance function defined in $\mathcal{D} \in \mathbb{R}^n$, continuous at 0.

The K-L algorithm enables to determine the solutions of the second kind Fredholm equation associated to C i.e. to find the $(\lambda_k, \varphi_k)_{k\geq 1}$ such that:

$$\int_{\mathcal{D}} C(s,t)\varphi_k(t)dt = \lambda_k\varphi_k(s) \ \ \forall s \in \mathcal{D} \tag{4.18}$$

where $(\lambda_{k\geq 1})$ is a non increasing sequeance of nonnegative values (the eigenvalues) and $(\varphi_{k\geq 1})$ the associated sequence of eigenfunctions, normalised by $\int_{\mathcal{D}} \|\varphi_k(s)\|^2 = 1$. They form an Hilbertian basis of $L^2(\mathcal{D}, \mathbb{R}^d)$.

The Mercer theorem shows that the covariance function C writes:

$$C(s,t) = \sum_{k=1}^{+\infty} \lambda_k\varphi_k(s)\varphi_k^\top(t) \ \ \forall (s,t) \in \mathcal{D} \times \mathcal{D} \tag{4.19}$$

The threshold s is used in order to select the most significant eigenvalues, i.e. all the eigenvalues such that:

$$K_s = min\Big\{k \in \mathbb{N} | \sum_{i=1}^{k} \lambda_i \geq (1-s) \times \sum_{i\geq 1}^{+\infty} \lambda_i\Big\} \tag{4.20}$$

To solve the eq. (4.18) we use the functional basis $(\theta_p)_{1\leq p\leq P})$ of $L^2(\mathcal{D}, \mathbb{R})$ with P elements defined in $\mathcal{D}$.

The solution is searched like:

$$\tilde{\varphi} = \sum_{p=1}^{P} \phi_{pk}\theta_p(t)$$

where $\phi_{pk} \in \mathbb{R}^d$ we note:

$$\Phi_k = \begin{pmatrix} \phi_{1k} \\ \cdots \\ \phi_{Pk} \end{pmatrix} \in \mathbb{R}^{Pd}$$

and $\Phi = (\Phi_1 | \ldots | \Phi_K)$ is the matrix of the K first modes of the Karhunen Loève decompositions The approximated Fredholm problem writes for all $k \geq 1$:

$$\int_{\mathcal{D}} C(s,t)\tilde{\varphi}_k(t)dt = \lambda_k\tilde{\varphi}_k(s) \ \ \forall s \in \mathcal{D}$$

Which enables to define the residual function $r : \mathcal{D} \to \mathbb{R}^d$ defined by:

$$r(s) = \int_{\mathcal{D}} C(s,t)\tilde{\varphi}_k(t)dt - \lambda_k\tilde{\varphi}_k(s) \tag{4.21}$$

The Fredholm problem writes:

$$r(s) = 0 \ \ \forall s \in \mathcal{D}$$

Which can be solved by the Galerkin or the collocation approach. The integrals in equation 4.21 can be evaluated with a singular value decomposition approach (SVD).

The singular value decomposition (SVD) approach is a particular case of the quadrature approach where the functional basis $((\theta_p^j(s))_{1\leq j\leq d, 1\leq p\leq P}$ of $L^2(\mathcal{D},\mathbb{R}^2)$ defined on $\mathcal{D}$ by:

$$\theta_p^j(s) = [C(s,s_p)]_{:,j}$$

The SVD approach is used when the covariance function is not explicitely known but only through K fields of the associated stochastic process $X : (X_1, ..., X_K)$.

it consist in:

- approximating C by its empirical estimator $\frac{1}{\tilde{K}}\tilde{X}\tilde{X}$ where $\tilde{X} = (X_1|...|X_K)$ and $\tilde{K} = K$ if the process is centered and $\tilde{X} = (X_{1-\mu}|...|X_{K-\mu})\tilde{K} = K-1$ otherwise, where $\mu = \frac{1}{K}\sum_{k=1}^{K} X_k$:
- taking the L vertices of the mesh of X as the L quadrature points.

We suppose now that $K < dL$ and we note $Y = \sqrt{W}X$ (see [29] for details).

As the matrix $\Theta = C$ is invertible, the Galerkin and collocation approaches are equvivalent and both lead to the following singular value problem for Y:

$$YY^\top \Psi_k = \tilde{K}\lambda_k \Psi_k \tag{4.22}$$

The SVD decomposition of $Y \in \mathcal{M}_{dL,\tilde{K}}(\mathbb{R})$ writes:

$$Y = U\Sigma V^\top$$

where we have $U \in \mathcal{M}_{dL,\tilde{K}}\mathbb{R}$, $\Sigma \in \mathcal{M}_{\tilde{K},\tilde{K}}(\mathbb{R}), V \in \mathcal{M}_{\tilde{K},\tilde{K}}(\mathbb{R})$ such that:

- $V^\top V = VV^\top = I_{\tilde{K}}$,
- $U\top U = I_{\tilde{K}}$,
- $\Sigma = \begin{bmatrix} \sigma_1 & & \\ & \ddots & \\ & & \sigma_{\tilde{K}} \end{bmatrix}$

Then the columns of U are the eignevectors of $YY^\top$ associated to the eigenvalues of σ_k^2. The modes and eigenvalues of a Fredholm problem are deducted for $k \leq \tilde{K}$:

$$\Phi_k = \frac{1}{\lambda_k}\sqrt{W}U_k\lambda_k = \frac{\sigma_k^k}{\tilde{K}}$$

We have:

$$\tilde{\varphi}(t) = \sum_{l=1}^{L} C(t,\xi_l)\phi_{l,k} \quad for \quad k \geq \tilde{K}$$

Where the most computationally intensive part is the computation of the SVD decomposition.

4.2.4 Example of Karhunen-Loève decomposition

For the period of 5 consecutive days with 450 point a PV production was simulated and used to create of a field model over an 1-d mesh. The threshold to select the most significant eigenvalues was set on 1e-06. Karhunen-Loève decomposition was created of a process with known trajectories and a functional chaos decomposition between the coefficients of the input and output processes was applied in the OpenTurns software [6]. The general procedure can be summarized in the following steps:

- Creation of a field model over an 1-d mesh
- Karhunen-Loéve decomposition of a process with known trajectories
- Projection of Fields
- Functional chaos decomposition between the coefficients of the input and output processes
- Build a metamodel of the whole field model

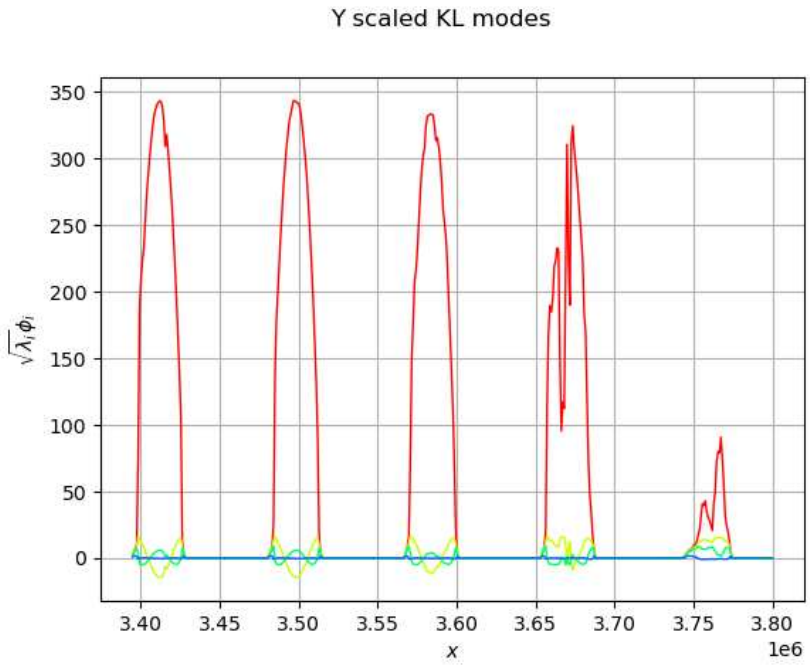

Figure 4.2: Karhunen-Loéve scaled modes.

The decomposition of the input process is presented in figure 4.3

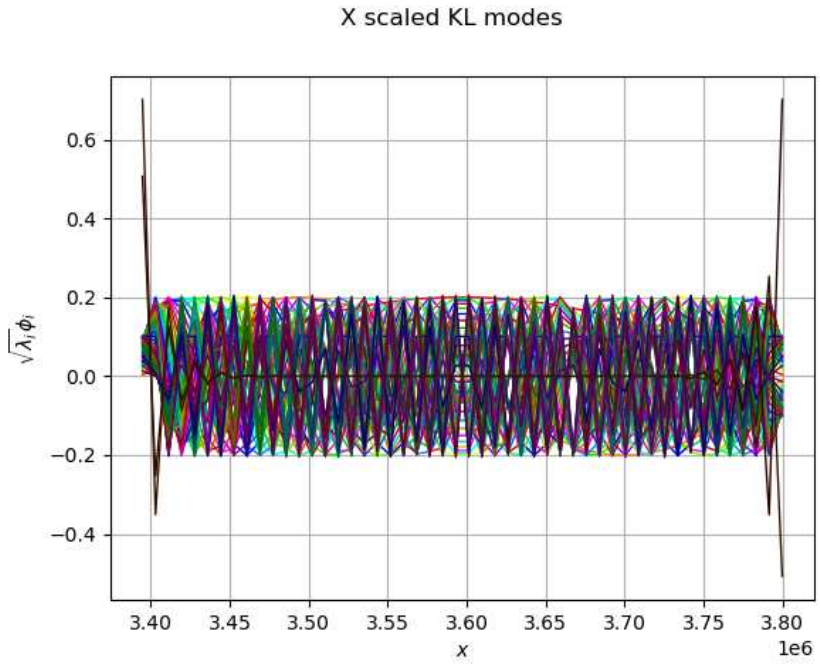

Figure 4.3: Karhunen-Loève decomposition of the input process.

The final meta-model is a composition of the KL function and the polynomial chaos meta-model. In the next chapter the PCE build meta-model is validated.

4.2.5 Artificial Neural Network (ANN) based meta-models

Lately the artificial neural networks (ANNs) has become popular in various applications. One of the domains where their properties can be used is using them as meta-models.

Artificial Neural Networks (ANN) are mathematical models which try to simulate the structure and functionalities of biological neural networks. The NN are composed of input layer, hidden layer and output layer (Figure 4.4) and can be classified as either single-layer or multilayer. A single-layer ANN consists of just one input and one output layer (Figure 4.4). On the other hand, a multi-layer ANN consists of one or more of the so-called hidden layers of neurons between the input and the output layers. Each layer is composed of computing units called neurons operating in parallel. This units are interconnected by weighed edges. The computing units or neurons perform simple operations and communicate the results to its neighboring units. The hidden layers are used to represent the relationships between the input layer and the output layer and allows a representation of the relationships among input variables. There are two main types of NN, namely Feed-forward neural networks (FNNs) and recurrent neural networks (RNNs). A RNN has neurons that transport a signal back through the network (at least one feedback connection in recurrent network) whereas FNNs feed outputs from individual neurons forward to one or more neurons or layers in the network [21].

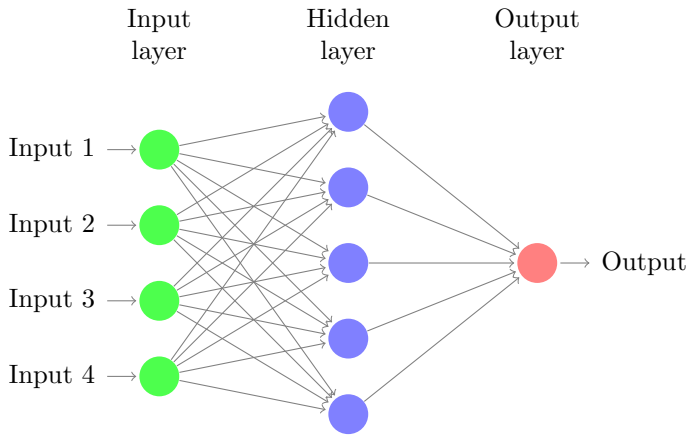

Figure 4.4: Example of Feed forward neural network.

From a mathematical viewpoint the NNs are composed of a set of nonlinear (sigmoidal) basis functions with free parameters w or weights that are adjusted to minimize the error between the output value of the NN and the real output for a given data. The iterative process of adjusting the weights is called training. The calculation of the output values using the weights is given by the equation:

$$f(X, w) = \hat{y}(X) = \psi(w_{0l}b + \sum_{j=1}^{h} w_{jl}\phi(w_{0j}b + \sum_{k=1}^{p} w_{ij}x_k)),$$

where X is an input vector with p entries, $X = (x_1, x_2, ..., x_p)$, p is the number of input variables, x_k is the k^{th} input signal, w is the weight vector, h is the number of hidden neurons, w_{ij} is the synaptic weight from i^{th} neuron to j^{th}, ϕ is the activation function from input layer to hidden layer and ψ is the activation function from hidden layer to output layer. The b is the bias factor.

An estimate $\hat{w}$ of w can be calculated by training process by minimizing the quadratic error function E:

$$E(w) = \sum_{i=1}^{n} (\hat{y}_i - y_i)^2,$$

where $\hat{y}_i = f(X_i, \hat{w})$ is the output of NN from the input X_i and n is the number of training samples.

Artificial Neural Network (ANN) as meta-models, had been successfully applied in several cases. Yuan and Guangchen [102] compared the fitness of ANN and Kriging in terms of meta-model based optimization. Kroetz et al. [51] contrasted performance of Kriging models against Neural Networks and Polynomial Chaos Expansion (PCE) meta-modelling techniques for a range of structural reliability problems and concluded that Kriging and ANN models converge more efficiently compared to PCE. Lu et al. [56] compared the approximation accuracy of the three surrogate models in groundwater remediation process. The results showed that the ANN and kriging models had better approximation accuracy and robustness than the PCE model.

4.2.6 Model Validation

Meta-models need to be validated before being used to confirm if it has the intended accuracy which is consistent with the application. The accuracy of the meta-model depends on the quality of the data set on which it was build and the meta-model type. There are several methods and measures to access the accuracy of the meta-model. It is not enough that the meta-model fits the

data on which is was developed it needs to be validated against new simulation points different from the ones used to build the meta-model [27].

The most common approach to validate the surrogate model is with a leave-one out cross validation method. The data-set $S\{X, Y\}$ consisting of N input-output data point pairs (x, y) where y is the model response at the design sample point x and N is the total number of model runs. In p-fold cross-validation, the initial data set is split into p- different subsets that is $S\{X, Y\} = S_1(X_1, Y_1), S_2\{X_2, Y_2\}, \ldots, S_p\{X_p, Y_p\}$ then the meta-model is fit p times, each times leaving out one of the subset from training and using the omitted subset to compute the error measure. One other option is to leave k- out of the validation process where all possible $\binom{N}{k}$ subsets of size k are left out and the meta-model is fit to each remaining set, the approach is more computationally intensive than p-fold cross-validation.

Through intensive testing Lin [53] found that the leave-one-out cross validation is not an appropriate measure of the accuracy instead the leave one out cross validation is actually a measurement for degrees of insensitivity of a meta-model to lost information [53]. According to the [36] the drawback of the cross validation method is that it's cost can become huge because of many meta-model fitting processes.

Another approach is the test sample approach [36] which consists in comparing the meta-model predictions on simulations not used in meta-model fitting process. This method requires new calculations with the computer code where for CPU time expensive codes it can be difficult to provide enough points. Another question is the localisation of these test points. The usual practice is to choose an independent Monte Carlo for the test sample but in the case where the sample size is small the proposed points can be badly localised [36]. The test sample approach can provide incorrect results for small sizes of the test sample [36].

Other available model selection validation techniques are:

- Modified leave one out [8], which uses a correction factor for the leave one out which was derived for the empirical error for ordinary least squares with small sample sizes [16] where the correction factor depends on the experimental design
- Kashyap information criterion (KIC) [87] an approximation to the Bayesian model evidence, which expresses the likelihood of observations given the model.
- Sparsity [3], using the idea that a larger basis should lead to a sparser solution when the necessary basis functions enter the model, unless the ratio of basis functions to model evaluations becomes too large.

Meta-model error

The validation method are based on comparing the meta-model predictions on simulation points not used in the meta-model fitting process. The results give the prediction residuals and the global quality measures such as the meta-model generalisation error and predictivity coefficient. The new sample points are called a test sample/validation sample.

Where the test sample approach consists in comparing the meta-model predictions not used in the meta-model fitting process. Because this method requires new calculations with the computer code it can be difficult to obtain sufficient number of prediction points to obtain the required accuracy in the case of time expensive code.

The error of the meta-model (surrogate model) can be estimated via the generalisation error defined as:

Generalisation error

$$\epsilon = E\Big[\Big(\mathbf{f}(X) - \widehat{f}(X)\Big)^2\Big] \tag{4.23}$$

where $\widehat{\mathbf{f}}$ denotes the surrogate model. The estimation of ϵ can be obtained with Monte Carlo simulation in the case when large amount of validation data is available.

The input vector $X_{val}^{(n)}$ and the response of the n-th validation data $Y_{val}^{(n)}$. The mean square error of data discrepancy is defined as:

$$\epsilon_{val} = \frac{1}{N_{val}} \sum_{n=1}^{N_{val}} \Big(\mathbf{f}(X_{val}^{(n)}) - \widehat{f}(X)_{val}^{(n)})\Big)^2 \tag{4.24}$$

and it converges to ϵ in the case the size of N_{val} goes to infinity. The quality of the meta-model can be measured with the coefficient of determination (called as well as predictivity coefficient Q_2) can be computed on the test sample which gives the percentage of the explained variance by the meta-model:

Coefficient of determination

$$R_{val}^2 = 1 - \frac{\epsilon_{val}}{Var(f_{val})} \tag{4.25}$$

Where:

$$Var(f_{val}) = \sum_{n=1}^{N_{val}} (f_{val}^{(n)} - \widehat{f}_{val})^2/(N_{val-1}) \tag{4.26}$$

and

$$\widehat{f}_{val} = \sum_{n=1}^{N_v al} f_{val}^{(n)}/N_{val} \tag{4.27}$$

The closer the R_{val}^2 is to 1 the more accurate is the prediction of $\widehat{f}$.

One of the possible issues of the meta-model is the over-fitting which means that the model has very small fitting error but a large prediction error and generally occurs when the model has too many parameters relative to the number of observations in the fitting set.

There are several measures of goodness of fit which take into account the residual error and the model complexity. One method is the generalised cross validation [18] and final prediction error [2]. Those error measures need to be evaluated on meta-models with various complexity fitted to the same data set where the model with the lowest value is selected. If the fitting error of the meta-model is defined as root mean squared error (RMSE) the generalised cross validation and the final prediction error is defined as:

$$RMSE_{GCV} = \frac{RMSE}{(1 - \frac{v}{n})^2} \tag{4.28}$$

and

$$RMSE_{FPE} = RMSE\frac{n + v}{n - v} \tag{4.29}$$

where n is the number of the fitting points and v is the number of model parameters.

4.3 Meta-model validation example

Before applying the polynomial chaos expansion the Karhunen-Loève decomposition of a sample of trajectories was computed. A numerical code for PV performance (PVZEN) was simulated for a period of 5 days in 15 minutes interval (450 points). Four different LHS sample sizes, namely 100, 250, 500 and 1000 were used to compare how the LHS sample size is affecting the accuracy of the PCE meta-model. The accuracy was calculated as a mean absolute percentage error (MAPE) between the model and meta-model defined as:

$$MAPE = \frac{1}{n}\sum_{t=1}^{n}\left|\frac{Y_t - \hat{Y}_t}{Y_t}\right| \times 100, \tag{4.30}$$

where Y_t is the simulated value with the model and $\hat{Y}_t$ is a simulated value with the meta-model. The absolute value in this calculation is summed for every point and divided by the number of points n. Multiplying by 100% makes it a percentage error. In general, more sample points give more information for the function but at the higher computational cost.

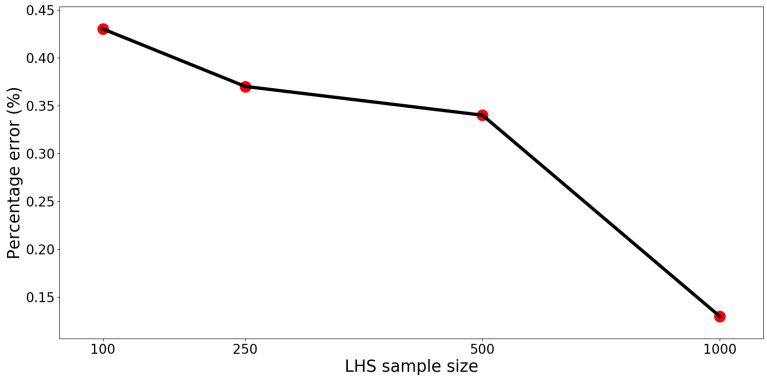

Figure 4.5: Accuracy of the meta-model based on the DOE sample size.

In Figure 4.5 the relative difference between meta-model and model is calculated for different LHS sample sizes. The mean absolute percentage error regarding the LHS sample size is between 0.13% and 0.43%. The mean absolute percentage error is comparable for three different sample sizes 100,250 and 500, 0.43%, 0.37%, 0.34% respectively. The meta-model build with 100 is selected as the final because of the satisfactory accuracy and short construction time.

Comparing the 5 days of PV production simulated with model vs meta-model with 3 sets of different parameters in Figure 4.6 shows good accuracy of the meta-model.

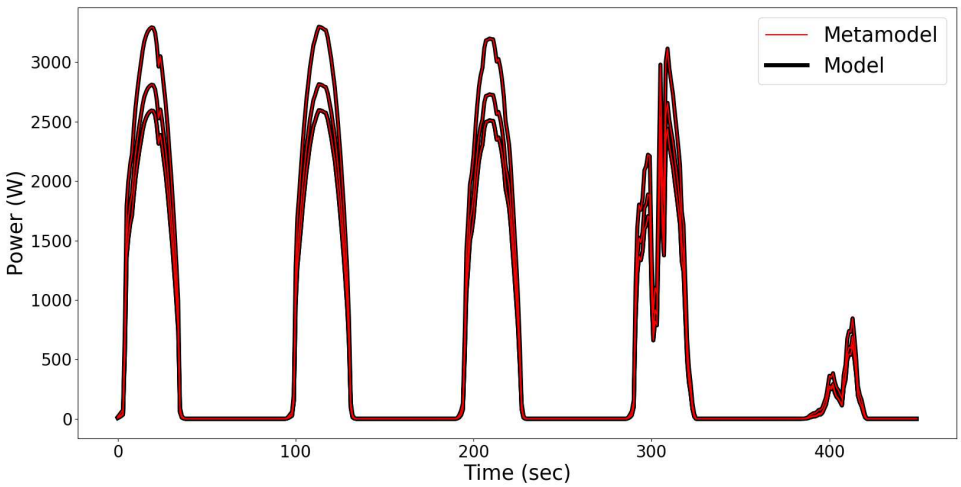

Figure 4.6: Comparing three realisations of the meta-model vs. model with same parameter values.

Calculating the coefficient of determination show good accordance of the meta-model with the model and it is 0.99986 in the ideal case it would be 1. For the meta-model validation a k-fold cross validation was used. With the cross validation the sample is divided in a learning sample and test sample. The test sample approach consists in comparing the meta-model predictions not used in the meta-model fitting process. The meta-model is estimated on the new points in the learning sample. The process is repeated several times where the meta model predictions are compared with the model predictions. The Figure 4.7 show 100 realisations of meta-model on the points not used in the meta-model construction process compared with 100 realisations of the model. For every simulation of the meta-model a model was simulated at the same time. On the Figure 4.7 a meta-model simulation of 500W of PV production corresponds almost perfectly to the 500W simulated with the model, all the points are on the diagonal line.

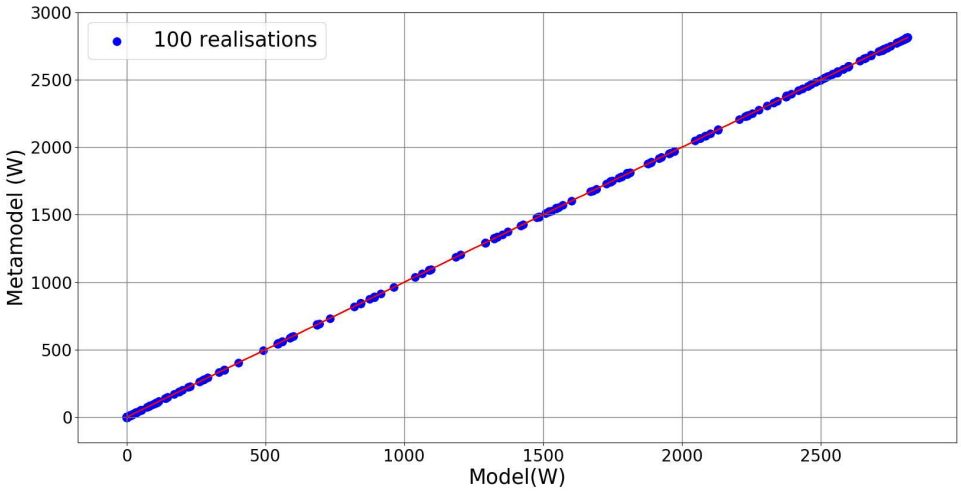

Figure 4.7: Meta model validation.

The figure 4.7 shows that the meta-model has a good predictivity, since the points are almost on the first diagonal.

4.4 Conclusion

Meta-model allows to emulate the computationally expensive codes with a relatively simple mathematical function that approximates the input/output relationship of the full code. The meta-modeling can be categorised according to sampling, model and model fitting.

The sampling of the meta-models evolves from the design of experiments presented in the chapter 2. The meta-models directly evolve from the design of experiment theory in which polynomial functions are used as a response surfaces or meta-models. Usually the polynomial functions are applied as meta-model, Sacks [80] proposed the use of Kriging based on stochastic models, to treat the deterministic computer response as a realization of a random function with respect to the actual system response.

For the non-linear problems the Kriging-models are more accurate but difficult to obtain, according to [98] Kriging is also more flexible in either interpolating the sample points or filtering noisy data. On the other hand a polynomial model is easy to construct, it is computationally cheap but it is less accurate than the Kriging model [40].

One of the most important steps of building meta-model is their validation. Meta-models need to be validated before being used as a surrogate of the computationally intensive codes. Lin [53] found that leave one out is an insufficient measurements for meta-model accuracy. The validated meta-model by leave one out could be far from the actual as the data points may not be able to capture the actual behaviour.

Currently meta-model is mostly used for approximating models and they behaviour where the models are usually used as "black-box" functions. According to [98] the focus on sampling should shift to how to generate a minimum number of sample points intelligently so that the meta-model reflects the real "black box" function of interest.

The results of the chapter show that the meta-model obtained with the PCE on the PV yield code shows almost perfect agreement with the initial model. The meta-model validation shows that the coefficient of determination is 0.99986 which means that the meta-model can explain almost all the variability of the model.

Chapter 5

Calibration

The chapter gives an overview of different calibration techniques and the application on the outdoor PV data. In the case where the IV curve measurements are available from the PV field the calibration is straightforward using a simple single diode model to estimate the parameter values in certain operating conditions. Because IV curves are usually not available from the PV field the calibration using only the maximum power is presented. Because of the model over-parameterization and measurements noise the parameter identification can be difficult. At the end more a robust calibration procedure using Approximate Bayesian Computation is presented

Contents

5.1 Calibration

Calibration consists of searching for a set of values of the unknown inputs such that the observed data fit as closely as possible to the corresponding outputs of model [47]. To solve the minimization problem usually many code calls from the model response represented by $f(x)$ are needed before reaching the optimal solution or desired accuracy with the set objective function. Verifying the model usually requires that the parameters are validated against experimental data where the model accuracy can be assessed. By tuning the parameters we can usually improve the model accuracy. The parameters can either be tuned manually or by an optimization aimed at minimizing the difference between experimental data and the model response.

Calibration intends to find the parameters by minimizing the sum of squared differences between the output and the experiments. The general approach of the calibration is summarized in the Figure 5.1.

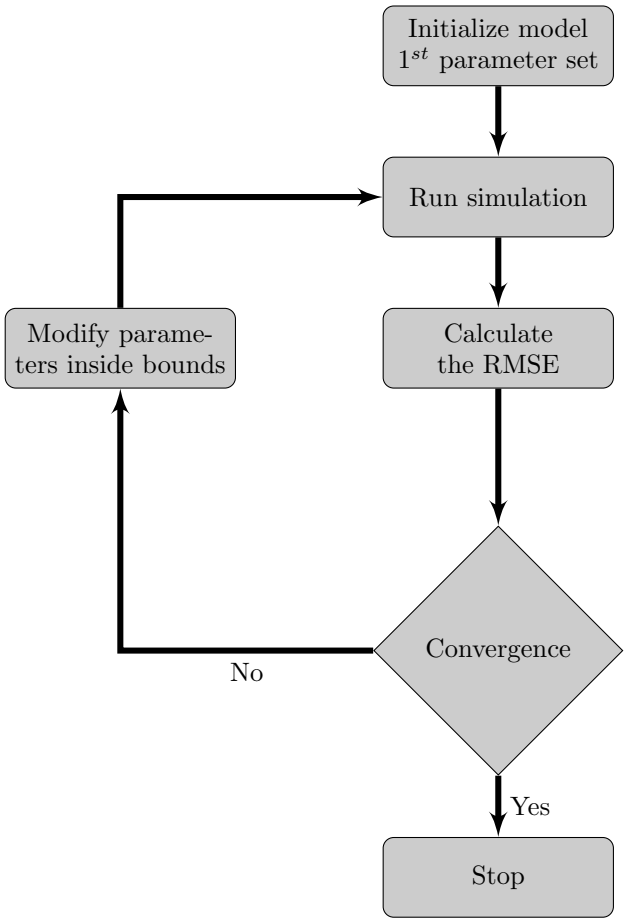

Figure 5.1: Calibration Loop.

The objective function considered is following:

Objective Function RMSE

$$Q_{obj}(\theta) = \sqrt{\frac{1}{2}\sum_{i=0}^{M}(Y^{sim}(t_i,\theta) - Y^{meas}(t_i))^2} \tag{5.1}$$

where Y^{sim} is the model output trajectory and Y^{meas} are the measurements. The parameters to be estimated are θ and M is the number of measurements at the time points t_i.

The calibration problem generally corresponds to the minimization of the objective function $Q_{obj}(\theta)$:

$$\begin{aligned} &minimize\ Q_{obj}(\theta) \\ &s.t\ \theta \in \Omega \end{aligned} \tag{5.2}$$

where Q_{obj}, $\mathbb{R}^n \to \mathbb{R}$, $\theta \in \mathbb{R}^n$ is the decision variable (parameters to calibrate) and $\Omega \subseteq \mathbb{R}^n$ is the constraint set (or feasible set). Here the s.t. is a short hand notation for 'subject to'. Typically, the set Ω is given in a functional form:

$$\Omega = \{\theta \in \mathbb{R}^n \mid g_i(\theta) \leq\ 0, i = 1, ..., m,\ h_j(\theta) = 0,\ j = 1, ..., k\} \tag{5.3}$$

for some functions $g_i\ , h_j : \mathbb{R}^n \to \mathbb{R}$.

An optimal solution θ^* (also referred to as the arg min of Q_{obj} over Ω) is a point in Ω that satisfies:

$$Q_{obj}(\theta^*) \leq\ Q_{obj}(\theta),\ \text{ for all } \theta \in \Omega \tag{5.4}$$

5.2 Optimization algorithms

There are many available optimization algorithms that can be used for solving a specific optimization problem. The optimization problems can be divided into local and global where the local ones attempts to find the local optimum without the guarantee that the local optimum will be the global one. In the cases with several local optima different results can be obtained depending on the starting conditions of the optimization. The majority of the optimization algorithms uses the gradient information to find the optimum solution. Gradient based algorithms are usually efficient and can solve problems with many design variables [15]. Gradient-based algorithms can identify only the local optima. One of the possible solutions in dealing with multiple local optima is to use a multi-start approach where multiple local searches are performed with different starting points [77].

If global optimum is needed, global optimization algorithms are used and can be classified into two main categories: deterministic and stochastic [101]. Deterministic algorithms solve an optimization problem with generating deterministic sequence of points which are converging to the global minimum. Such algorithms will give the same results every time and behave predictably. To apply deterministic algorithms the optimisation problem should have certain mathematical properties.

On the other hand the stochastic optimization algorithms are using randomly generated points which are used for non-linear local optimization search procedures. Compared to the deterministic approaches they usually have fewer restrictions and do not require any gradient information.

The drawbacks of the stochastic algorithms include poor constraint-handling abilities, problem specific parameter tuning and limited problem size [96]. Typical stochastic optimization algorithms include genetic algorithms, evolutionary strategies, particle swarm optimization and simulated annealing. The selected algorithms will be presented in the following section.

5.3 Gradient-Based Algorithms

Gradient based optimization algorithm are using the gradient information to find the optimum solution of the objective function. The gradient information is usually obtained using finite difference gradient calculations. Gradient based techniques are popular because they are efficient (in terms of function evaluations to find the optimum), can solve problems with multiple design variables and require little parameter tuning. The drawbacks of the gradient based approaches are that they can locate only a local optimum.

Another disadvantage is that they are not efficient at solving discrete optimization problems and are difficult to implement [96]. The difference between various gradient based optimization algorithms is how they determine the search direction.

Newton's Method

Newton method is one of the classical gradient based optimization algorithm. The algorithm is an unconstrained algorithm that is derived from second-order Taylor series expansion of the objective function about the initial design point x^0.

$$f(x) \approx f(x^0) + \bigtriangledown f(x^0)^T(x - x^0) + \frac{1}{2}(x - x^0)^T H(x^0)(x - x^0) \tag{5.5}$$

Where $H(x^0)$ is the Hessian matrix that contains the second-order gradient information of the objective function. We need to assume that the Hessian matrix is invertible. Differentiating the equation with respect to x and setting the results equal to zero according to the Karush-Kuhn-Tucker conditions, results in update formula for the current design point:

$$x = x^0 - H(x^0)^-1 \bigtriangledown f(x^0) \tag{5.6}$$

In this form the method uses a fix step size of 1 and the search direction is provided by $-H(x^0)^-1 \bigtriangledown f(x^0)$. The Newthon's method has a quadratic rate of convergence requiring only a single step to obtain the optimum for any positive definite quadratic function. The rate of convergence of Newton method is at least quadratic if the following conditions are satisfied:

1. $f'(x) \neq 0 \ \forall \, x \in I$ where I is the interval $[a - r, a + r]$, (where a is the zero of the function $f(a) = 0$, and x_0 is the starting value of x) for some $r \geq |a - x_0|$;
2. $f''(x)$ is continuous $\forall \, x \in I$
3. x_0 is sufficiently close to the root a

The method has a quadratic convergence rate which is desirable, but the computational cost associated with obtaining the second-order gradient information in the Hessian matrix makes the method impractical in most cases [96].

Fleetcher-Reeves

The Fleetcher-Reves uses the conjugate search direction to reach the optimum. The conjugate directions are obtained from the information obtained from the previous iteration. It has the advantage of small computer memory requirements [96].

Broyden-Fleetcher-Goldfarb-Shanno (BFGS)

The BFGS makes use of the information obtained from the previous n iterations to find a new search direction. Numerical experiments indicate that BFGS is method is the most efficient variable metric

method. The BFGS creates an approximation of the Hessian matrix where this approximation is updated after each iteration with the first-order gradient information from that iteration. The method is known as quasi-Newton method [96].

5.4 Gradient Free Based Algorithms

The development of gradient-free optimization algorithms-also referred as a black box optimization-was driven by the increasing complexity of optimization problems in simulation studies where gradient information is rarely available. Even if gradient information is available it can be difficult and unreliable to compute it. Non-gradient optimization methods do not require gradient information to converge to the optimum solution. These methods rely on function evaluations of the objective function to reach convergence.

5.4.1 Nelder-Mead simplex algorithm

The Nelder-Mead algorithm starts with a initial set of points that forms a simplex. In each iteration the objective function values at the corner points of the simplex determine the worst corner points. The algorithm replaces the worst points with new vertex in a way that results in the new simplex. Candidate replacement points are obtained by transforming the worst vertex with various operations on the centroid of current simplex [75].

5.4.2 Generalized pattern search (GPS)

GPS generalizes direct pattern search. At the beginning of a new iteration, GPS search by explanatory moves. From the current iteration GPS defines a set of points that form a pattern, determined by a step and generating a matrix that spans in $\mathbb{R}^n$ [75].

5.5 Evolutionary algorithms

Evolutionary algorithms are based on principles of biological evolution and became popular in the last three decades. Evolutionary algorithms do not require any gradient information and make use of a populations set to find the optimum design. The methods are inspired by phenomena from nature and have the advantage of being extremely robust to find a global or near global optimum. The drawbacks associated with these algorithms are high computational costs, poor constraint-handling abilities, problem-specific parameter tuning and limited problem size [96].

The well known evolutionary algorithms are the Genetic Algorithm (GA) [41], which was inspired by Darwin's principle of survival of the fittest and Particle Swarm Optimization (PSO) which is based on the social model [22].

The basic steps of Genetic Algorithm (GA) are illustrated in the figure bellow.

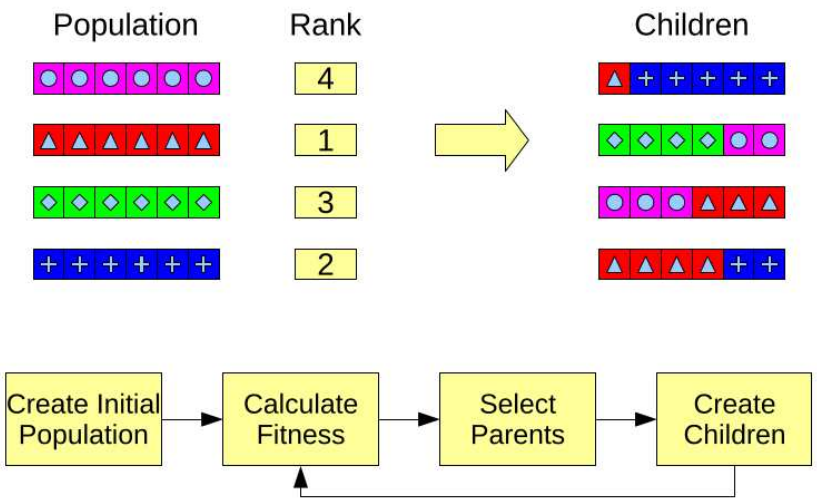

Figure 5.2: Basic evolutionary algorithm [96].

The first step is to create a random initial population where the population size does not change during the optimization. The population is ranked based on the fitness of the objective function of each individual and parents are randomly selected for reproduction. The parent designs are selected in such way that the individuals with the higher rank have a higher probability of being selected. The next generation is created by mixing the selected parents with cross over. The next generation is ranked again and the whole process is repeated until convergence is reached.

5.5.1 Covariance Matrix Adaptation Evolution Strategy (CMA-ES)

CMA-ES is a stochastic, derivative-free methods for numerical optimization of non-linear or non-convex continuous optimization problems [30]. It is broadly based on the principle of biological evolution, namely the repeated interplay of variation (via recombination and mutation) and selection: in each generation (iteration) new individuals (candidate solutions, denoted as x) are generated by variation, usually in a stochastic way, of the current parental individuals. Then, some individuals are selected to become the parents in the next generation based on their fitness or objective function value $f(x)$. Like this, over the generation sequence, individuals with better and better f-values are generated. Problem can be stated as: Given an objective function:

$$f : \chi \subset \mathbb{R}^n \longrightarrow \mathbb{R} \tag{5.7}$$

Minimize f in a black-box scenario (direct search, no gradients)

Figure 5.3: Black-Box Scenario.

The problem domain specific knowledge is used only within the black-box. Objective is

- convergence to a global essential infimum of f as fast as possible
- find $x \in \chi$ with small $f(x)$ value using as few black-box calls as possible

The optimization is based on stochastic search:
Initialize distribution parameters θ, set population size $\lambda \in \mathbb{N}$ while not terminate:

- Sample distribution $P(x|\theta) \longrightarrow x_1, ..., x_\lambda \in \mathbb{R}^n$
- Evaluate f on $x_1, ..., x_\lambda$
- Update parameters $\theta \longrightarrow F_\theta(\theta, x_1, ..., x_\lambda, f(x_1, ..., f(x_\lambda))$

For the application of the CMA-ES, an initial guess, an initial standard deviation (step-size, variables should be defined such that the same standard deviations can be reasonably applied to all variables) and, possibly, the termination criteria (e.g. a function tolerance) need to be set by the user [30]. With CMA-ES calibration we are not taking into account the discrepancy between the model output and the measured data. With CMA-ES the best possible set of parameter values are calibrated to match as closely as possible to the observed values.

Bayesian Calibration of Computer Models

In the Bayesian calibration context the relationship between the observations z_1, the true process $\zeta(\cdot)$ and the computer model output $\eta(\cdot, \cdot)$ can be represented with in the equation as presented by the Kennedy and O'Hagan [47]

$$z_i = \zeta(x_i + e_i) = p\eta(x_i, \theta) + \delta(x_i) + e_i \tag{5.8}$$

Where e_i is the observation error for the ith observation, p is an unknown regression parameter and $\delta(\cdot)$ is a model inadequacy (model discrepancy) function that is independent of the code output $\eta(\cdot, \cdot)$. The discrepancy between the model output and the measured data is modelled as an occurrence of a Gaussian process that yields a random function over the domain of input variable space. In this context calibration can be used to calibrate code on the data collected on the PV site to forecast the behaviour of the PV plant over the next period.

Carmassi [13] was focusing on the Bayesian calibration of a PV plant to reduce the uncertainty of the PV yield assessment. To reduce the discrepancy or model error of the computational code various Bayesian calibration approaches were presented. The overall uncertainty of PV forecast was reduced for approximately 4%. The drawback of the approach is not considering degradation in the PV production forecast which could have a big impact on the Levelized Cost of Electricity (LCOE).

5.6 Calibrating when IV curve measurements are available

From an EDF monitoring test site located in a "Csa" dry-summer or Mediterranean climate (according to the Köppen-Geiger climate classification) large quantities of data were collected in 1 minute interval. 8 years of IV curves measurements from Poly Si 60 cells module were used to estimate the difference in parameter values at the first year of the installation and in one year after 8 years of outdoor operation. The number of data points in each period were comparable. Maximum power point and the fill factor were extrapolated from the I-V curves. Weather data includes irradiance in plane of array, ambient temperature and module temperature. Missing values, outliers representing measurement or sensor error were omitted from analysis.

Selecting IV curves

To evaluate the parameter values in different operating conditions the narrow window method is used (Figure 5.4) where parameters are extracted at certain outdoor temperature and irradiance

conditions, initially chosen from standard IEC 61853-1. Without translating to STC conditions the uncertainty of the measurements is reduced. We defined narrow windows with a range of G $\pm 2W/m^2$ and T$\pm 1°C$. The size of this window is a compromise between sufficient number of data points and acceptable spread between IV curves measured within the same year. Data from high irradiation conditions are used since they show less spread and additional filtering of 2 standard deviations around the mean values was used to additionally control the spread of measured and estimated values.

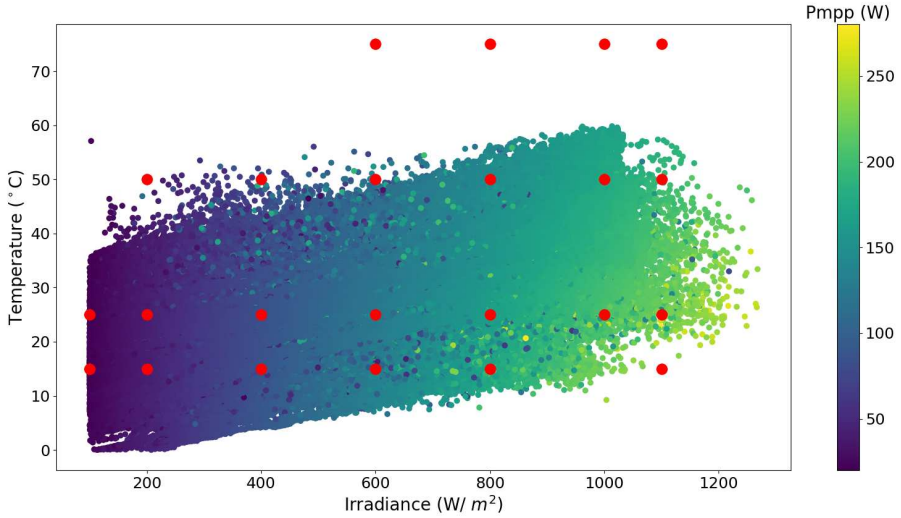

Figure 5.4: Data points where IV curves are available shown over the irradiance and temperature domain. The initial reference points are depicted in red.

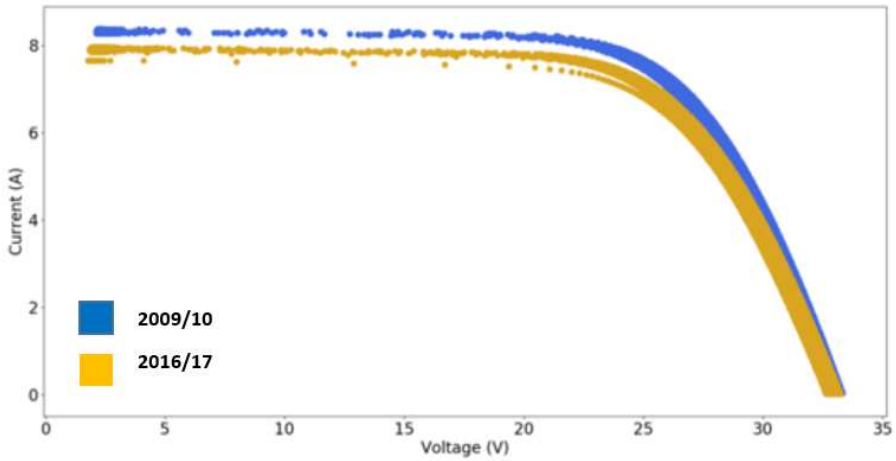

Figure 5.5: Example of selected IV curves at irradiance=1000 $\pm 2W/m^2$ and module temperature T = 50 $\pm 1°C$.

5.6.1 Parameter Estimation with a Single Diode Model

The focus of the approach is to track the evolution of estimated single diode parameters from measured IV curves in stable irradiation and temperature conditions to gain insights into the degradation of PV devices. The evolution of single diode parameters, namely the series resistance (R_s) and shunt resistance (R_{sh}) could at least partially reveal the fundamental mechanisms of degradation and their influence on the open circuit voltage V_{oc}, short circuit I_{sc} and P_{mpp}. Therefore, both R_s and R_{sh} need to be recognized and we need to understand their evolution with

changing irradiance and temperature conditions in order to improve the module performance forecast. The IV curves for the parameter estimation were selected in 4 different outdoor operating conditions from the narrow windows method namely (Figure 5.4):

- $1000W/m^2 - 50\,C^\circ$
- $1000W/m^2 - 45\,C^\circ$
- $950W/m^2 - 45\,C^\circ$
- $900W/m^2 - 40\,C^\circ$

High irradiation conditions were chosen because the IV curves variation is reduced. The initial parameter values for calibration with CMA-ES were estimated from the first year IV-curve measurement at 4 different operating conditions.

The absolute error of CMA-ES optimization that is acceptable for convergence was set on the 1.e-5 function value and the optimization procedures converged for every IV curve parameter estimation in around 5000 iterations with the Root Mean Square Error (RMSE) between 0.005-0.008. Figure 5.6 shows the convergence of parameters over the number of iterations.

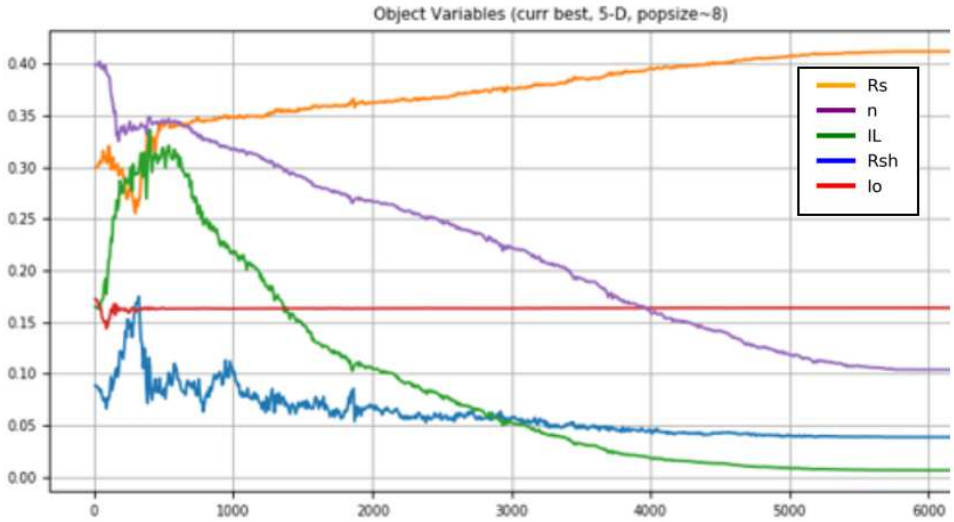

Figure 5.6: Convergence of parameters for a single IV-curve.

The change of photo current averaged over all operating conditions Figure 5.7 is -4.7% where the values of photo current do not show any temperature dependencies.

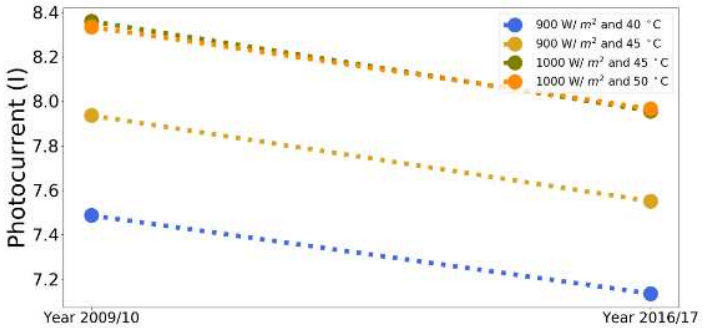

Figure 5.7: Evolution of photo current in various operating conditions.

Comparing the values of series resistance at the beginning of the lifetime and after 8 years of field operation in 4 different operating conditions do not shows any changes in the slope (figure 5.8). Averaging over all operating conditions the increase in R_s is 9.4% after 8 year. The values of the R_{sh} do not show considerable changes after 8 years of outdoor operation.

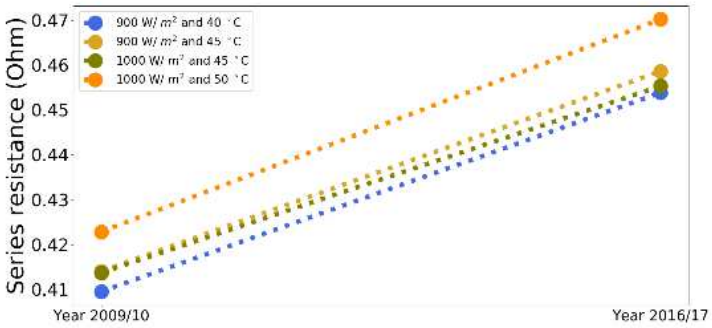

Figure 5.8: Evolution of series resistance in various operating conditions.

In order to improve the module performance forecast and service life prediction the temporal evolution of the parameter and their dependency on changing irradiance and temperature conditions needs to be understood (Figure 5.9). Currently the temperature dependency is not modelled. Moreover a estimation with confidence interval or hypothesis test should be done to draw conclusions because the uncertainty has to be taken into account.

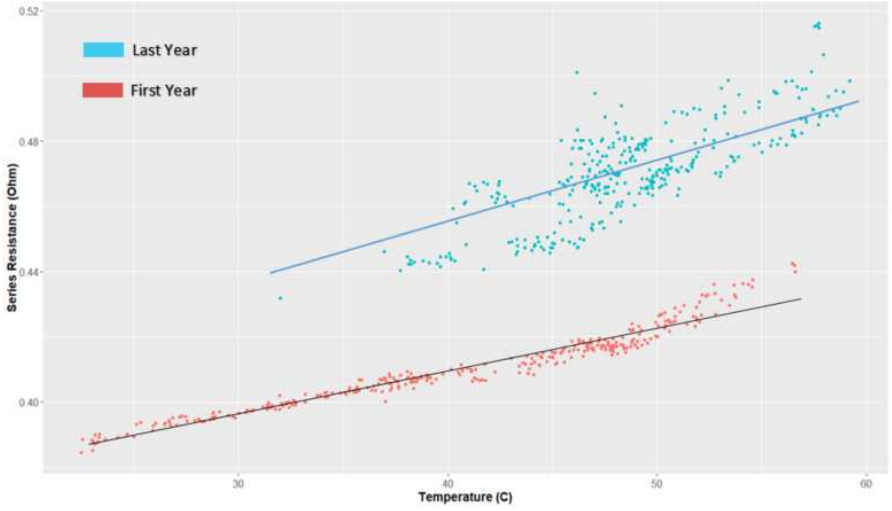

Figure 5.9: Series Resistances temperature dependence.

5.6.2 Conclusion

The approach of outdoor IV curves parameter estimation methodology was applied to study the degradation process on PV. The method with IV curve measurement relies on single diode circuit based model of PV electrical characteristics. The approach is based on a narrow window method of different environmental conditions (irradiation and temperature) combinations and allows to analyze the outdoor data without the conversion to STC conditions.

The results show that the main aging factor of fielded PV module is the decrease of short-circuit current where the main power loss is supposed to be caused by the optical degradation of the PV

modules followed by the increase of series resistance. Possible degradation modes affecting the analyzed module are yellowing or browning of EVA, delamination and appearance of bubbles or anti-reflecting coating degradation. Increase in series resistance suggest that there is a possible corrosion on metal bars or interconnections in the PV modules.

5.7 Calibration related issues

In many physical models the parameters are not directly measurable but only accessible indirectly through their impact on measured entities which are typically some time varying signals responding to some applied perturbations. Before calibrating the model and estimating the model parameters the question that needs to be answered is if the model structure is identifiable.

A model is said to be identifiable when, given an infinite amount of data, it is possible to uniquely estimate the true values of the model parameters. The uniqueness property implies that different values of the model parameters generate different probability distributions of the observable variables. Conversely if two or more sets of parameters generate identical distributions of the observed values the model is not identifiable. The parameter identification problem is often an ill-posed problem (it is a problem whose solution is not unique).

In some cases is may be still possible to uniquely identify a subset of model parameters in this case the model is partially identifiable [52].

Ordinary differential equation Ordinary Differential Equation (ODE) models often contain a large number of parameters that must be determined from measurements by parameter estimation. For a parameter estimation procedure to be successful, there must be a unique set of parameters that can have produced the measured data. In the model calibration and parameter estimation process the identifiability analysis addresses the question whether is it possible to uniquely recover the model parameters from a given set of data. For ordinary differential equation models (ODE) the problem can be divided into two groups:

- Practical or numerical identifiability: practical calibration issues which comes with the real data: measurement noise, bias etc.
- Structural identifiability: the property of structural identifiability is independent of real experimental data. The structural identifiability is determined as follows:

Let $f(x)$ be a fixed model structure with a set of parameters $x = (x_1, ..., x_{n_x})$. $f(x)$ describes the relationship between input variables and observables. Let us denote by $f(x) = f(x^*)$ the equality of the input-output behaviour of the model structure obtained for the two parameter sets x, x^*. A parameter $x_i = (1, ..., n_x)$ is structurally identifiable if the equality $f(x) = f(x^*)$ implies that the $x_i = x_i^*$ that is:

$$f(x) = f(x^*) \Rightarrow x_i = x_i^* \tag{5.9}$$

A model is structurally globally (or locally) identifiable if all its parameters are structurally globally (or locally) identifiable. A model is non-identifiable if at least one of its parameters is non-identifiable. A mathematical rigorous definition of structural identifiability is given by Walter and Pronzato [97]. In short, the identifiability issue can be described as the phenomenon that the distribution of the observed data from physical system does not uniquely determine the value of the corresponding calibration parameter given the computer model [99].

5.7.1 Sensitivity Based Identifiability

The idea of the sensitivity analysis can be also used to evaluate the "locally-at-a-point" identifiability of the unknown parameters [61]. The sensitivity based identifiability does not require experimental data, and does not directly use the model structure information. A nominal parameter value is required for the sensitivity based approach. The parameter identifiability is evaluated with respect to a specific point in a parameter space.

The sensitivity of measurable model responses with respect to parameter values can be used to assess the identifiability of unknown parameters. If the locations and the number of time points at which the model responses will be measured have been given, denoted by $t_1 \leq t_2 \leq \cdots \leq t_N$, then the sensitivity coefficient at each time point $t_k (k = 1, 2, ..., N)$ for a given nominal parameter vector θ^* is defined as:

$$s_{ij}(t_k) = \frac{\partial y_i(t_k, \theta^*)}{\partial \theta_j} \tag{5.10}$$

where $y_i (i = 1, 2, ..., d)$ denotes the i^{th} component of $y (y \in \mathbb{R}^d)$ and θ_j the $j^{th} (j = 1, 2, ..., q)$ component of $\theta (\theta \in \mathbb{R}^q)$. The sensitivity matrix for all time points is defined as:

$$S_{dN \times q} = \begin{pmatrix} s_{11}(t_1) & \cdots & s_{1q}(t_1) \\ \cdots & \ddots & \cdots \\ s_{d1}(t_1) & \cdots & s_{dq}(t_1) \\ \vdots & \vdots & \vdots \\ s_{11}(t_N) & \cdots & s_{1q}(t_N) \\ \cdots & \ddots & \cdots \\ s_{d1}(t_N) & \cdots & s_{dq}(t_N) \end{pmatrix} \tag{5.11}$$

There are various identifiability analysis techniques which have been developed based on this sensitivity matrix. Generally the larger the sensitivity coefficients are, the more sensible the model response is with respect to the changes of parameters. A parameter is likely to be practically identifiable if the model output is highly sensitive to small perturbations of this parameter, otherwise the parameter is likely to be practically unidentifiable [61]. In the case there is a high correlation between any of two parameters in the model it is probable that they will be indistinguishable from each other. There are many available methods: the correlation method, the principle component analysis method [42], the orthogonal method [37] to check the model parameters sensitivity.

5.8 Calibration when only power measurements are available

IV curves are rarely available from real PV power plants. Usually the information about P_{mpp} is available and sometimes separated values of I_{mpp} and V_{mpp}. The current method uses only the P_{mpp} data together with the PV data sheet values and corresponding weather files.

One of the issues with calibrating only the P_{mpp} data is the possibility of multiple solutions in the calibration process. The Pmpp is calculated as a

P_{mpp}

$$P_{mpp} = I_{mpp} \times V_{mpp} \tag{5.12}$$

5.8.1 Available data

The model code represents a test plant of 12 series connected panels installed on EDF site Les Renardieres in Moret sur Loing, France. Data is available for a period of multiple months where the instantaneous power (P_{mpp}) is recorded every 10 seconds. The production data and weather files are constantly checked for any recording errors. In the computational code the change in weather conditions has an instantaneous effect on the power without any delay. The input variables contain all the weather data:

- t: the UTC time since the beginning of the year in seconds,
- L: the latitude in °
- l: the longitude in °
- I_g: global irradiance (GHI) (normal incidence of the sun ray to the panel) in W/m^2
- I_d: diffuse irradiation (DGI) (horizontal incidence of the sun ray to the panel) in W/m^2
- T_e ambient temperature in °C

The weather file variables were averaged over the period of 10 minutes. Entries without recorded data were removed from analysis.

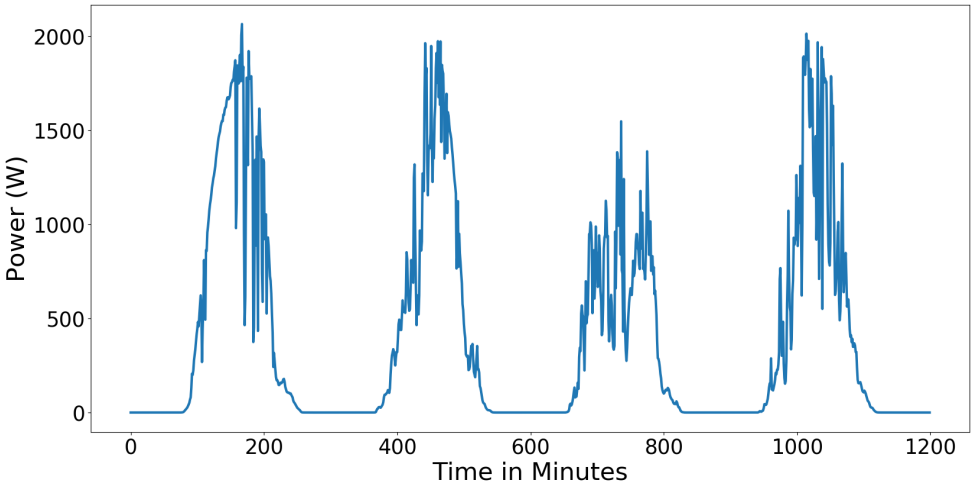

Figure 5.10: Example of simulated PV production for a period of 4 days with real meteorological data.

Example of simulated PV production for a period of 4 days starting at 1^{st} August 2014 with the weather file from the EDF PVZEN PV plant located in Les Renardieres in 5 minute time step (Figure 5.10). The simulated PV production with Dymola is highly volatile because of the passing clouds above the irradiation sensor. The simulation with the Dymola software needs approximately 40 seconds to compute the P_{mpp} on the personal computer with $i5$ 2 Ghz processor.

5.8.2 Calibration on Outdoor Data

Single day of P_{mpp}, PV production data from the EDF monitored site PVZEN was used to tune the computational code parameters to the observed values. Usually because of the numerical approximations and input file measurement errors we are not able to mimic fully the physical

process. Even with the best possible set of parameters there will be a discrepancy between the code output and observed data.

Dictionary of used terms:

- **NOMINAL** Simulated PV performance with the data sheet values of PV manufacturer with the technology related parameters
- **MEASURED** the real measured outdoor PV performance data
- **CALIBRATED** Calibrated parameter values obtained with **CMA-ES**

The nominal values of parameters are obtained from module data-sheet values while the values of R_s and R_{sh} are obtained from fitting the IV curves from analyzed modules. Nonlinear least-squares fitting algorithm had been applied to fit the double diode model parameters and extract the values of R_s and R_{sh}.

5.8.3 Parameter constraints

Prior to the calibration process the parameter bounds needs to be defined. Most parameters in the model are limited to a specific range taken from the literature or based on the expert knowledge. It is common procedure to set the parameters range acceptable to the analysis. The defined bounds need to have a physical meaning so that the interpretation of the calibration results is meaningful. The parameter constrains are the same as those used for the sensitivity analysis of the model.

Parameters	**Nominal Value**	**Bound**
I_{sc} (A)	5.44	[4,9]
R_s (Ω)	0.00012	[0.00001,0.0009]
R_{sh} (Ω)	0.14745	[0.015,0.45]
Ms	3	[2.8,3.2]
nDs	1	[0.8,1.1]
A_r	0.17	[0.12,0.25]

Table 5.1: Parameter constraints for calibration.

The convergence criteria for CMA-ES calibration was set on 2000 function evaluations or tolerance of 0.05 on RMSE where the calibration was terminated after one of the two defined criteria was reached. For the calibration the parameters are normalized to have a comparable sensitivity.

Parameters	**Nominal value**	**Calibrated**
I_{sc} (A)	5.44	6.895
R_s (Ω)	0.00012	0.000078
R_{sh} (Ω)	0.14745	0.4499
Ms	3	3.199
nDs	1	1.199
A_r	0.17	0.12
$RMSE$	98.26	89.56

Table 5.2: Calibrated parameters.

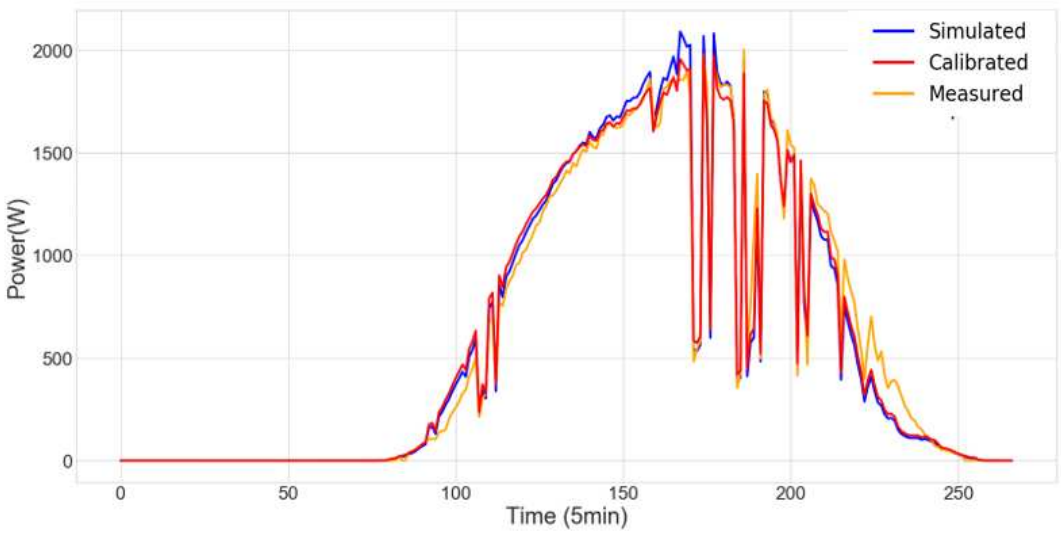

Figure 5.11: Calibrating a single day of PV production.

With the new set of the parameters the overall improvement of the RMSE of the calibrated model (optimized) is around 15%. On the figure 5.11 is evident that the discrepancy between the computational code and measured values is still substantial regardless of the calibration. To see if the calibration procedure is converging 2000 function evaluations are plotted against parameter values.

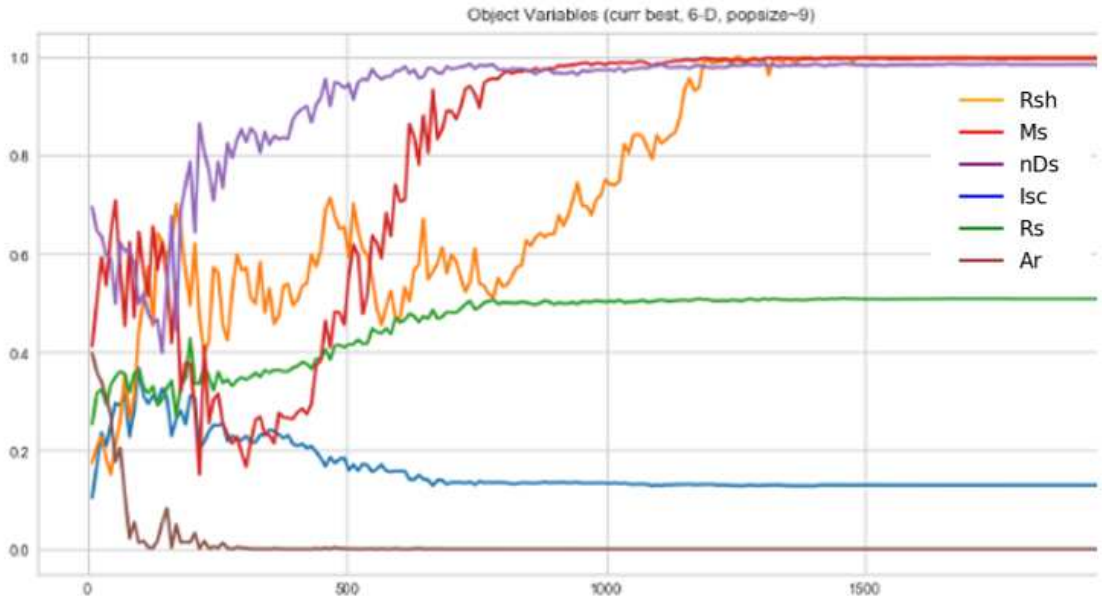

Figure 5.12: Number of function evaluations vs normalized parameters values with initial bounds.

The parameters on the figure 5.12 reached the minimum or maximum calibration bounds during the calibration procedure.

- R_{sh} Shunt Resistance **MAX**
- M_s Temperature exponent of the saturation current **MAX**
- nDs Diode Ideality Factor **MAX**

- A_r Transmission factor**MIN**

The calibration result on the outdoor data shows that the calibration is not converging because the parameter values are reaching their boundaries. The parameter bounds for the calibration could be increased for the calibration to converge without reaching the defined boundaries, but in this case the physical interpretation of the parameters would be meaningless. The possible issue is that the calibration model is overparameterized i.e. model having more parameters than can be estimated from the data.

5.8.4 Structural identifiability

Structural identifiability is a property of a model structure that ensures that parameters can be uniquely (globally or locally) determined from knowledge of the input-output behaviour of the system [46]. The theory is explained in detail in chapter 5.7.

The data was simulated with Dymola with known parameter values and then calibrated to see how will the estimated parameter values differ from the initial ones. The convergence criteria for CMA-ES calibration was set on 2000 function evaluations or tolerance of 0.05 on RMSE where the calibration was terminated after one of the two defined criteria was reached.

The calibration was performed on one two day period simulated with nominal values. A weather file of 10 minute time step was used to generate data point for the period. The initial parameter values for calibration where chosen at random from the LHS obtained sample.

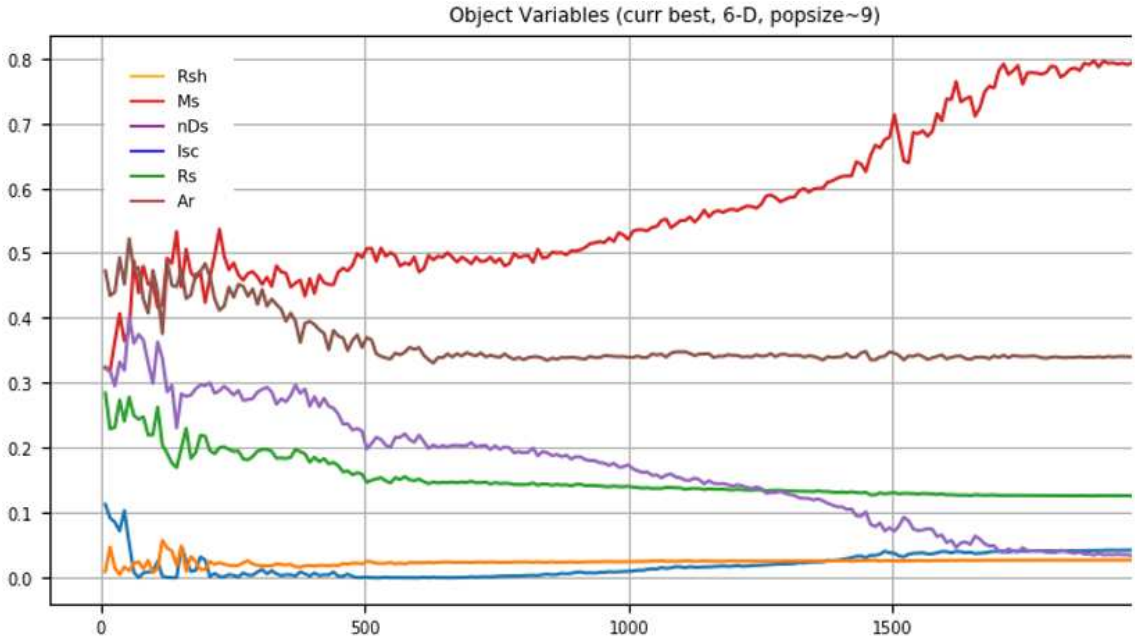

Figure 5.13: Calibration with 6 parameters, not stabilized after 2000 function evaluations.

Observing the evolution of parameters with the number of function evaluations the parameters are not stabilizing even after 2000 function evaluations.

Parameters	Nominal	Calibrated
nDs	1	0.82
R_s (Ω)	0.00012	0.0.00049
R_{sh} (Ω)	0.14745	0.1228
Ms	3	3.34
I_{sc} (A)	5.44	4.631
A_r	0.17	0.14
$RMSE$		24.21

Table 5.3: Calibrating 6 parameters.

Comparing the calibrated parameter values with the nominal values show large differences. The calibration is not converging and the RMSE remains relatively high. Simulating and comparing the daily PV production with the calibrated and nominal parameter values show small discrepancy (Figure 5.14), while the difference in nominal vs calibrated parameter values is large.

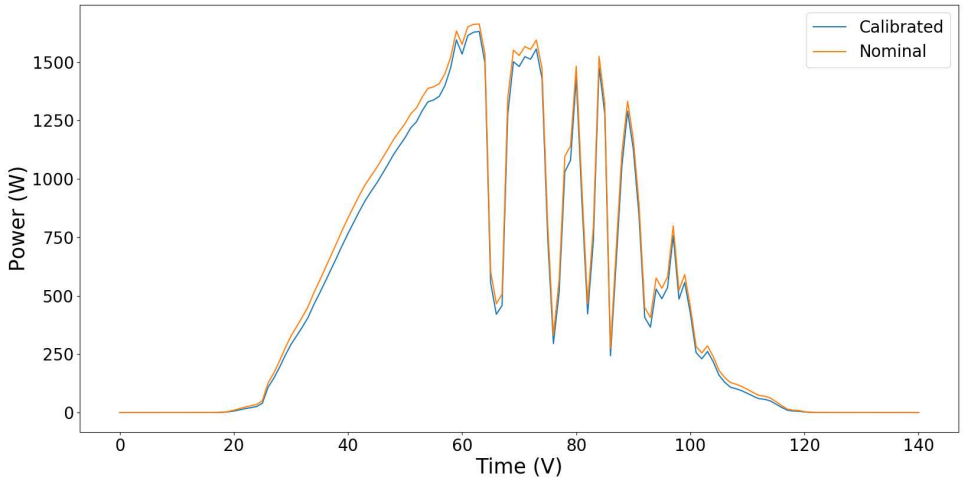

Figure 5.14: Comparison of the PV production with the calibrated and nominal parameter values.

Reducing the number of parameters

One of the possible issue is the overparameterization of the model we are trying to calibrate. Parameters were removed from the model and just the most influential ones were chosen for calibration. Parameters nDs and R_s were chosen based on the sensitivity analysis results like the most influential ones. All the parameters are scaled to the interval [0, 1] to be comparable.

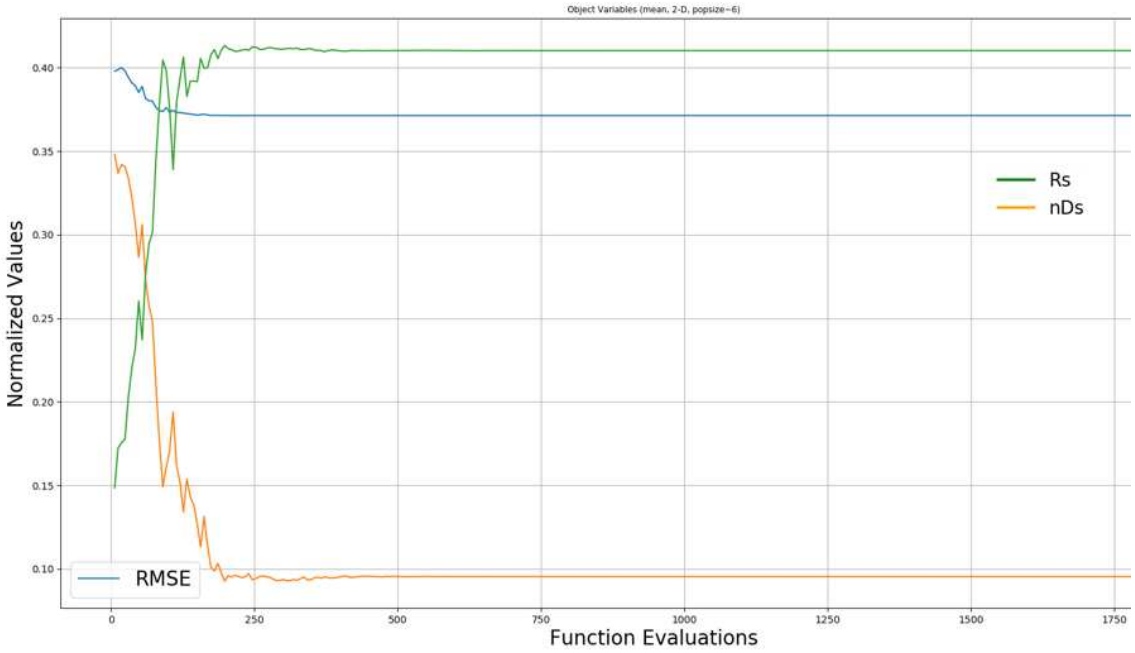

Figure 5.15: Calibration with 2 parameters.

For two parameters R_s and nDs the RMSE stabilizes after approx. 150 function evaluations at the value 0.22. The model synthetic model parameters are identifiable.

Parameters	**Nominal**	**Calibrated**
nDs	1	0.99164
R_s (Ω)	0.00012	0.000121
$RMSE$		0.021

Table 5.4: Calibrating 2 parameters.

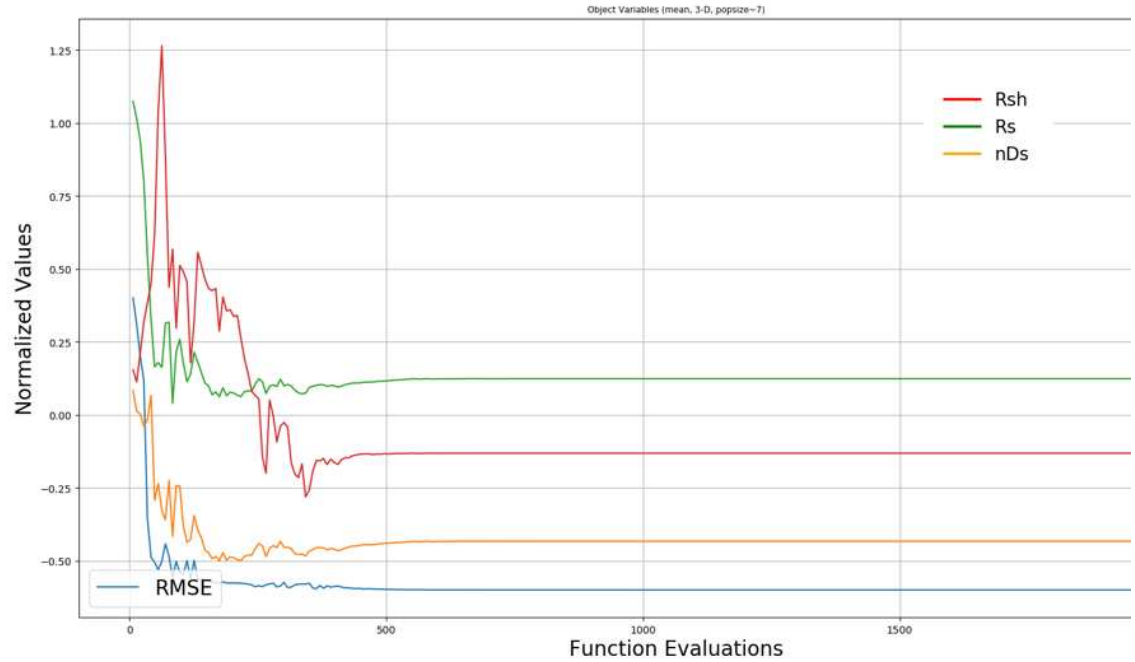

Figure 5.16: Calibration with 3 parameters.

With the reduced number of parameters the model is clearly identifiable on the synthetic simulated data. Additional parameters will be included into the calibration procedure to see which parameters are unidentifiable.

Parameters	**Nominal**	**Calibrated**
nDs	1	0.999
R_s (Ω)	0.00012	0.00012
R_{sh} (Ω)	0.14745	0.14742
$RMSE$		0.00172

Table 5.5: Calibrating 3 parameters.

With 3 parameters (Diode Ideality Factor-nDs, Series Resistance-R_s and Shunt Resistance R_{sh}) the parameters of the model on the simulated data are fully identifiable, the calibrated parameters are equal to the initial ones with the RMSE equal to 0.00172. The results on the structural identifiability show that the model with the reduced number of parameters is identifiable.

The accuracy of the calibrated parameters depends on the discrepancy between the computational code and the measured values. One of the issues in the calibration procedure are the initial parameter constraints. The parameter bounds were defined with the physical meaning of all the possible parameter values while in the calibration procedure the normalized values were reaching the bounds of the possible defined values. With the new parameter bounds the RMSE is improved but the parameter values are far from nominal ones.

Because the calibration procedure is performed on the noisy outdoor data the discrepancy between the simulated and measured data is causing convergence issues. A new approach which is more robust is presented in the following section.

5.9 Approximate Bayesian Computation (ABC)

The approximate Bayesian computation (ABC) algorithm is introduced as a alternative to deal with model selection and parameter estimation. The ABC is a class of computational methods based on the principles of Bayesian statistics (Equation 5.14).

Bayes theorem

$$p(\theta|y) = \frac{p(y|\theta)p(\theta)}{p(y)} \tag{5.13}$$

Where:

- $p(\theta|y)$ = posterior
- $p(y|\theta)$ = likelihood
- $p(\theta)$ = prior
- $p(y)$ = evidence

In the classic statistical inference the likelihood function has the central importance since it expresses the likelihood of the observed data under a particular statistical model and quantifies the selection of parameter values and models. The ABC method allows one to avoid the evaluation of the likelihood function which can be computationally costly.

The basic idea of the likelihood-free ABC algorithm was first described by Rubin [76] in 1984 where the method was presented in the intuitive way where he states that 'Bayesian statistics and Monte Carlo methods are ideally suited to the task of passing many models over one data set'. It offers an almost automated resolution of the difficulty with models which are intractable but can be simulated from. Rubin does not promote this simulation method in situations where the likelihood is not available but rather exhibits it as an intuitive way to understand posterior distributions from a frequentist perspective, because parameters from the posterior are more likely to be those that could have generated the observed data.

The ABC method was firstly proposed in population genetics by Tavare et al in 1997 [95], who introduced approximate Bayesian computational methods as a rejection technique bypassing the computation of the likelihood function via a simulation from the corresponding distribution. The algorithm can be written as:

Algorithm 1 Likelihood-free rejection sampler

```
for i=1 to N do
  repeat
    Generate θ from the prior distribution π(·)
    Generate D sample from the likelihood f(·|θ)
  until ρ{D, D_obs} ≤ ε
  set θ=θ_true
end for
```

In the case of model selection and parameter estimation Abdessalem et al. [1] implemented the likelihood-free ABC method in non-linear system identification problems. The results showed that the method is quite promising for parameter estimation from complex systems. Work from

Hazra et al [31] applied the ABC with the Monte Carlo Markov Chain approach for the parameter estimation from noisy degradation measurement. They show that the method is highly efficient compared to the traditional likelihood-based models without compromising the numerical accuracy.

Approximate Bayesian Computation (ABC) avoids the direct evaluation of likelihood function and approximates it with generated synthetic data from model simulations.The logic behind ABC is that θ^* should be a sample from the posterior distribution as long as the distance between the observed and measured values is less than some positive value.

The vector of the model parameter is denoted as $\theta = \{x_1, x_2, x_3\}$ and the observed data is denoted as $D_{obs} = \{y_1, y_2, ..., y_n\}$. The ABC algorithm approximates the posterior distribution $f(\theta|D_{obs})$ by generating samples from a joint distribution of the parameter vector θ and simulated data D using forward modeling and accept-reject mechanism.

To avoid the likelihood evaluation, first a set of candidate parameter vectors $\{\theta_1, \theta_2, ...\}$ is generated by sampling from the prior density $f(\theta)$ and then simulates the corresponding set of complete data sets $\{D_1, D_2, ...\}$ from a model $\mathcal{M}(D|\theta)$ and accepts the combinations of $\{\theta_n, D_n\}$ which satisfy the condition $\rho(D, D_{obs}) \leq \epsilon$ where the ϵ is a defined threshold measure.The final results from the algorithm are the samples of parameter vectors and simulated data from the distribution $f(\theta, D|\rho(D, D_{obs}) \leq \epsilon)$. The approximated posterior distribution can be written as:

$$f(\theta|D_{obs}) = \int f(\theta, D|\rho(D, D_{obs}) \leq \epsilon dD \tag{5.14}$$

where $f(\theta|D_{obs})$ is the marginal ABC posterior of θ.

5.9.1 The ABC rejection Algorithm

The D is accepted with tolerance $\epsilon \geq 0$ if:

$$\rho(\widehat{D}, D) \leq \epsilon \tag{5.15}$$

the distance measure $\rho(D, D_{obs})$ is the discrepancy between D and D_{obs} based on defined metric. A positive tolerance is necessary since is almost impossible that the simulation is equal to the data. The outcome of the ABC rejection algorithm is a sample of parameter values with the smallest discrepancy between the simulated D and D_{obs}. The accepted θ are approximately distributed according to the desired posterior and obtained without explicitly evaluating the likelihood function. The whole procedure can be summarised in the Figure 5.17

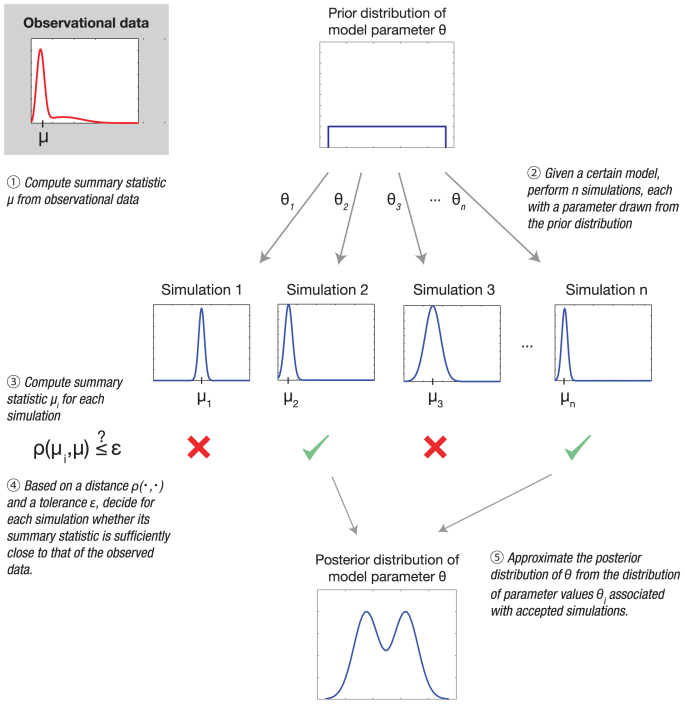

Figure 5.17: Parameter estimation by Approximate Bayesian Computation [94].

5.10 Available Data

The data consist of 1 day of 15 minute time step PV measurements from Bolzano airport (EURAC) 2 x 10 Kyocera poly crystalline modules with the nominal power of 4200 Wp were used for analysis.

The measured data consist of:

- $P_{mpp}AC$ Power at maximum power point in alternating current (W)
- $P_{mpp}DC$ Power at maximum power point in direct current (W)
- I_{mpp} Current at maximum power point (A)
- V_{mpp} Voltage at maximum power points (V)

The measured weather files are following:

- DHI Diffuse Horizontal Irradiation (W/m^2)
- GHI Global Horizontal Irradiation (W/m^2)
- POA Plane of Array Irradiation (W/m^2)
- Module temperature (°C)
- Ambient Temperature (°C)
- Wind Speed (m/s)

The electrical performance of the modules was simulated with the Dymola code using the two diode physical model. For the weather input files the GHI, DHI, ambient temperature and wind speed was used.

The computer code considered is deterministic and can be denoted as:

$$f_c = (X, \theta) \tag{5.16}$$

$$\theta \longmapsto y$$

The computer code does not take X as an input parameters because they represent the meteorological variables (input variables). The parameter vector θ has 28 variables related to the electrical properties of the PV panels and mounting configuration.

A single day PV performance was simulated with the nominal parameter values. The nominal parameter values were determined from the manufacturer data sheet. Most parameters in the physical model are limited to a specific range taken from the literature or based on the expert knowledge. The parameters for calibration were selected based on the sensitivity analysis results and because of their relation to the degradation processes.

To approach the posterior distribution of the model parameters 6000 uniform random samples from the model parameter space were generated and used as an input data for the computational code realisations. The ABC calibration is based on the equation 5.9. The discrepancy between the model and the measured data is added as a Gaussian noise.

The information about the computational code can be obtained from studying the probability distribution of the output from 6000 simulations the best 1 % of results (60) with the smallest RMSE were selected for comparison. The computational time for generating 10000 samples from the model was approximately 16 hours.

Parameters	**Nominal**	**Calibrated**
R_s (Ω)	0.000129	0.000118
R_{sh} (Ω)	0.1790	0.18561
I_{sc} (I)	6.54	6.4419
$RMSE$		1.8628

Table 5.6: Approximate Bayesian Calibration comparison.

Using the ABC to calibrate the code to the outdoor measured power shows good accordance with the nominal values of the parameters. The drawback of the ABC method is that is computationally intense, calibrating a single day with 10000 function evaluations takes approximately 16 hours on a $i5$ 2 Ghz personal computer .

5.11 Calibration on meta-models

The main motivation of using the meta-model is for the purpose of calibrating complex computer codes that are often too time expensive to be used directly for optimization purposes. Instead of optimization of the full computer model the meta-model is optimized where computational burden of large number of function evaluations is avoided. Meta-model based calibration is suitable for problems with the limited number of design variables.

Meta-model based calibration simplifies the direct optimization because the implicitly represented stochastic response of the simulation is replaced by an explicit deterministic meta-model response function. Validating the meta-model is a crucial step because using a meta-model which approximated the original objective function badly cannot lead to reliable calibration results. Calibration and parameter estimation adds an additional source of uncertainty into the calibration process where the calibration success is directly related to the accuracy of the meta-model.

The main steps of meta-model optimization are shown in the figure: 5.18.

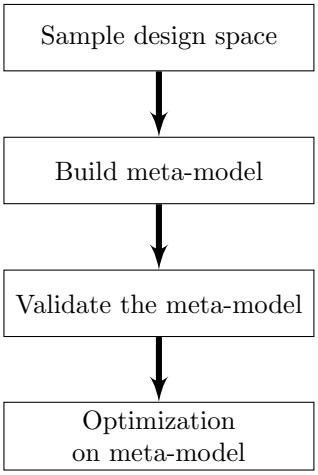

Figure 5.18: Meta-model based optimization.

5.12 Example of meta-model calibration

To compare the structural identifiability of the model vs meta-model 5 days of PV production were simulated with known (nominal) parameter values and same input weather measurements. The structural identifiability is the possibility to uniquely estimate the true values (nominal) of the model parameters where the parameter values are known (noise free measurements). The estimated parameters with model and meta-model should be the same as the nominal values from which the model/meta-model was simulated. The meta-model was build with the PCE expansion explained in the chapter 4. Before applying the polynomial chaos expansion the Karhunen-Loéve decomposition of a sample of trajectories was computed. For the model space explorations 100 samples from LHS were used.

Both model vs. meta-model were calibrated with the CMA-ES (Covariance Matrix Adaptation-Evolution Strategy) with the same nominal parameter values. The calibration with the full model with 2000 function evaluations takes approximately 10 hours while on the meta-model it takes approximately 3 seconds on a personal computer with $i5$ 2 Ghz.

Parameters	**Nominal**	**Bounds**
R_s (Ω)	0.000129	[0.0001-0.00025]
R_{sh} (Ω)	0.1790	[0.07-0.25]
I_{sc} (I)	6.54	[6-9]

Table 5.7: Selected parameters with their bounds

Table 5.7 shows the selected parameters nominal values and the corresponding bounds used for calibration with CMA-ES.

Parameters	**Nominal**	**Calibrated Model**	**Calibrated Meta-model**
R_s (Ω)	0.000129	0.000128	0.00013
R_{sh} (Ω)	0.1790	0.17951	0.1791
I_{sc} (I)	6.54	6.539	6.5419
$RMSE$		1.178	1.702

Table 5.8: Model vs meta-model calibration results.

Comparing the calibration results (table 5.8) show no difference in estimated parameters. With the meta-model we are able to highly improve the calibration efficiency while not sacrificing the accuracy of the calibrated parameters. The difference between the calibrated parameters R_s, R_{sh} and I_{sc} is minimal. The $RMSE$ in both cases is almost identical.

5.13 Conclusion

The objective of the chapter is to obtain reliable and precise parameter values from the noisy outdoor measurements. Calibrating the model in a various times in the lifetime of a PV plant could help to understand the degradation mechanism behind performance loss and use they temporal evolution for service life models.

When IV curves are available from the PV plant the parameter values obtained with calibration can be used to diagnose the health state of the PV system. The parameters were identified where the biggest performance drop was related to the loss of photo-current I_{sc} followed by the increase of series resistance R_s while the shunt resistance does not show any change over the period.

Because the IV curves are rarely available from the monitored PV sites other methods using reduced information are needed.

The presented approach which uses only the P_{mpp} value of the outdoor PV plant shows that the parameters obtained are not accurate enough to be used for service life modeling. The accuracy of the calibrated parameters depends on the discrepancy between the computational code and the measured values. One of the issues in the calibration procedure are the initial parameter constraints. The parameter bounds were defined with the physical meaning of all the possible parameter values while in the calibration procedure the normalized values were reaching the bounds of the possible defined values. With the new parameter bounds the RMSE is improved but the parameter values are far from nominal ones.

Checking the structural identifiability of the computational code shows that the model is identifiable with reduced numbers of parameters. Because of the noisy outdoor measurements the more robust Approximate Bayesian calibration is presented. The ABC method is applied on the single day of measured data where it shows good agreement with the initial nominal parameter values. The drawback of the method is that is time consuming and not suitable for calibrating multiple years of outdoor data. To overcome this issue the surrogate or meta-model are presented.

To run the calibration on the meta-models the surrogate has to be as close as possible to the initial numerical code otherwise the calibration of the parameters could loose they physical sense. The sampling design and the number of samples have direct influence on the accuracy of the meta-model where the main goal is to find a compromise between the meta-model accuracy and the required number of DOE experiments for their construction.

Signatures of Degradation Mechanisms from Fielded Photovoltaic Plant Monitoring Data

Nikola Hrelja, Mike Van Iseghem, Eric Lajoie-Mazenc, Merlin Keller, Mohammed Meftah, Eric Moulines, David Moser, Sascha Lindig

***Abstract*— The degradation of the performance of a photovoltaic (PV) plant over its lifetime can be estimated with various performance loss rate methods. These methods are not suitable for identifying root causes and degradation mechanisms from field data, because they only provide the overall sum of reversible and irreversible power loss mechanisms. The physics-based understanding and modeling of the performance using only the Pmpp (Power at maximum power point) from power plants where IV curves are not available can be used to estimate circuit parameters that reflect degradation over time and evaluate the system's state of health. In this paper, we propose an algorithm that aims to identify the degradation related parameters by calibrating the EDF PV yield model (PVNOV) based on the double diode model with the observed PV plant data. Approximate Bayesian computation was used for the calibration. The algorithm has been validated on simulated synthetic data (Digital Power Plant) with a known circuit parameter degradation evolution and an added Gaussian noise and discrepancy to check the uniqueness of the extracted circuit parameters. The results show that the evolution of the selected circuit parameters using only the Pmpp can be estimated. The proposed algorithm has been applied on 8 years of PV plant outdoor data. Our analysis indicates that the power decrease on the studied modules can be attributed to the decrease in the short circuit current (Isc) from 8.58A to 7.8A while the series (Rs) and shunt resistance (Rsh) parameters do not show any significant change over the period of 8 years.**

***Index Terms*—Photovoltaic (PV) system degradation, double diode model, sensitivity analysis, calibration, approximate Bayesian computation.**

I. Introduction

THE PV plant's service life is mainly determined by the stability and resistance of PV modules to different internal and mechanical loads. These loads are closely related to differences in climatic exposure depending on the location of the installation and affect various module technologies differently. The degradation rates and prevailing degradation mechanisms will be different depending on the chosen technology and its geographical location. Certain degradation modes are more severe in specific climatic conditions [1].

Estimating the degradation and understanding the underlying mechanisms is important to reveal the expected service life of a PV plant. Several performance loss rate (PLR) calculating methodologies have been proposed which are based on various statistical approaches [2], [3], [4]. These methods are suitable to estimate the degradation rates but they fail to provide any insight into the degradation mechanisms. On the other hand, methods like IV curve fitting to the single or double diode model can be applied to relate the circuit parameter changes to the efficiency losses and underlying degradation mechanisms [5], [6].

The IV curves measured at the module level provide detailed information about the performance. Parameters obtained from IV curves, namely the open circuit voltage, short circuit voltage, maximum power point voltage and current, and series and shunt resistance, can provide critical information about the performance loss. A number of different models exist to fit measured IV curves. Some models represent the full IV curves using the single diode equivalent circuit models such as PVSyst [7] and the De Soto Single Diode Model (CEC) [8]. Other models such as SANDIA PV Array Performance Model (SAPM) [9] and the Loss Factor Model (LFM) [10], [11], [12] estimate only key points on the IV curves such as the maximum power point (Vmp, Imp), short circuit current (Isc) and open circuit voltage (Voc). The LFM also estimates performance losses due to series and shunt resistances. However, outdoor measurements are rarely taken in the field to evaluate fault conditions and/or degradation.

Another approach using the Suns-Vmp method [13] reconstructs the IV curves by using the natural illumination-dependent and temperature-dependent evolution of circuit parameters (e.g. Series resistance) which may enable to identify the dominant degradation modes. The drawbacks are that both current and voltage at maximum power are required.

Since IV curves are rarely available from the PV plant monitoring data, the challenge is to estimate the parameters

Manuscript received August XX, 2020. This project has received funding from the European Union's Horizon 2020 research and innovation program within the framework of the "Solar Train" project under the Marie Skodowska-Curie GA No 721452. *(Corresponding author: Nikola Hrelja.)*

N. Hrelja, M. Van Iseghem and E. Lajoie-Mazenc are with the EDF R&D, site des Renardières, 77818 Moret-sur-Loing, FR (phone: +33160736149; e-mail: nikola.hrelja@edf.fr; mike.van-iseghem@edf.fr; eric.lajoie-mazenc@edf.fr,).

M. Keller and M. Meftah are with the EDF R&D, Chatou, 6 Quai Watier , 78400 Chatou, FR (e-mail: merlin.keller@edf.fr; mohammed.meftah@edf.fr).

E. Moulines is with the CMAP École Polytechnique, Route de Saclay, 9128 Palaiseau, FR (e-mail: eric.moulines@polytechnique.edu).

D. Moser and S. Lindig are with the Institute for Renewable Energy, EURAC Research, Viale Druso 1, 39100 Bolzano, IT (e-mail: david.moser@eurac.edu; sascha.lindig@eurac.edu).

of the PV diode using only the measured Pmpp and the corresponding weather file. In this paper, the proposed approach is focused on the PV diode circuit parameter extraction from the PVNOV, EDF's PV performance model using field measurements of Pmpp from polycrystalline modules and weather data. The precise evolution of degradation-related parameters from the historical PV performance data could help link performance losses to relevant degradation mechanisms and better understand the evolution of power degradation.

II. Method

The method is based on calibrating the selected circuit parameters from PVNOV at various times and monitoring their evolution to gain insights regarding the degradation modes. In this section, we will present the model, model parameter selection and the calibration method.

A. Model

To mimic the behavior of PV power plants, models have been developed which intend to be as close as possible to the PV system. Electricité de France (EDF)'s existing PV performance model (PVNOV) [14], written in the Modelica software, enables the user to model the electrical behaviour of any PV device under given meteorological conditions. The configuration of the PV plant assumes a uniform behaviour of every cell/module/array without considering any mismatch between modules.

The PVNOV contains several modeling layers:

1. Double diode model
2. Thermo-physical model (based on thermal exchanges), for details see [14]

Optical reflections are taken into account in the model to estimate the effective irradiance on the module. According to Martin and Ruiz [15], the transmission coefficient can be obtained by:

$$FT_B = \frac{T_{dirt}}{T_{clean}}\left[1 - \frac{exp\left(-\frac{\cos\Phi_s}{a_r}\right) - exp\left(-\frac{1}{a_r}\right)}{1-\exp\left(-\frac{1}{a_r}\right)}\right] \quad (1)$$

Where $\frac{T_{dirt}}{T_{clean}}$ and a_r depend on the dirtiness of the module and Φ_s is the angle of incidence. Each component of the global irradiance is reduced by a specific transmission coefficient described in [16].

The PVNOV model takes two kinds of inputs: *variables* and *parameters*. The variables are measured during the field experiments and include weather variables and module temperature, while the parameters are physical values defining the physical model:

$$f_{\text{mod}} = (x, \theta) \quad (2)$$

The computer model is formulated as f_{mod}. θ represents the parameter vector of the double diode model; see Table II for an example. x represents the meteorological variables, namely global horizontal irradiation (GHI), diffuse horizontal irradiation (DHI) and ambient temperature (T). Wind speed and soiling were not yet considered here. However, the thermal transient behaviour of PV modules is included in the model [14].

The nominal values of physical parameters are obtained from the module datasheet while the values of Rs and Rsh are obtained from fitting the IV curves from analyzed modules. The nonlinear least-squares fitting algorithm had been applied to fit the double diode model parameters and extract the values of Rs and Rsh.

B. Parameter selection

Prior to the calibration, the most influential parameters need to be identified and prioritized while the non-influential inputs are fixed to their nominal values. At the same time, the selected parameters need to be related to degradation mechanisms. The Morris method [17] for global sensitivity analysis (SA) was used for the selection of parameters from Table I.

TABLE I
SELECTED PARAMETERS

Physical parameter	
Alpha (%/K)	Current temperature coefficient
Isc (A)	Short circuit current
Rseries (Ω)	Series resistance
Rshunt (Ω)	Shunt resistance
Cr (A/m^2K^3)	Saturation current temperature exponent 2
Cs (A/m^2K^3)	Saturation current temperature exponent 1
Mr	Coefficient of recombination 2
Ms	Coefficient of recombination 1
nDr	Diode ideality factor 2
nDs	Diode ideality factor 1

The Morris method evaluates the influence of each input parameter by considering the impact of its variation on the model output while considering all the other parameters as constant. The Morris method enables the user to identify variables which can be neglected in the subsequent study. Before the analysis, the model parameter bounds need to be defined in the range of possible realizations of the physical system. The parameter bounds are usually determined empirically or by using 10% around the nominal value defined in the model (Table II).

TABLE II
PARAMETER NOMINAL VALUES WITH BOUNDS USED FOR SENSITIVITY ANALYSIS

Parameter	Nominal value	Bounds
Alpha (%/K)	0.037	[0.034-0.042]
Isc (A)	8.36	[6.0-9.0]
Rseries (Ω)	0.45	[0.35-0.9]
Rshunt (Ω)	650	[450-1000]
Cr (A/m^2K^3)	0.630	[0.450-0.842]
Cs (A/m^2K^3)	3291.9	[3003.8-3505.2]
Mr	2.5	[2.25-2.75]
Ms	3	[2.8-3.4]
nDr	2	[1.9-2.2]
nDs	1	[0.9-1.2]

In the Morris method, the variations of each parameter are quantified by elementary effect (EE) denoted as $\mu*$ and the standard deviation of the EE denoted as σ.

This method has two interesting properties:

1. Large $\mu*$ values mean the j-th input parameter contributes to the dispersion of the output.
2. A parameter with a large σ over mu ratio means high non-linear effects on the output or interaction with at least one parameter.

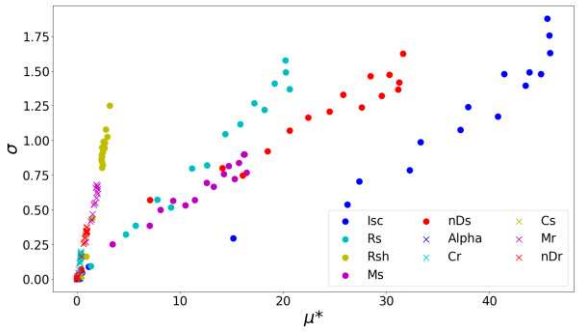

Fig. 1. Morris indices obtained on the single day of PV simulation from PVNOV

In fig 1, we simulated a full day (from 7.30-19:30) in 15-minute time intervals and Morris indices were obtained for each time step. The influence of some parameters seems to depend on the time of the day:

1. Since they have high mu values. the parameters Isc, nDs, and Rs contribute to the dispersion of the output.
2. Since its sigma over mu is elevated, the parameter Rsh seems to have a non-linear effect on the model output.

The parameters Isc, Rs, and Rsh were selected for final analysis. The selected parameters influence the power output and can be linked with various degradation mechanisms. The evolution of series and shunt resistances represents the summation of several loss mechanisms in a solar cell. Losses due to resistance introduced in cell solder bonds, emitter and base regions, cell metallization and cell-interconnect busbars contribute to the value of Rs [18]. Shunt resistance can result from imperfections on the device surface as well as from leakage currents across the edge of the cell. The Rsh value represents any parallel high conductivity paths across the solar cell junction. A decrease in Rsh reduces the current output whereas an increase in Rs results in a drop in the voltage output. The effect of reduced Rsh values is especially severe at low light levels, as there would be less light-generated current.

Work by Dyk and Meyer on crystalline silicon modules demonstrated that by increasing Rs from 0.36 to 1.8 both the Pmpp and fill factor (FF) were reduced by 25%, making it clear that the performance is strongly influenced by increased series resistance values [19]. Therefore, the evolution of Isc, Rs, and, Rsh needs to be recognized and understood to improve the module service life forecast.

C. Calibration

In general, the calibration problem can be represented as finding the best possible model parameter θ using (2) which fits the observed data $D_{obs}(x_i)$ at the same experimental conditions x_i as good as possible. We assume that for some well-chosen θ the calibration model can be represented as:

$$\begin{aligned} &D_{obs}(x_i) = f_{\mathrm{mod}}(x_i,\theta) + \varepsilon_i + \eta \\ &with: \forall_i \in [1,\ldots,n]\ \varepsilon_i \overset{iid}{\sim} N(0,\sigma^2), \\ &\eta \sim N(0,\sigma^2) \end{aligned} \tag{3}$$

Compared to the physical system, computer models are rarely perfect or exact due to the simplifications of complex physical phenomena, numerical approximations, and measurement uncertainties. Even if the computer model parameters are well-calibrated, there will be a gap between the physical system and its corresponding computer model known as code error or discrepancy. The random Gaussian noise ε in (3) represents the measurement uncertainty while the systematic Gaussian noise η represents the discrepancy between the model and the measured data. Both ε and η are independent and identically distributed random variables (*iid*).

D. Approximate Bayesian Computation

For complex models, the likelihood function might be computationally very costly to evaluate. Approximate Bayesian computation (ABC) replaces the calculation of the likelihood function by simulating the model that produces an artificial data set and comparing it with the observed data [20]. The logic behind the ABC is that θ should be a sample from posterior distribution as long as the distance between the observed and simulated values is less than some positive value. The pseudocode for ABC algorithm can be written as:

ABC LIKELIHOOD FREE REJECTION ALGORITHM

for *i=1 to N* ***do***
repeat
Generate θ from the prior distribution π (•)
Generate $\hat{D}$ sample from model f (θ)
until $\rho\{\hat{D}, D_{obs}\} \leq \varepsilon$
set $\theta=\theta_{true}$
end for

With the rejection algorithm, a set of parameter points is first sampled from the prior distribution using a uniform distribution U *(min (θi), (max (θi))* with the defined bounds for parameter values. The ABC algorithm approximates the posterior distribution $f(\theta|\ D_{obs})$ by generating samples from parameter vector θ and simulating data $\hat{D}$ using forward modeling and accept-reject mechanism. With the given sampled parameter point θ, a data set $\hat{D}$ is simulated under the statistical model using (3). The process is repeated *N*

times. If the generated $\hat{D}$ is significantly different from the observed data D_{obs}, the sample parameter is discarded. The $\hat{D}$ is accepted with tolerance $\varepsilon \leq 0$ if:

$$\rho_i = \left(\sqrt{\sum_{i=1}^{n} \frac{D_{obs} - \hat{D}_i}{N}} \right) \leq \varepsilon \quad (4)$$

The distance measure ρ is the discrepancy between the $\hat{D}$ and D_{obs}, based on the root mean square error (RMSE) in every simulation. Positive tolerance is necessary since it is almost impossible for the simulated data to be equal to the observed data. The outcome of the ABC rejection algorithm is a sample of parameter values θ with the smallest discrepancy ρ using (4). The accepted θ are approximately distributed according to the desired posterior and obtained without explicitly evaluating the likelihood function. In our case, the ABC approach showed more robust results on noisy outdoor data than the ones obtained with classical calibration approaches and enabled us to add the code error or discrepancy into the statistical model (3).

III. Digital Power Plant

Before applying the ABC calibration algorithm on the outdoor PV plant measurements, the method was applied on a Digital Power Plant (DPP). The DPP enables simulating PV production from the PVNOV [14] code with defined evolution of selected parameters, namely: Isc, Rs, and, Rsh. The DPP was simulated for a period of 8 years where Isc followed a pre-defined monthly linear decrease, the parameter Rs followed a predefined monthly linear increase and the parameter Rsh was kept constant (see Table III).

TABLE III
Parameter Nominal Values and Their Linear Degradation Evolution

Parameter	Nominal value	Degradation after 8 years	Change
Isc (A)	8.36	7.34	-12%
Rseries (Ω)	0.45	0.90	+100%
Rshunt (Ω)	650	650	0%

The motivation for using the DPP is to check the uniqueness of the extracted circuit parameters. Every month, five days of PV production from the DPP were selected for calibration because this provides enough data points and reduces the computational cost. The aim is to accurately capture the known evolution of parameters over 96 months. Every month 10000 models were simulated using equation (3) with parameter samples generated from a uniform distribution. The bounds of parameters are defined in Table II. All the other parameters were kept at their nominal values. The set of 200 parameters (2%) with the smallest threshold ρ from (4) on RMSE was selected. Because of the field measurement uncertainty, the noise was added to the data set simulated with the DPP to better represent typical field data. The added levels of noise correspond to the ones present in the field data. The noise and discrepancy in equation (3) was added in two ways:

1. Random Gaussian noise (ε) of 2% on instantaneous values.
2. Systematic Gaussian noise or discrepancy (η) of 2% on the monthly period of simulation.

The short circuit current was estimated on 96 points (see Fig.2). The red intervals on every estimation point are the values of the 95% confidence intervals calculated on 10.000 ABC function evaluations. The calibration of a single month with the ABC took approximately 4 hours on a computer with an Intel(R) Core (TM) i5-6200U CPU using 16 GB of RAM, running Windows 10.

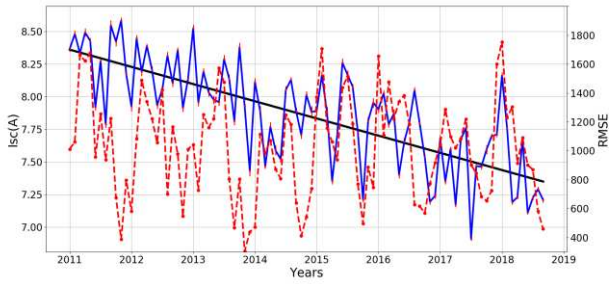

Fig. 2. The estimated evolution of short circuit current values (blue line) together with the defined evolution of Isc from DPP (straight black line) and the RMSE (red dashed line)

In Fig. 2, the evolution of Isc is shown over the period of 8 years. The calibrated values of Isc show volatility because of different outdoor operating conditions and added Gaussian noise. Comparing the average values of Isc in the first vs. last operating year shows comparable values with those set in the DPP.

Fig. 3 shows the evolution of the Rs over the period of 8 years on the Digital Power plant. The values of the Rs are comparable to those set initially in the DPP. The 95% confidence intervals show that small changes in Isc cause significant changes in the Pmpp while small changes in Rsh do not cause any noticeable change in the Pmpp.

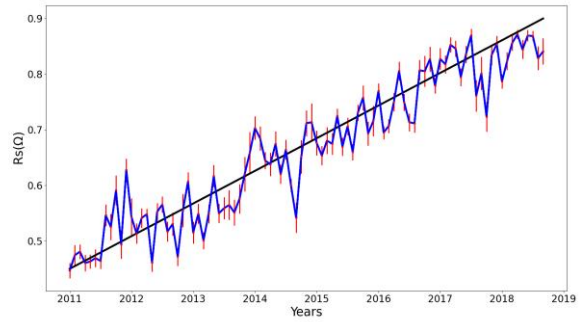

Fig. 3. The estimated evolution of series resistance together with defined evolution of Rs from DPP (straight black line)

The values of shunt resistance are increasing over the period of 8 years which suggests that there is an interaction between the parameters Rs and Rsh and they are not independent (Fig.

4). After a certain increase in Rs, the Rsh values are increasing as well.

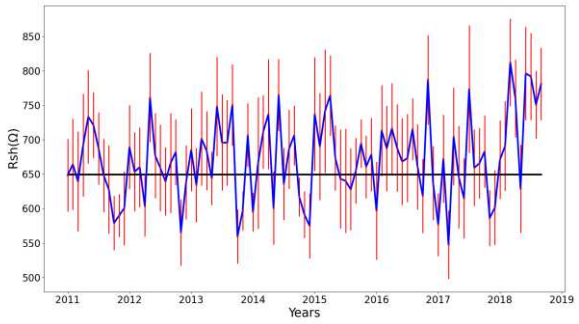

Fig. 4. The estimated evolution of shunt resistance together with the defined evolution of Rsh from DPP (straight black line)

The DPP enables to simulate a pre-defined degradation evolution of selected parameters which are then estimated with the ABC method. The method is capable of tracking the evolution of parameters where the calibrated values of Isc and Rs correspond to the values set in DPP.

IV. Application on Field Data

In this section, the algorithm was tested on the EURAC data set with more than 8 years of recorded field data. The corresponding plant is installed at the Bolzano airport in Italy. The analysis shows the temporal evolution of calibrated physical circuit parameter values over a period of 8 years with a monthly resolution on polycrystalline modules.

A. *Description of the field data*

The PV plant installed in Bolzano (IT) consists of 10 polycrystalline modules (210 Wp) connected in a string. According to the Köppen–Geiger classification, the installation climate is CFB (temperate oceanic climate). Data is available over the period of 8 years where instantaneous power is recorded in 15-minute intervals together with ambient temperature, global horizontal irradiance, diffuse horizontal irradiance, plane of array irradiance, and wind speed. Missing values, outliers representing measurement or sensor error were omitted from the analysis if their values were out of the range of two standard deviations from the monthly mean values. First, the nominal parameter values of the PV modules were used to create an exact twin of the power plant with PVNOV and simulate the PV performance (Table IV). The output of the code is a time series of over 8 years of instantaneous power with a time step of 15 minutes.

TABLE IV
PARAMETER NOMINAL VALUES WITH BOUNDS

Parameter	Nominal value	Bounds
Isc (A)	8.58	[6-9]
Rseries (Ω)	0.45	[0.25-0.80]
Rshunt (Ω)	600	[250-1000]

The PR was calculated on both the simulated and measured data and aggregated to daily values. A second filter was applied so that plane of array (POA) irradiation of less than 100 W/m^2 and more than 1200 W/m^2 was removed from analysis. This was done to remove outliers and measurement errors.

The PR is calculated by dividing the final yield *Yf* by the reference yield Y_{REF} [5] (Eq. 5).

$$PR = \frac{Y_f}{Y_{REF}} = \frac{P_{AC}/P_{STC}}{G_{POA}/G_{STC}} \quad (5)$$

The yields are ratios of measured values of power or irradiance with values obtained under standard test conditions (STC) of 1000 W/m^2. In Fig. 5, the average daily PR on measured and simulated PV performance is shown.

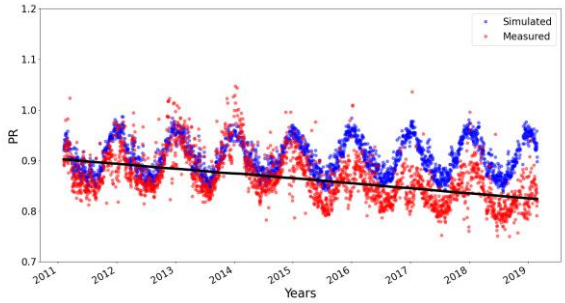

Fig. 5. Comparing the PR calculated on the measured (red) and simulated data (blue). The line is the estimated degradation rate of measured PV data.

The discrepancy between the PR calculated on measured and simulated PV performance is increasing over time and can be attributed to the degradation of the fielded PV. The degradation was estimated with linear regression. Dividing the overall degradation rate with the number of analyzed years yields the average estimated degradation rate 0.84% per year.

B. *ABC calibration on the field data*

The calibration was performed over 94 months. For every month, five days were selected in outdoor operating conditions. In Fig. 6 the average plane of array (POA) irradiation and ambient temperature was calculated for selected periods.

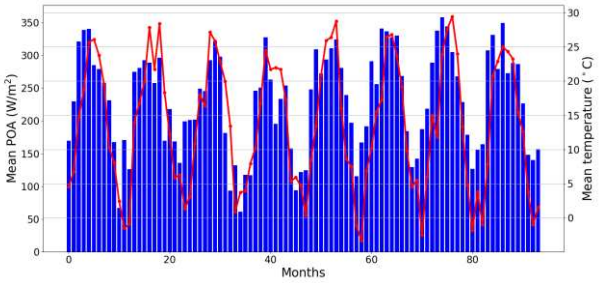

Fig. 6. The average POA irradiation (blue) and the ambient temperature (red line) on selected days.

Every month, 10.000 models were simulated using equation (3) with parameter samples generated from a uniform distribution using the bounds for parameter values from Table IV. All the other model parameter values were retained at their nominal values. The set of 200 parameters (2%) with the smallest threshold ρ (4) on *RMSE* was selected. The calibration of a single month with the ABC took approximately 4 hours.

From the calibration results, there is a clear decrease in the value of Isc within a period of 8 years (see Fig.7). The variability of the calibrated parameter Isc is high because of varying operating conditions and model discrepancy.

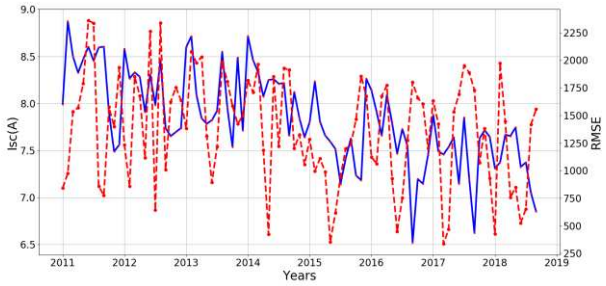

Fig. 7. Evolution of Isc on field data from Bolzano (blue line) and the corresponding RMSE (red dashed line)

Comparing the values of short circuit current in selected months shows reduced parameter variability (Fig. 8).

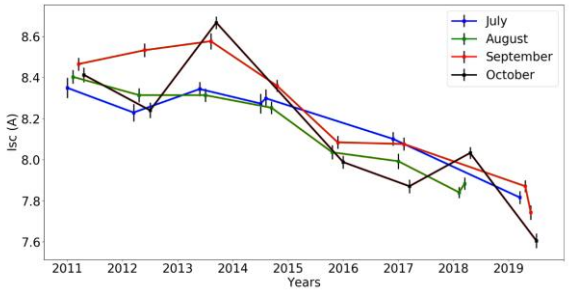

Fig. 8. Evolution of Isc in selected months on field data from Bolzano

The evolution of Rs (Fig.9) does not show any increase over the period of 8 years. The variability of the parameter is high and can be attributed to the measurement noise and model discrepancy.

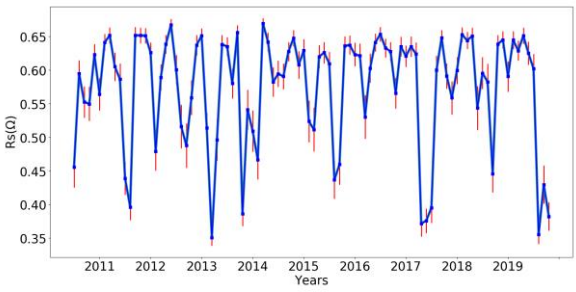

Fig. 9. Evolution of Rs on field data from Bolzano

Evolution of Rsh on the field data does not show any considerable long term trend over the period of 8 years (Fig.10). It is expected that the Rsh values will be decreasing over time.

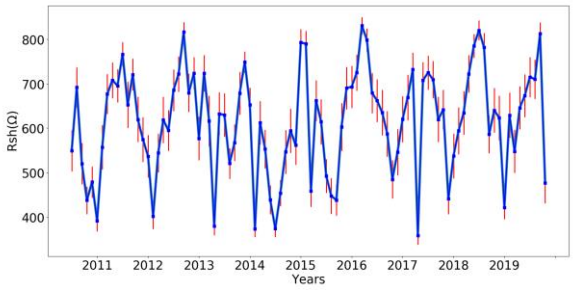

Fig. 10. Evolution of Rsh on field data from Bolzano

In order to check the variability and investigate possible seasonal effects of both parameters, specific months with more stable weather conditions were selected. The estimated parameters Rs and Rsh do not show any trend in their evolution (see Fig.11 and 12).

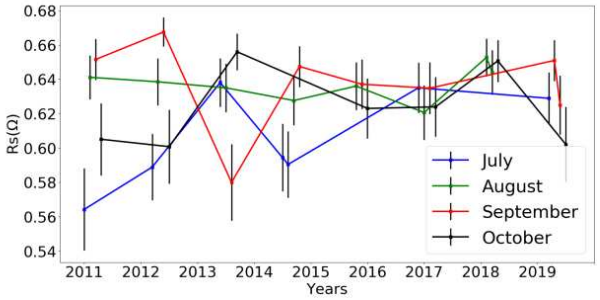

Fig. 11. Evolution of Rs in selected months on field data from Bolzano

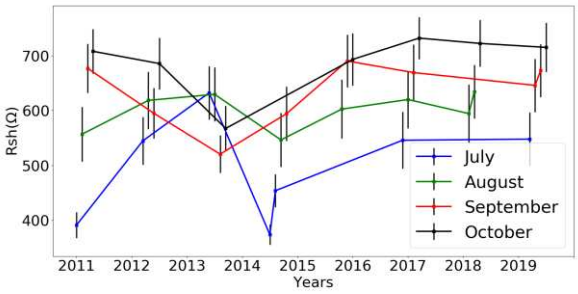

Fig. 12. Evolution of Rsh in selected months on field data from Bolzano

The evolution of the Rs does not show any change in the selected months (see Fig. 11). The values of Rs are closely related to the manufacturing quality and the possible explanation is that an 8-year period is not enough to see Rs related degradation modes like corrosion of the busbars in this particular climate.

V. Discussion and Conclusion

We present a method to estimate the Rs, Rsh, and Isc parameters from fielded PV systems by creating a digital twin

of a power plant and calibrating the selected parameters with respect to observed Pmpp values using the ABC method.

In the first case, the algorithm was validated on a digital power plant (DPP) with a known parameter degradation evolution where it was demonstrated that it can be used to track the parameter (Isc, Rs) evolution over time with added Gaussian noise and discrepancy. One of the findings on DPP is that the parameters Rs and Rsh are not independent. After Rs reached some threshold value, it affected the values of the Rsh. Next, the algorithm was applied to fielded PV system data where the degradation of Isc was tracked over 8 years. The presented approach allows us to relate the power loss of the PV system to certain degradation mechanisms and extends the classical performance rate degradation approaches. The method enables tracking the evolution of physical parameters related to the degradation mechanisms using only standard Pmpp and meteorological data from the field.

Results on the analyzed power plant show that the main aging factor is a decrease in the short circuit current where the power loss is probably related to optical degradation of the PV modules.

This might be caused by yellowing and/or browning of the EVA, delamination, and appearance of bubbles or degradation of anti-reflecting coating. No traceable change of Rs was observed in the analysed data. The results could indicate that the period of 8 years is not enough for the development of corrosion-related degradation modes on analysed modules. The results need to be validated with a visual inspection on the field and a full IV characterization of the analysed modules. Currently, the calibration algorithm considers all the modules operating under identical conditions without considering mismatch or non-uniformity in modules. For future improvements of the algorithm, the mismatch between the modules and the non-uniformity needs to be integrated into the calibration process because it can add substantial differences in the parameter estimation. The double-diode model parameters can be generalized to include nonlinear shunt resistance and temperature and illumination-dependent series resistance. The algorithm was tested on a single fielded crystalline silicon system and should be applied to more field data to compare the results. The algorithm should be tested on thin-film technologies where the physical parameter evolutions could be different from those observable on silicon modules. In the future parameter evolution, tracking will enable a better understanding of the state of a power plant and its expected evolution.

ACKNOWLEDGMENT

This project has received funding from the European Union's Horizon 2020 research and innovation programme within the framework of the "Solar-Train" project under the Marie Sklodowska- Curie GA No 721452.

REFERENCES

[1] D. C. Jordan, T. J. Silverman, J. H. Wohlgemuth, S. R. Kurtz, and K. T. VanSant, 'Photovoltaic failure and degradation modes', *Prog. Photovolt. Res. Appl.*, vol. 25, no. 4, pp. 318–326, 2017, doi: 10.1002/pip.2866.

[2] D. C. Jordan, T. J. Silverman, B. Sekulic, and S. R. Kurtz, 'PV degradation curves: non-linearities and failure modes', *Prog. Photovolt. Res. Appl.*, vol. 25, no. 7, pp. 583–591, 2017, doi: 10.1002/pip.2835.

[3] S. Lindig, I. Kaaya, K.-A. Weiss, D. Moser, and M. Topic, 'Review of Statistical and Analytical Degradation Models for Photovoltaic Modules and Systems as Well as Related Improvements', *IEEE J. Photovolt.*, vol. 8, no. 6, pp. 1773–1786, Nov. 2018, doi: 10.1109/JPHOTOV.2018.2870532.

[4] M. Meftah, E. Lajoie-Mazenc, M. Van Iseghem, R. Perrin, D. Boublil, and K. Radouane, 'A Less Environment-Sensitive and Data-Based Approach to Evaluate the Performance Loss Rate of PV Power Plants', Sep. 2019, doi: 10.4229/EUPVSEC2019-5CV.4.3.

[5] X. Ma *et al.*, 'Data-Driven I–V Feature Extraction for Photovoltaic Modules', *IEEE J. Photovolt.*, vol. 9, no. 5, pp. 1405–1412, Sep. 2019, doi: 10.1109/JPHOTOV.2019.2928477.

[6] T. J. Peshek *et al.*, 'Insights into metastability of photovoltaic materials at the mesoscale through massive I–V analytics', *J. Vac. Sci. Technol. B*, vol. 34, no. 5, p. 050801, Aug. 2016, doi: 10.1116/1.4960628.

[7] A. Mermoud and T. Lejeune, "Performance Assessment of A Simulation Model For PV Modules Of Any Available Technology," in *25th European Photovoltaic Solar Energy Conference*, Valencia,

[8] CEC, "California Solar Initiative Incentive Calculators," 2013. [Online]. Available: http://csi-epbb.com/documentation.aspx.

[9] D. L. King, W. E. Boyson and J. A. Kratochvil, "Photovoltaic Array Performance Model," Sandia National Laboratories, Albuquerque, NM, 2004.

[10] C. B. Jones *et al.*, 'Quantify Photovoltaic Module Degradation using the Loss Factor Model Parameters', in *2017 IEEE 44th Photovoltaic Specialist Conference (PVSC)*, Washington, DC, Jun. 2017, pp. 3488–3493, doi: 10.1109/PVSC.2017.8366400.

[11] S. Ransome and J. Sutterlueti, 'Adaptable PV Performance Modelling for Industrial Needs'. *35th European Photovoltaic Solar Energy Conference and Exhibition,* 2018, doi: 10.4229/35thEUPVSEC20182018-5CV.1.28

[12] S. Ransome and J. Sutterlueti, 'Quantifying long term PV performance and degradation under real outdoor and IEC 61853 conditions using high quality module IV measurements', *36th European Photovoltaic Solar Energy Conference and Exhibition,* 2019, doi: 10.4229/EUPVSEC20192019-5CV.4.35.

[13] X. Sun, R. V. K. Chavali, and M. A. Alam, 'Real-time monitoring and diagnosis of photovoltaic system degradation only using maximum power point—the Suns-Vmp method', *Prog. Photovolt. Res. Appl.*, vol. 27, no. 1, pp. 55–66, 2019, doi: 10.1002/pip.3043.

[14] B. Braisaz, P. Dupeyrat, A. Lindsay, K. Radouane, 'An Advanced Model of PV Power Plants Based on Modelica®', *28th Eur. Photovolt. Sol. Energy Conf. Exhib.*, pp. 3644–3648, Nov. 2013, doi: 10.4229/28thEUPVSEC2013-5AO.9.4.

[15] N. Martin, J.M. Ruiz, 'Calculation of the PV modules angular losses under field conditions by means of analytical model', *Solar Energy Materials and Solar Cells,* Volume 70, Issue 1, pp. 25-38, 2001.

[16] T. M. Klucher, 'Evaluation of models to predict insolation on tilted surfaces', *Solar Energy*, Volume 23, Issue 2, pp 111-114, 1979.

[17] M. D. Morris, 'Factorial Sampling Plans for Preliminary Computational Experiments', *Technometrics*, vol. 33, no. 2, pp. 161–174, May 1991, doi: 10.1080/00401706.1991.10484804.

[18] 'Solar cells: operating principles, technology, and system applications / Martin A. Green | National Library of Australia'. https://catalogue.nla.gov.au/Record/1555330 (accessed Jun. 11, 2020).

[19] E. E. van Dyk and E. L. Meyer, 'Analysis of the effect of parasitic resistances on the performance of photovoltaic modules', *Renew. Energy*, vol. 29, no. 3, pp. 333–344, Mar. 2004, doi: 10.1016/S0960-1481(03)00250-7.

[20] S. A. Sisson, Y. Fan, and M. A. Beaumont, 'Overview of Approximate Bayesian Computation', *ArXiv180209720 Stat*, Feb. 2018, Accessed: Jun. 11, 2020. [Online]. Available: http://arxiv.org/abs/1802.09720.

Chapter 6

Conclusion and perspectives

The objective of the thesis is to better understand the mechanism behind the degradation of photovoltaic plants. The objective is important to industrial companies like EDF because the degradation of the photovoltaic plants directly relates to the profitability of the photovoltaic investments and it can reveal the expected service life of a PV plant. In this context, it is essential to accurately quantify and define all the relevant risk factors of long term performance losses. The general framework of this thesis is the photovoltaic degradation related parameter calibration. The degradation of PV modules is closely related to the variation of the internal parameters of the solar cell namely the short circuit current I_{sc}, the series resistance R_s and the shunt resistance R_{sh}. Tracking the evolution of those parameters could reveal certain degradation mechanisms on the fielded photovoltaic systems.

In the case, IV curves are available the single diode model of the PV cell can be utilized. The model provides a good compromise between accuracy and simplicity while avoiding the complexity of the double diode model. The double diode model is presented which allows to model junction recombination by adding a second diode in parallel and it is integrated into the EDF's numerical code for simulating photovoltaic performance.

In the third part of the thesis, a sensitivity analysis was performed on two models to identify which parameter has the most influence on the model output. For the sensitivity analysis, Morris and Sobol's method were used. The results on both models show that the short circuit current followed by the series resistance and shunt resistance are the most influential parameters which at the same time can be related to various degradation mechanisms.

In the fourth chapter of the thesis, the identification of the degradation related parameters was performed using two different approaches. In the case when IV curve measurements are available from the PV monitoring sites the parameter estimation is straightforward. The IV curves are extracted in various narrow windows of stable irradiance and temperature conditions to gain insights into the degradation of PV devices. The parameter calibration from measured IV curves was performed using the Covariance Matrix Adaptation Evolution Strategy (CMA-ES). The IV curve measurements are available for 8 years. The results show that the main aging factor of the fielded PV module is the decrease of short-circuit current where the main power loss is mostly caused by the optical degradation of the PV modules followed by the increase of series resistance.

Because usually, only limited data is available from the PV plants the challenge is how to estimate the physical parameters of the PV diode behavior using only the measured P_{mpp} data and the corresponding weather file. Before the calibration process, the parameter bounds need to be defined so that they have physical meaning. Calibrating the computational code using only

the measured power is causing convergence issues because the parameter values are reaching their boundaries. The structural identifiability of the code was tested where the results show that the model is over parameterized and the number of parameters needs to be reduced. With the reduced number of parameters, the model is identifiable. To get more robust parameter values the Approximate Bayesian Calibration was applied (ABC).

The meta-models are introduced in chapter 5. To avoid the computational burden of expensive code calls the code is replaced with the surrogate or meta-model. For building the meta-models the design of experiment was used. For the appropriate design, the Latin Hypercube Design was used. To run the calibration on the function which emulates the photovoltaic performance model we are risking that the calibrated parameter will loose their physical sense so the meta-model needs to be as close as possible to the actual model. Polynomial chaos expansion was used for meta-model building. For building the meta-model various LHS sample sizes were compared to study their influence on the meta-model accuracy. The validation of the meta-model shows that the meta-model can be used as a surrogate for the time expensive code without sacrificing the accuracy of the calibrated parameters. An example of calibration on real data is presented together with the results.

In the last chapter, the paper "Signatures of Degradation Mechanisms from Fielded Photovoltaic System Monitoring Data " is presented. In the paper 8 years of outdoor measurements from poly crystalline modules are used for calibration on a monthly resolution. Before the calibration the method was validated on the Digital Power Plant (DPP) with known parameter degradation evolution of short circuit current, shunt and series resistance and added Gaussian noise and discrepancy. The calibration results show that the parameters of the model can be estimated on the synthetic data. The method was then applied to the outdoor measurements. The results from the outdoor measurements show that the physical model parameter values can be estimated from the outdoor monitoring data. The results show that the main mechanisms affecting the degradation of the modules are related to the decrease of the short-circuit current.

The presented approach extends the classical performance rate degradation approaches with physical parameter tracking. It would be interesting to apply the method on various module technologies and compare the results. The results of the study should be confirmed with the field inspection and full characterization of the fielded modules. The focus of future studies should be the temporal evolution of parameters together with the outdoor operating conditions in order to understand their interactions and identify possible degradation mechanisms.

Currently, the calibration algorithm considers all the modules operating under identical conditions without considering mismatch or non-uniformity in modules. For the future improvements of the algorithm, the mismatch between the modules and the non-uniformity needs to be integrated into the calibration process because it can add substantial differences in parameter estimation. One of the possible drawbacks is that the method will not be able to identify unique parameter values when there is a large discrepancy between the measured PV power and the simulated one. This kind of discrepancy occurs when the quality of the power measurements or the weather file is poor. Before applying the method the quality of the input data needs to be checked. For future studies, the approach can be extended with multi-objective optimization while it could improve the identifiability of the model with additional added parameters.

One of the drawbacks of the proposed approach is the number of needed meta-models, because for every month of calibration a meta-model needs to be built. Building the meta-model with a certain number of LHD design samples is time consuming and where the number of LHD samples needed should be reduced as much as possible but without sacrificing the accuracy of the obtained

parameters. It could be interesting to study deeper the surrogate models and their application in calibration problems. Trying out various DOE design which could be adapted to the intended application with the minimal needed code calls. Where the DOE should be a compromise between the required accuracy of the meta-model and time expense.

The method can be extended with the service life prediction models where the evolution of the selected parameters can be forecast. One of the drawbacks of this approach is that it can not reveal any degradation mechanism which is not already present in the data. The historical photovoltaic data available for analysis is quite recent and we can not expect to see certain degradation modes that are related to the corrosion of the models.

The presented method can be applied for a novel machine learning algorithms based on the physical models which can track the parameters from fielded PV modules in real-time and make predictions about their future evolution.

Bibliography

[1] Anis Ben Abdessalem et al. "Model selection and parameter estimation in structural dynamics using approximate Bayesian computation". In: *Mechanical Systems and Signal Processing* 99 (2018), pp. 306–325.

[2] Hirotugu Akaike. "Statistical predictor identification". In: *Annals of the institute of Statistical Mathematics* 22.1 (1970), pp. 203–217.

[3] Negin Alemazkoor and Hadi Meidani. "Divide and conquer: An incremental sparsity promoting compressive sampling approach for polynomial chaos expansions". In: *Computer Methods in Applied Mechanics and Engineering* 318 (2017), pp. 937–956.

[4] François Bachoc. "Parametric estimation of covariance function in Gaussian-process based Kriging models. Application to uncertainty quantification for computer experiments". PhD thesis. 2013.

[5] Michaël Baudin et al. "Open TURNS: An industrial software for uncertainty quantification in simulation". In: *arXiv preprint arXiv:1501.05242* (2015).

[6] Michaël Baudin et al. "Openturns: An industrial software for uncertainty quantification in simulation". In: *Handbook of uncertainty quantification* (2017), pp. 2001–2038.

[7] Gal Berkooz, Philip Holmes, and John L Lumley. "The proper orthogonal decomposition in the analysis of turbulent flows". In: *Annual review of fluid mechanics* 25.1 (1993), pp. 539–575.

[8] Géraud Blatman and Bruno Sudret. "Adaptive sparse polynomial chaos expansion based on least angle regression". In: *Journal of Computational Physics* 230.6 (2011), pp. 2345–2367.

[9] Géraud Blatman and Bruno Sudret. "Use of sparse polynomial chaos expansions in adaptive stochastic finite element analysis". In: *Prob. Eng. Mech* (2009).

[10] Andrew J Booker et al. "A rigorous framework for optimization of expensive functions by surrogates". In: *Structural optimization* 17.1 (1999), pp. 1–13.

[11] Francesca Campolongo, Jessica Cariboni, and Andrea Saltelli. "An effective screening design for sensitivity analysis of large models". In: *Environmental modelling & software* 22.10 (2007), pp. 1509–1518.

[12] Mathieu Carmassi. "Uncertainty quantification and calibration of a photovoltaic plant model: warranty of performance and robust estimation of the long-term production." PhD thesis. 2018.

[13] Mathieu Carmassi et al. "Bayesian calibration of a numerical code for prediction". In: *arXiv preprint arXiv:1801.01810* (2018).

[14] Solar Cell. *Working principle of solar cells*. https://www.electrical4u.com/solar-cell/, Last accessed on 2020-02-18. 2017.

[15] Bruno M Chaparro et al. “Material parameters identification: Gradient-based, genetic and hybrid optimization algorithms”. In: *Computational Materials Science* 44.2 (2008), pp. 339–346.

[16] Olivier Chapelle, Vladimir Vapnik, and Yoshua Bengio. “Model selection for small sample regression”. In: *Machine Learning* 48.1-3 (2002), pp. 9–23.

[17] IE Commission et al. “International Standard IEC 61724: Photovoltaic System Performance Monitoring—Guidelines for Measurements, Data Exchange and Analysis”. In: *IEC* (1998).

[18] Peter Craven and Grace Wahba. “Smoothing noisy data with spline functions”. In: *Numerische mathematik* 31.4 (1978), pp. 377–403.

[19] Thierry Crestaux, Olivier Le Maıtre, and Jean-Marc Martinez. “Polynomial chaos expansion for sensitivity analysis”. In: *Reliability Engineering & System Safety* 94.7 (2009), pp. 1161–1172.

[20] David DeGraaff, Ryan Lacerda, Zach Campeau, et al. “Degradation mechanisms in Si module technologies observed in the field; their analysis and statistics”. In: *NREL 2011 Photovoltaic Module Reliability Workshop*. 2011.

[21] Ke-Lin Du and Madisetti NS Swamy. *Neural networks and statistical learning*. Springer Science & Business Media, 2013.

[22] Russell Eberhart and James Kennedy. “A new optimizer using particle swarm theory”. In: *MHS’95. Proceedings of the Sixth International Symposium on Micro Machine and Human Science*. Ieee. 1995, pp. 39–43.

[23] EDF. *The EDF Group pours all its energies into the new Solar Power Plan with a view to developing 30 GW of solar capacity in France by 2035*. https://www.edf.fr/en/edf/the-edf-group-pours-all-its-energies-into-the-new-solar-power-plan-with-a-view-to-developing-30-gw-of-solar-capacity-in-france-by-2035, Last accessed on 2020-01-15. 2017.

[24] PV Education. *Double Diode Model*. https://www.pveducation.org/pvcdrom/ characterisation/double-diode-model, Last accessed on 2020-01-30. 2019.

[25] Robert Faivre et al. *Analyse de sensibilité et exploration de modèles: application aux sciences de la nature et de l’environnement*. Editions Quae, 2016.

[26] Jessica Franco et al. “Minimum Spanning Tree: A new approach to assess the quality of the design of computer experiments”. In: *Chemometrics and intelligent laboratory systems* 97.2 (2009), pp. 164–169.

[27] Linda Weiser Friedman and Israel Pressman. “The metamodel in simulation analysis: Can it be trusted?” In: *Journal of the Operational Research Society* 39.10 (1988), pp. 939–948.

[28] Mircea Grigoriu. “Evaluation of Karhunen–Loève, spectral, and sampling representations for stochastic processes”. In: *Journal of engineering mechanics* 132.2 (2006), pp. 179–189.

[29] Nathan Halko et al. “An algorithm for the principal component analysis of large data sets”. In: *SIAM Journal on Scientific computing* 33.5 (2011), pp. 2580–2594.

[30] Nikolaus Hansen. “The CMA evolution strategy: a comparing review”. In: *Towards a new evolutionary computation*. Springer, 2006, pp. 75–102.

[31] Indranil Hazra, Mahesh D Pandey, and Noldainerick Manzana. “Approximate Bayesian computation (ABC) method for estimating parameters of the gamma process using noisy data”. In: *Reliability Engineering & System Safety* 198 (2020), p. 106780.

[32] Mohammad Hejri et al. “On the parameter extraction of a five-parameter double-diode model of photovoltaic cells and modules”. In: *IEEE Journal of Photovoltaics* 4.3 (2014), pp. 915–923.

[33] Toshimitsu Homma and Andrea Saltelli. “Importance measures in global sensitivity analysis of nonlinear models”. In: *Reliability Engineering & System Safety* 52.1 (1996), pp. 1–17.

[34] Thomas Huld et al. “A power-rating model for crystalline silicon PV modules”. In: *Solar Energy Materials and Solar Cells* 95.12 (2011), pp. 3359–3369.

[35] Bart GM Husslage et al. “Space-filling Latin hypercube designs for computer experiments”. In: *Optimization and Engineering* 12.4 (2011), pp. 611–630.

[36] Bertrand Iooss et al. “Numerical studies of the metamodel fitting and validation processes”. In: *arXiv preprint arXiv:1001.1049* (2010).

[37] John A Jacquez and Peter Greif. “Numerical parameter identifiability and estimability: Integrating identifiability, estimability, and optimal sampling design”. In: *Mathematical Biosciences* 77.1-2 (1985), pp. 201–227.

[38] Ulrike Jahn et al. *Review on infrared and electroluminescence imaging for PV field applications: International Energy Agency Photovoltaic Power Systems Programme: IEA PVPS Task 13, Subtask 3.3: report IEA-PVPS T13-12: 2018*. International Energy Agency, 2018.

[39] Amit Jain and Avinashi Kapoor. “Exact analytical solutions of the parameters of real solar cells using Lambert W-function”. In: *Solar Energy Materials and Solar Cells* 81.2 (2004), pp. 269–277.

[40] Ruichen Jin, Wei Chen, and Timothy W Simpson. “Comparative studies of metamodelling techniques under multiple modelling criteria”. In: *Structural and multidisciplinary optimization* 23.1 (2001), pp. 1–13.

[41] Holland John. *Adaptation in natural and artificial systems*. 1992.

[42] Ian T Jolliffe. “Discarding variables in a principal component analysis. I: Artificial data”. In: *Journal of the Royal Statistical Society: Series C (Applied Statistics)* 21.2 (1972), pp. 160–173.

[43] Will Usher Jon Herman. *Sensitivity Analysis Library*. https://salib.readthedocs.io/en/latest/, Last accessed on 2020-01-30. 2019.

[44] Dirk C Jordan et al. “Photovoltaic failure and degradation modes”. In: *Progress in Photovoltaics: Research and Applications* 25.4 (2017), pp. 318–326.

[45] Vengazhiyil Roshan Joseph. “Space-filling designs for computer experiments: A review”. In: *Quality Engineering* 28.1 (2016), pp. 28–35.

[46] Johan Karlsson, Milena Anguelova, and Mats Jirstrand. “An efficient method for structural identifiability analysis of large dynamic systems”. In: *IFAC Proceedings Volumes* 45.16 (2012), pp. 941–946.

[47] Marc C Kennedy and Anthony O’Hagan. “Bayesian calibration of computer models”. In: *Journal of the Royal Statistical Society: Series B (Statistical Methodology)* 63.3 (2001), pp. 425–464.

[48] Jack PC Kleijnen. “Kriging metamodeling in simulation: A review”. In: *European journal of operational research* 192.3 (2009), pp. 707–716.

[49] Katerina Konakli and Bruno Sudret. “Polynomial meta-models with canonical low-rank approximations: Numerical insights and comparison to sparse polynomial chaos expansions”. In: *Journal of Computational Physics* 321 (2016), pp. 1144–1169.

[50] Marc Kontges et al. *Review of Failures of Photovoltaic Modules*. International Energy Agency, 2014.

[51] Henrique M Kroetz, Rodolfo K Tessari, and André T Beck. "Performance of global metamodeling techniques in solution of structural reliability problems". In: *Advances in Engineering Software* 114 (2017), pp. 394–404.

[52] Marc Lavielle and Leon Aarons. "What do we mean by identifiability in mixed effects models?" In: *Journal of pharmacokinetics and pharmacodynamics* 43.1 (2016), pp. 111–122.

[53] Yao Lin. "An efficient robust concept exploration method and sequential exploratory experimental design". PhD thesis. Georgia Institute of Technology, 2004.

[54] Sascha Lindig et al. "Review of Statistical and Analytical Degradation Models for Photovoltaic Modules and Systems as Well as Related Improvements". In: *IEEE Journal of Photovoltaics* 8.6 (2018), pp. 1773–1786.

[55] Michel Loève. "Probability Theory. 1955". In: *Princeton NJ: Von Nostrand* ().

[56] Jiannan Luo and Wenxi Lu. "Comparison of surrogate models with different methods in groundwater remediation process". In: *Journal of Earth System Science* 123.7 (2014), pp. 1579–1589.

[57] Wei Luo et al. "Potential-induced degradation in photovoltaic modules: a critical review". In: *Energy & Environmental Science* 10.1 (2017), pp. 43–68.

[58] George Makrides et al. "Degradation of different photovoltaic technologies under field conditions". In: *2010 35th IEEE Photovoltaic Specialists Conference*. IEEE. 2010, pp. 002332–002337.

[59] Bill Marion et al. "Performance parameters for grid-connected PV systems". In: *Conference Record of the Thirty-first IEEE Photovoltaic Specialists Conference, 2005.* IEEE. 2005, pp. 1601–1606.

[60] Michael D McKay, Richard J Beckman, and William J Conover. "Comparison of three methods for selecting values of input variables in the analysis of output from a computer code". In: *Technometrics* 21.2 (1979), pp. 239–245.

[61] Hongyu Miao et al. "On identifiability of nonlinear ODE models and applications in viral dynamics". In: *SIAM review* 53.1 (2011), pp. 3–39.

[62] Max D Morris. "Factorial sampling plans for preliminary computational experiments". In: *Technometrics* 33.2 (1991), pp. 161–174.

[63] Max D Morris and Toby J Mitchell. "Exploratory designs for computational experiments". In: *Journal of statistical planning and inference* 43.3 (1995), pp. 381–402.

[64] Daryl Myers. *Evaluation of the Performance of the PVUSA Rating Methodology Applied to Dual Junction PV Technology: Preprint (Revised)*. Tech. rep. National Renewable Energy Lab.(NREL), Golden, CO (United States), 2009.

[65] John Norton. "An introduction to sensitivity assessment of simulation models". In: *Environmental Modelling & Software* 69 (2015), pp. 166–174.

[66] Carl Osterwald et al. "Degradation analysis of weathered crystalline-silicon PV modules". In: *Conference Record of the Twenty-Ninth IEEE Photovoltaic Specialists Conference, 2002.* IEEE. 2002, pp. 1392–1395.

[67] Kurt Palmer and Michael Realff. "Optimization and validation of steady-state flowsheet simulation metamodels". In: *Chemical Engineering Research and Design* 80.7 (2002), pp. 773–782.

[68] Benjamin Braisaz Patrick Dupeyrat Amy Lindsay. "An Advanced Model of PV Power Plants Based on Modelica". In: *European Photovoltaic Solar Energy Conference and Exhibitions*. PVSEC. 2013.

[69] Timothy J Peshek et al. "Insights into metastability of photovoltaic materials at the mesoscale through massive I–V analytics". In: *Journal of Vacuum Science & Technology B, Nanotechnology and Microelectronics: Materials, Processing, Measurement, and Phenomena* 34.5 (2016), p. 050801.

[70] Giovanni Petrone, Giovanni Spagnuolo, and Massimo Vitelli. "Analytical model of mismatched photovoltaic fields by means of Lambert W-function". In: *Solar energy materials and solar cells* 91.18 (2007), pp. 1652–1657.

[71] Alexander Phinikarides et al. "Review of photovoltaic degradation rate methodologies". In: *Renewable and Sustainable Energy Reviews* 40 (2014), pp. 143–152.

[72] Luc Pronzato. "Minimax and maximin space-filling designs: some properties and methods for construction". In: *ournal de la Societe Française de Statistique, Societe Française de Statistique et SocieteMathematique de France* 158.1 (2017), pp. 7–36.

[73] Michael Quintana et al. "Commonly observed degradation in field-aged photovoltaic modules". In: *Conference Record of the Twenty-Ninth IEEE Photovoltaic Specialists Conference, 2002.* IEEE. 2002, pp. 1436–1439.

[74] Laiz Reis, Jose Robert Camacho, and Deborah Novacki. "The Newton Raphson method in the extraction of parameters of PV modules". In: *Proceedings of the International Conference on Renewable Energies and Power Quality (ICREPQ'17), Malaga, Spain*. 2017, pp. 4–6.

[75] Luis Miguel Rios and Nikolaos V Sahinidis. "Derivative-free optimization: a review of algorithms and comparison of software implementations". In: *Journal of Global Optimization* 56.3 (2013), pp. 1247–1293.

[76] Donald B Rubin. "Bayesianly justifiable and relevant frequency calculations for the applies statistician". In: *The Annals of Statistics* (1984), pp. 1151–1172.

[77] Ann-Britt Ryberg, Rebecka Domeij Bäckryd, and Larsgunnar Nilsson. *Metamodel-based multidisciplinary design optimization for automotive applications*. Linköping University Electronic Press, 2012.

[78] Bassem Saassouh, Bruno Sudret, and Géraud Blatman. "Uncertainty analysis based on polynomial chaos expansions using Open TURNS". In: ().

[79] Jerome Sacks, Susannah B Schiller, and William J Welch. "Designs for computer experiments". In: *Technometrics* 31.1 (1989), pp. 41–47.

[80] Jerome Sacks et al. "Design and analysis of computer experiments". In: *Statistical science* (1989), pp. 409–423.

[81] Shuichi Sakamoto and Togashi Oshiro. "Field test results on the stability of crystalline silicon photovoltaic modules manufactured in the 1990s". In: *3rd World Conference onPhotovoltaic Energy Conversion, 2003. Proceedings of*. Vol. 2. IEEE. 2003, pp. 1888–1891.

[82] Andrea Saltelli. "Making best use of model evaluations to compute sensitivity indices". In: *Computer physics communications* 145.2 (2002), pp. 280–297.

[83] Andrea Saltelli et al. *Sensitivity analysis in practice: a guide to assessing scientific models*. Vol. 1. Wiley Online Library, 2004.

[84] Katharina Schulze et al. “Untersuchung von Alterungseffekten bei monokristallinen PV-Modulen mit mehr als 15 Betriebsjahren durch Elektrolumineszenz-und Leistungsmessung”. In: *Proc. 28. Symposium Photovoltaische Solarenergie*. 2012.

[85] Stefan Sellner et al. “Advanced PV module performance characterization and validation using the novel Loss Factors Model”. In: *2012 38th IEEE Photovoltaic Specialists Conference*. IEEE. 2012, pp. 002938–002943.

[86] Stefan Sellner et al. “Understanding PV module performance: Further validation of the novel loss factors model and its extension to AC arrays”. In: *27th EU PVSEC* (2012), pp. 3199–3204.

[87] Qian Shao et al. “Bayesian sparse polynomial chaos expansion for global sensitivity analysis”. In: *Computer Methods in Applied Mechanics and Engineering* 318 (2017), pp. 474–496.

[88] Timothy W Simpson, Dennis KJ Lin, and Wei Chen. “Sampling strategies for computer experiments: design and analysis”. In: *International Journal of Reliability and Applications* 2.3 (2001), pp. 209–240.

[89] Ilya M Sobol. “Sensitivity estimates for nonlinear mathematical models”. In: *Mathematical modelling and computational experiments* 1.4 (1993), pp. 407–414.

[90] Michael Stein. “Large sample properties of simulations using Latin hypercube sampling”. In: *Technometrics* 29.2 (1987), pp. 143–151.

[91] Bruno Sudret. “Global sensitivity analysis using polynomial chaos expansions”. In: *Reliability engineering & system safety* 93.7 (2008), pp. 964–979.

[92] Bruno Sudret. “Polynomial chaos expansions and stochastic finite element methods”. In: *Risk and reliability in geotechnical engineering* (2015), pp. 265–300.

[93] Xingsu Sun, Raghu Vamsi Krishna Chavali, and Muhammad Ashraful Alam. “Real-Time monitoring and diagnosis of photovoltaic system degradation only using maximum power point- the Suns-Vmp method”. In: *Progress in Photovoltaic* 27.27 (2017), pp. 55/66.

[94] Mikael Sunnåker et al. “Approximate bayesian computation”. In: *PLoS computational biology* 9.1 (2013), e1002803.

[95] Simon Tavaré et al. “Inferring coalescence times from DNA sequence data”. In: *Genetics* 145.2 (1997), pp. 505–518.

[96] Gerhard Venter. “Review of optimization techniques”. In: *Encyclopedia of aerospace engineering* (2010).

[97] Eric Walter and Luc Pronzato. “Identification of parametric models”. In: *Communications and control engineering* 8 (1997).

[98] Gary Wang and Songqing Shan. “Review of metamodeling techniques in support of engineering design optimization”. In: *Journal of Mechanical design* 129.4 (2007), pp. 370–380.

[99] Fangzheng Xie and Yanxun Xu. “Bayesian Projected Calibration of Computer Models”. In: *arXiv preprint arXiv:1803.01231* (2018).

[100] Dongbin Xiu and George Em Karniadakis. “The Wiener–Askey polynomial chaos for stochastic differential equations”. In: *SIAM journal on scientific computing* 24.2 (2002), pp. 619–644.

[101] Adel Younis and Zuomin Dong. “Trends, features, and tests of common and recently introduced global optimization methods”. In: *Engineering Optimization* 42.8 (2010), pp. 691–718.

[102] Ren Yuan and Bai Guangchen. "Comparison of neural network and Kriging method for creating simulation-optimization metamodels". In: *2009 eighth IEEE international conference on dependable, autonomic and secure computing*. IEEE. 2009, pp. 815–821.

[103] Brian Zaharatos. "Statistical modeling of photovoltaic device performance". PhD thesis. Colorado School of Mines. Arthur Lakes Library, 2015.

Appendix: A

Technical scheme to generate trajectories

Technical scheme to generate trajectories with required properties is as follows [83]:

For a model with k parameters a trajectory can be seen in the form of a matrix B^* with dimension $(k+1) \times k$, whose rows are the vectors $x^{(1)}, x^{(2)}, ..., x^{(k+1)}$. To build B^* we first need to build a matrix B, whose dimensions are $(k+1) \times k$, with elements that are 0's and 1's so that for every column index $j, j = 1, ..., k$, there are two rows of B that differ only in the j^{th} entry. A convenient choice for B is a strictly lower triangular matrix of 1's:

$$B = \begin{bmatrix} 0 & 0 & 0 & \cdots & 0 \\ 1 & 0 & 0 & \cdots & 0 \\ 1 & 1 & 0 & \cdots & 0 \\ 1 & 1 & 1 & 0 & \cdots \\ \cdots & \cdots & \cdots & \cdots & \cdots \end{bmatrix}$$

The sampling matrix is defined as:

$$B^* = (x^* + (\Delta/2) \times [(2B - J_{k+1,k}) \times D^* + J_{k+1,k}]) \times P^*$$

where $J_{k+1,k}$ is a $(k+1)$ matrix of 1's and x^* is a randomly chosen base value of X. D^* is a k-dimensional diagonal matrix where each element is either $+1$ or -1 with equal probability. P^* is a *k-by-k* random permutation matrix in which each row contains one element equal to 1 while all the other elements are 0, and no two columns have 1's in the same position.

Example:

For three input factors x_1, x_2 and x_3 all uniformly distributed in [0,1] for $p = 4$ number of levels. The levels are $\{0, 1/3, 2/3, 1\}$. Suppose that the $\Delta = 2/3$, and the randomly generated x^*, D^* and P^* are as following:

$$x^* = [0, 1/3, 1/3] \qquad D^* = \begin{bmatrix} -1 & 0 & 0 \\ 0 & 1 & 0 \\ 0 & 0 & 1 \end{bmatrix} \qquad P^* = \begin{bmatrix} 0 & 0 & 1 \\ 1 & 0 & 0 \\ 0 & 1 & 0 \end{bmatrix}.$$

For those values,

$$(\Delta/2)[(2B - J_{k+1,k})D^* + J_{k+1,k}] = \begin{bmatrix} \Delta & 0 & 0 \\ 0 & 0 & 0 \\ 0 & \Delta & 0 \\ 0 & \Delta & \Delta \end{bmatrix}$$

and then

$$B^* = \begin{bmatrix} 1/3 & 1/3 & 2/3 \\ 1/3 & 1/3 & 0 \\ 1 & 1/3 & 0 \\ 1 & 1 & 0 \end{bmatrix}$$

The trajectory obtained is $x^{(1)} = (1/3, 1/3, 2/3)$, $x^{(2)} = (1/3, 1/3, 0)$, $x^{(3)} = (1, 1/3, 0)$, $x^{(4)} = (1, 1, 0)$

Appendix: B

Saltelli sampler

The Salteli sampler [82] is defined as:

Generate a $(N, 2k)$ matrix of randomly selected parameters x from defined parameter space, where k is the number of inputs. Define two matrices A and B. Use the first k columns of the matrix as matrix A, and the remaining k columns as matrix B. N is called a base sample and can vary from few hundreds to a few thousands.

$$A = \begin{bmatrix} x_1^{(1)} & x_2^{(1)} & \cdots & x_i^{(1)} & \cdots & x_k^{(1)} \\ x_1^{(2)} & x_2^{(2)} & \cdots & x_i^{(2)} & \cdots & x_k^{(2)} \\ \cdots & \cdots & \cdots & \cdots & & \\ x_1^{(N-1)} & x_2^{(N-1)} & \cdots & x_i^{(N-1)} & \cdots & x_k^{(N-1)} \\ x_1^{(N)} & x_2^{(N)} & \cdots & x_i^{(N)} & \cdots & x_k^{(N)} \end{bmatrix}$$

$$B = \begin{bmatrix} x_{k+1}^{(1)} & x_{k+2}^{(1)} & \cdots & x_{k+i}^{(1)} & \cdots & x_{2k}^{(1)} \\ x_{k+1}^{(2)} & x_{k+2}^{(2)} & \cdots & x_{k+i}^{(2)} & \cdots & x_{2k}^{(2)} \\ \cdots & \cdots & \cdots & \cdots & & \\ x_{k+1}^{(N-1)} & x_{k+2}^{(N-1)} & \cdots & x_{k+i}^{(N-1)} & \cdots & x_{2k}^{(N-1)} \\ x_{k+1}^{(N)} & x_{k+2}^{(N)} & \cdots & x_{k+i}^{(N)} & \cdots & x_{2k}^{(N)} \end{bmatrix}$$

Define a matrix C_i formed by all columns of B except the i^{th} column, which is taken from A:

$$C_i = \begin{bmatrix} x_{k+1}^{(1)} & x_{k+2}^{(1)} & \cdots & x_i^{(1)} & \cdots & x_{2k}^{(1)} \\ x_{k+1}^{(2)} & x_{k+2}^{(2)} & \cdots & x_i^{(2)} & \cdots & x_k^{(2)} \\ \cdots & \cdots & \cdots & \cdots & & \\ x_{k+1}^{(N-1)} & x_{k+2}^{(N-1)} & \cdots & x_i^{(N-1)} & \cdots & x_{2k}^{(N-1)} \\ x_{k+1}^{(N)} & x_{k+2}^{(N)} & \cdots & x_i^{(N)} & \cdots & x_{2k}^{(N)} \end{bmatrix}$$

Compute the model output for all the input values in the sample matrices A, B and C_i.

ECOLE
DOCTORALE
DE MATHEMATIQUES
HADAMARD

Titre : Signatures de mécanismes de dégradation des centrales photovoltaïques

Mots clés : Dégradation de performance, Centrales photovoltaïques, Analyse de sensibilité, Méta-modèles, Estimation d'un modèle non linéaire, Calcul bayésien approximatif

Résumé : La dégradation de la performance des centrales PV (photovoltaïque) au cours de leur durée de vie est généralement déterminée par la variation de la puissance au point de puissance maximale (Power at maximum power point P_{mpp}). Cependant, la même quantité de pertes en P_{mpp} peut avoir des causes multiples, qui ont, chacune, des évolutions différentes dans le temps. Le modèle physique d'EDF est une version sophistiquée d'un modèle à 2 diodes. Ce modèle dépend de paramètres dont les valeurs évoluent au cours du temps et peuvent reflètent ainsi les processus de dégradation.
Lorsque les mesures des courbes courant-tension (courbes IV) sont disponibles, les paramètres du modèle physique peuvent être directement estimés. Toutefois les mesures de la courbe IV sont rarement effectuées sur les sites de production de PV et l'estimation des paramètres du modèle à 2 diodes est difficile à partir du nombre limité de variables mesurées. Le défi que nous nous attachons à relever est l'estimation des paramètres du modèle en utilisant uniquement le P_{mpp}, et la météo, permettant ainsi une évaluation plus précise de l'état de santé du système, plutôt que d'estimer uniquement la mesure de la perte de performance. Une analyse de sensibilité (Morris et Sobol) a été réalisée sur différents modèles physiques photovoltaïques, à savoir le modèle à diode unique et le code d'EDF. Les trois paramètres les plus influents identifiés par notre méthodologie sont ont la résistance-série (Rs), la résistance shunt (Rsh) et le courant de court-circuit (Isc). Ces paramètres identifiés ont été utilisés dans la calibration du modèle de performance PV.
L'algorithme proposé vise à identifier la distribution *a posteriori* des paramètres en calibrant le code de calcul en fonction des données observées. L'inférence bayésienne a été menée à l'aide de la m´méthode ABC (Approximate Bayesian Computation) car la vraisemblance des observations est un code de calcul et n'a pas d'expression close. Comme l'exécution du code de calcul est chronophage. Une expansion en chaos polynomial (PCE) a été utilisée comme modèle de substitution pour remplacer le code original et accélérer l'inférence. L'algorithme a été validé sur des données synthétiques simulées (Digital Power Plant) auxquelles nous avons ajouté un bruit de mesure gaussien, une erreur systématique et un scénario d'évolution de d´dégradation des paramètres.

Title : Signatures of Degradation Mechanisms from Photovoltaic Plants

Keywords : Photovoltaic degradation, Sensitivity analysis, Design of Experiment, Calibration

Abstract : The degradation of the PV (Photovoltaic) performance over its lifetime is usually determined with the variation of Power at maximum power point (Pmpp). However, the same amount of Pmpp loss can have different causes, which have, each, different expectations of evolution with time. The EDF physical performance model is a sophisticated version of a 2-diode model and contains parameters that can reflect degradation over time. When IV curves measurements are available from the field the parameters of the physical model can be straightforwardly estimated. While the IV curve measurements are rarely available from the PV production sites the parameter, estimation is challenging since only limited data about the observed system is available. Estimating the model parameters using only Pmpp is the challenge here allowing a more precise evaluation of the health state of the system, rather than estimating only the performance loss metric.
A sensitivity analysis (Morris and Sobol) was performed on different photovoltaic physical models, namely the single diode model and the EDF code. The three most influential parameters identified by our methodology are the series resistance (Rs), the shunt resistance (Rsh) and the short-circuit current (Isc). These identified parameters were used in the calibration of the PV performance model. The proposed algorithm aims to identify posterior distribution of parameters by calibrating the computational code to the observed data with a robust Approximate Bayesian Computation (ABC) method. The ABC method expresses the probability of the observed data under a prior statistical model with certain parameter values. Polynomial Chaos Expansion (PCE) was used as a meta-model to replace the original code which was found to be too computationally expensive.
The algorithm has been validated on simulated synthetic data (Digital Power Plant) with an added Gaussian noise, some systematic discrepancy and a known parameter degradation evolution. The results on the synthetic data show that the evolution of parameters can be estimated in noisy measurement conditions